Universität Hamburg
Department Physik

TIME DOMAIN NUMERICAL CALCULATIONS OF THE SHORT ELECTRON BUNCH WAKEFIELDS IN RESISTIVE STRUCTURES

Dissertation
zur Erlangung des Doktorgrades
des Fachbereichs Physik
der Universität Hamburg

vorgelegt von

Andranik Tsakanian
aus Eriwan (Armenien)

Hamburg
2010

Gutachter der Dissertation: Prof. Dr. Jörg Rossbach
Prof. Dr. Ursula van Rienen

Gutachter der Disputation: Prof. Dr. Jörg Rossbach
Prof. Dr. Markus Drescher

Datum der Disputation: 19 Oktober 2010

Vorsitzender des Prüfungsausschusses: Dr. Georg Steinbrück

Vorsitzender des Promotionsausschusses: Prof. Dr. Joachim Bartels

Dekan der Fakultät für Mathematik,
Informatik und Naturwissenschaften: Prof. Dr. Heinrich H. Graener

TIME DOMAIN NUMERICAL CALCULATIONS OF THE SHORT ELECTRON BUNCH WAKEFIELDS IN RESISTIVE STRUCTURES

Dissertation
Submitted for Doctoral Degree in Physics
at Hamburg University

Presented by
Andranik Tsakanian

Abstract

The acceleration of electron bunches with very small longitudinal and transverse phase space volume is one of the most actual challenges for the future International Linear Collider and high brightness X-Ray Free Electron Lasers. The exact knowledge on the wake fields generated by the ultra-short electron bunches during its interaction with surrounding structures is a very important issue to prevent the beam quality degradation and to optimize the facility performance. The high accuracy time domain numerical calculations play the decisive role in correct evaluation of the wake fields in advanced accelerators.

The thesis is devoted to the development of a new longitudinally dispersion-free 3D hybrid numerical scheme in time domain for wake field calculation of ultra short bunches in structures with walls of finite conductivity. The basic approaches used in the thesis to solve the problem are the following. For materials with high but finite conductivity the model of the plane wave reflection from a conducting half-space is used. It is shown that in the conductive half-space the field components perpendicular to the interface can be neglected. The electric tangential component on the surface contributes to the tangential magnetic field in the lossless area just before the boundary layer. For high conducting media, the task is reduced to 1D electromagnetic problem in metal and the so-called 1D conducting line model can be applied instead of a full 3D space description. Further, a TE/TM ("transverse electric - transverse magnetic") splitting implicit numerical scheme along with 1D conducting line model is applied to develop a new longitudinally dispersion-free hybrid numerical scheme in the time domain.

The stability of the new hybrid numerical scheme in vacuum, conductor and bound cell is studied. The convergence of the new scheme is analyzed by comparison with the well-known analytical solutions. The wakefield calculations for a number of structures are performed and a good agreement with known analytical and numerical results is obtained. The new hybrid scheme was applied to calculate the wake potentials for the various components of FLASH linear accelerator at DESY and the European XFEL project.

Numerische Berechnung im Zeitbereich der begleitenden Felder kurzer Elektronen Pakete in Strukturen mit endlicher Leitfaehigkeit

Dissertation
zur Erlangung des Doktorgrades des Fachbereichs Physik
der Universität Hamburg

vorgelegt von
Andranik Tsakanian

Zusammenfassung

Die Beschleunigung von Elektronen-Paketen mit sehr kleinen Abmessungen im longitudinalen und transversalen Phasenraum ist eine der wichtigsten Herausforderungen für den zukünftigen internationalen Linearbeschleuniger (ILC) und für Freie-Elektronen-Röntgen-Laser mit sehr hoher Brillanz. Die genaue Kenntnis der begleitenden Felder, die von sehr kurzen Elektronen Paketen in Wechselwirkung mit den umgebenden Strukturen erzeugt werden, ist sehr wichtig um eine Verschlechterung der Strahlqualität zu verhindern und die Leistung der Anlage zu optimieren. Sehr genaue Berechnungen im Zeitbereich sind entscheidend um die begleitenden Felder in hochentwickelten Beschleuniger Strukturen richtig zu bestimmen.

Diese Arbeit ist der Entwicklung eines neuen dreidimensionalen dispersionsfreien numerischen Hybridschemas im Zeitbereich gewidmet, um die begleitenden elektromagnetischen Felder zu berechnen, die entstehen wenn sehr kurze Ladungspaketen durch Strukturen mit endlich leitfähigen Wänden fliegen. Die wesentlichen Näherungen die hier benutzt werden sind die folgenden. Für Materialien mit hoher aber endlicher Leitfähigkeit wird das Modell der Reflexion an einem leitfähigen Halbraum verwendet. Es wird gezeigt daβ im leitfähigen Halbraum Feldkomponenten senkrecht zur Grenzfläche vernachlässigt werden können. Die elektrische Tangentialkomponente in der Oberfläche ergibt sich dabei als Reaktion auf das tangentiale magnetische Feld im verlustfreien Bereich knapp vor der Grenzschicht. Für sehr gut leitfähige Medien vereinfacht sich die Aufgabe in das eindimensionale elektromagnetische Problem in Metall, auf das sich das sogenannte verlustbehaftete Linienleitungsmodell anwenden läβt, statt einer vollständig dreidimensionalen Beschreibung. Zudem wird eine TE/TM ("transversal elektrisch - transversal magnetisch") Aufspaltung eines impliziten, dispersionsfreien numerischen Verfahrens zusammen mit einem verlustbehafteten Linienleitungsmodell angewandt um ein neues dispersionsfreies numerisches Hybridschema im Zeitbereich zu entwickeln.

Die Stabilität des neuen numerischen Hybridschemas wird untersucht in Vakuum, im leitfähigen Bereich und in der verbindenden Zelle. Die Konvergenz des neuen Schemas wird ermittelt und mit bekannten analytischen Lösungen verglichen. Die begleitenden elektromagnetischen Felder werden für eine Reihe von Strukturen berechnet und dabei gute Übereinstimmung mit bekannten analytischen und numerischen Ergebnissen erzielt. Das neue Hybridschema wurde verwendet um begleitende Felder in zahlreichen Komponenten von FLASH und vom europäischen Freie-Elektronen Laser Projekt zu charakterisieren.

ACKNOWLEDGMENTS

Contents

List of Tables

List of Figures

Chapter 1. Introduction

The acceleration of electron bunches with very small longitudinal and transverse phase space volume is one of the most actual challenges in advanced linear accelerators for fundamental and applied research. The preservation of small phase space volume of accelerated electron bunches is one of the basic requirement to reach the projected luminosity in future International Linear Collider (ILC) [1] and to drive high brightness X-Ray Free Electron Lasers (XFEL) [2-6].

The European X-Ray FEL project [3] is aiming to generate ultra-short pulses of spatially coherent photon beams with wavelengths down to 0.1 nm and the brilliance of about 10^{33} ph/mm^2/mrad^2/0.1%BW. The process adopted to generate the X-ray pulses is Self-Amplified-Spontaneous-Emission (SASE) [7-10].

In SASE process, the high energy electron beam in undulator section interacts with the transverse electric field of radiation due to transverse velocity of electrons in undulator magnet and produces an electron energy modulation on the scale of radiation wavelength λ_r. The electron energy modulation in turn modifies the electron trajectory in the undulator producing the microbunching of the electrons at the scale λ_r. Electrons bunched within a wavelength emit radiation in phase, thus producing a larger intensity that leads to more energy modulation and more bunching, leading to exponential growth of the radiation until saturation is reached.

In order the SASE process to occur the electron beam must match the transverse phase space occupied by a transversally coherent radiation, i.e. in terms of the electron beam natural emittance ε (transverse phase space area) and radiation wavelength λ_r, this condition reads as $\varepsilon \le \lambda_r / 4\pi$.

Another important condition to electron beam parameters for SASE FEL is the limit to beam energy spread σ_E to prevent the widening of the spontaneous radiation line and the reduction of the growth rate due to Landau damping. In SASE FEL theory this limit is given by the dimensionless FEL parameter ρ and read as $\sigma_\epsilon / E << \rho$, where E is the accelerated particle nominal energy. The typical limit to relative energy spread for X-ray SASE FEL is of the order of $\sigma_\epsilon / E << 10^{-4}$. In addition, in order for the FEL to operate in the saturation mode with reasonable undulator length a high electron peak current (short bunches) is required.

In the European XFEL project [3], the electron bunches with normalized projected emittance of 1.4 μm and bunch charge of 1nC are accelerated up to 17.5 GeV energy in superconducting linear accelerator. The X-rays are then generated in about 200 m long undulator section. The required peak current of 5kA is reached in two magnetic chicanes where the initially 2mm (rms) long bunch is compressed down to 25 μm at the entrance to main linac.

In a real machine, as the beam propagates along the accelerator, it interacts with the surrounding structure and excites the electromagnetic fields that act back to the trailing particles of the bunch [11]. These fields, known as the wakefields, affect the beam performance as the excited fields in general have longitudinal and transverse components. The effects of these wake fields, are evaluated in time domain by introducing the longitudinal and transverse wake potentials that represent the integrated Lorenz force in longitudinal and transverse directions acting on the trailing test particles. The longitudinal wake potential produces an extra energy spread within the bunch, while the transverse wake potential lead to beam rms emittance growth.

The beam propagating along the accelerator interacts with various types of the elements such as accelerating structures, bellows, transitions, collimators, couplers, small gap undulators etc, which in general have different geometries and electrodynamical properties. Therefore, the exact knowledge on the wake fields generated during these interactions is very important both from the beam physics point of view (preservation of beam small emittance and energy spread) and with regard to the new technical solutions for various components.

Summarizing the above considerations, the first physical motivation of the presented thesis is driven by achievement and preservation of the small phase space volume of the charge particles beams in advanced accelerators.

The thesis is devoted to one important topic of this problem - the exact calculation of the longitudinal and transverse wake fields excited by short electron bunches in various accelerator structure components with finite conductivity walls.

1.1. Numerical Methods for Wake Field Calculation

The computation of the wake potentials always played an important role in particle accelerator physics [11-20]. With the progress of the new generation of the accelerator facilities with extremely low beam emittance and energy spread the exact solutions for the wake potentials become the barest necessity, as the relative effects of their impact to beam parameters are tangible.

The development of advanced accelerators is accompanied with the improvement and modification of the facility characteristics that require careful modeling and examination of the effects that impact the beam quality. In advanced electron light sources the technical solutions for small gap undulators and wigglers, high vacuum performance, cures of resistive instabilities [21-23], prevention of the static charge [24], shielding of external radiation [25-26] imply the usage of various types of complicated vacuum chamber configurations having both geometrical and constructive peculiarities. These complications along with the stringent requirements to the beam quality recently drove rigorous numerical and analytical study of the longitudinal and transverse wake fields for various types of structures. On the other hand the exact analytical solutions for the wake fields are available for the structure with relatively simple geometry [27-31].

Thus the practical way of calculating and studying the electromagnetic fields in real 3-dimensional (3D) structures is the application of numerical methods.

The numerical codes are an important tool for the wake field simulations [32-40], however they not always give appropriate results especially for the very short bunch length and the structures with walls of finite conductivity. The basic approach for the numerical calculations of the electromagnetic fields in three-dimensional structures is the discretization of the Maxwell equations in space and time domains. The correct numerical simulations of the wake fields require the longitudinal mesh step smaller than the bunch rms length. In addition, the phase and group velocity of the numerical waves differ from the physical one that lead to dispersive accumulative numerical errors. More complications arise for the structures with finite conductive walls, since to model the waves in conductor more dense geometrical meshes in comparison with free space are required. This leads to the considerable reduction of time step that increases the numerical dispersion error and corrupts the simulation.

Various Maxwell grid equation (MGE) based numerical codes have been developed to solve the 2D and 3D wake field problems in frequency and time domains [40, 52, 53] but usually without resistive wall losses.

To make the numerical simulations of beam dynamics in accelerators the particle-in-cell (PIC) method [35] is an effective approach. The electromagnetic fields in many PIC codes are computed using the finite-difference time domain (FDTD) method [36, 37]. As any numerical mesh approach the conventional FDTD scheme [38], used in MAFIA [39], TBCI [40] and other wake and PIC codes, suffers from numerical grid dispersion, i.e. the group velocity of the numerical waves is slower than the physical one. Hence, the high energy particles can travel in vacuum faster than their own radiation. This effect is commonly referred to as numerical Cherenkov radiation [41], which due to its accumulative character corrupts the simulation.

Several numerical approaches [42-45] are proposed to reduce the accumulated dispersion error of numerical simulations for all angles and for given frequency range. These methods require the usage of larger spatial stencils and a special treatment of the material interfaces.

In the accelerator applications the domain of interest is very long in the longitudinal direction (well-defined direction of the beam motion) and relatively narrow in the transverse plane. In addition, the electromagnetic fields change very fast in the direction of bunch motion but they are relatively smooth in the transverse plane. Therefore the development of numerical algorithms with cancellation or reduction of the numerical dispersion in longitudinal direction is very important.

It is known that the conventional FDTD method is dispersion free along grid diagonals and that this property can be used effectively in numerical simulations [46]. However, in this case the only solution is to take equal mesh steps in all three directions.
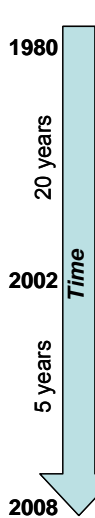
		Non-dispersive in longitudinal direction	Second order convergence	Volume Conductivity	Surface Conductivity (IBC-TD)
1980	BCI/TBCI	No	No	No	No
	NOVO	Yes	No	No	No
	ABCI	No	No	No	No
	MAFIA	No	No	Yes	Yes
	XWAKE	No	Yes	No	No
	Gdfidl	No	No	Yes	No
2002	Tau3P	No	Yes	No	No
	ECHO	Yes	Yes	No	No
	CST	No	Yes	Yes	Yes
	PBCI	Yes	Yes	No	No
2008	NEKCEM	No	Yes	No	No
	This work	Yes	No	No	Yes

Table 1. *Not exhaustive list of available numerical codes.*

Alternatively, a semi-implicit numerical scheme without dispersion in longitudinal direction with simpler conformal treatment of material interfaces and the usage of non-equidistant grids has been developed in [47-50].

Shown in Table 1 are the numerical codes developed during last 30 years. Also presented are the properties of the numerical schemes implemented in those codes, like numerical dispersion and convergence. The third column shows whether the code can model volume conductivity. From the numerical codes listed in Table 1 only MAFIA [39], CST Microwave Studio [51] and Gdfidl can model structures with walls of finite conductivity. In the last column the surface conductivity option is given in the mean of Impedance Boundary Condition modeling in Time Domain (IBC-TD). This option is important especially for high conductive materials like Aluminum (Al), Copper (Cu) and etc. However in those codes the Yee conventional FDTD scheme is implemented. Thus the algorithms suffer from numerical dispersion and are inefficient for ultra short bunches.

To model ultra short bunches and to prevent the numerical dispersion in longitudinal direction, the dispersion-free numerical scheme is proposed in [52] that is implemented in code ECHO. The dispersion-free numerical scheme enables use of a moving mesh frame concept without loosing the accuracy of calculation. Another relatively new numerical code applicable for ultra short bunches and with a dispersion-free algorithm is the PBCI code [53]. Note that both codes are unable to model the finite conductive materials (Table 1).

To calculate the wake field of ultra-short bunches in resistive structures, it is necessary to develop a new time-domain numerical scheme that would effectively match the resistive boundary conditions and would be dispersion-free in the longitudinal direction.

1.2 Overview and Main Results

The thesis is devoted to the development of a new 3D dispersion-free hybrid numerical scheme in time domain for wake field calculation of ultra short bunches in structures with walls of finite conductivity. The main issue in numerical simulation of 3D electrodynamic problems with conductive boundaries is stipulated by the wavelength contraction in conductor with respect to free space [60,76]. For short bunches, this leads to very dense 3D mesh in conductor region with respect to free space.

The basic approaches used in the thesis to solve the problem are the following. For finite but high conductivity material it is shown that the incident waves are transmitted perpendicular to the boundary surface and only the tangential components of electric and magnetic fields survive in the conducting media. Thus for high conducting media, the task is reduced to 1D electromagnetic problem in metal and the so-called 1D conducting line model can be applied instead of a full 3D space description. Further, TE/TM ("transverse electric - transverse magnetic") splitting implicit dispersion-free numerical scheme along with 1D conducting line model is applied to develop a new dispersion-free hybrid numerical scheme in time domain.

The stability of the new hybrid numerical scheme in vacuum, conductor and bound cell is studied. The stability conditions have been tested and confirmed by a number of numerical experiments. The convergence of the new scheme is analyzed by comparison with the well-known analytical solutions. The wakefield calculations for a number of structures are performed and a good agreement with known analytical and numerical results is obtained.

The thesis consists of introduction, three chapters, summary and bibliography.

Chapter 2 of the thesis is devoted to the time domain numerical modeling of one-dimensional electromagnetic problems with Impedance Boundary Condition (IBC). In this chapter an explicit and implicit numerical schemes are introduced for electromagnetic field calculations in the metal and in the vacuum regions. The stability analyses of those two schemes for both regions are performed. For IBC modeling in time domain the matching of the numerical schemes (explicit and implicit) in vacuum and in metal is achieved. The stability analyses of the so-called hybrid (matched) numerical schemes are performed. Stability analysis has shown the implicit hybrid scheme to be unconditionally stable. For the conductor part the stable space step strongly depends on both the time step and vacuum space step. It is shown that the hybrid numerical scheme has a second-order convergence.

In **Chapter 3** the overview of the TE/TM implicit 3D numerical scheme [33, 52, 67] is given. This time-domain numerical scheme is dispersion-free in longitudinal direction and valid for structures with perfect conducting walls. It is especially efficient for the wakefield calculations excited by ultra-short relativistic bunches. The analysis shows that the TE/TM numerical scheme is much more accurate in long-time simulations than the conventional FDTD approach. This scheme has been applied for development of a new hybrid numerical scheme that includes conductive boundaries.

The **Chapter 4** is devoted to a new hybrid numerical scheme for calculating the wakefields excited by ultra-short bunches in structures with walls of finite high conductivity. Based on the TE/TM splitting numerical scheme described in Chapter 3 a new longitudinally dispersion-free algorithm for resistive structures is developed. The time domain impedance boundary condition in each boundary cell is approximated by one-dimensional EM model described in Chapter 2. The realization of this new hybrid 3D implicit numerical scheme is done for rotationally symmetric geometries and staircase approximation of the boundary surface. A good agreement of the numerical simulations with the well-known analytical results and CST Particle Studio simulations are obtained. The new hybrid scheme was applied to calculate the wake potentials for the various components of FLASH linear accelerator at DESY and the European XFEL project.

Chapter 2.

Time Domain Numerical Modeling of 1D Electromagnetic Problems with Impedance Boundary Conditions

In this Chapter the time domain numerical model of one-dimensional electromagnetic problems with Impedance Boundary Conditions (IBC) is derived. The explicit and implicit numerical schemes are introduced for electromagnetic field calculations in the metal and vacuum regions. The stability analyses of those two schemes for both regions are performed. For IBC modeling in time domain the matching of the numerical schemes (explicit and implicit) in vacuum and in metal is achieved. The stability analyses of the so-called hybrid (matched) numerical schemes (explicit and implicit) are performed.

Consider the plane electromagnetic wave with electric $\vec{E}$ and magnetic $\vec{H}$ components incident normal to the vacuum-conductor boundary surface (Fig.1).
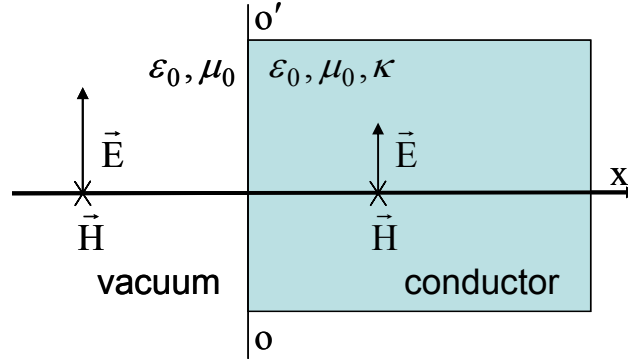
Figure 1. *Plane wave scattering on metallic surface.*

In Cartesian coordinate system and normalized time, variable $\tau \equiv ct$, the 1D integral Maxwell equations are given as

$$\oint \vec{H} d\vec{l} = \iint_S \left[\vec{J} + \frac{1}{Z_0} \frac{\partial \vec{E}}{\partial \tau} \right] d\vec{s}$$

$$\oint \vec{E} d\vec{l} = -Z_0 \iint_S \frac{\partial \vec{H}}{\partial \tau} d\vec{s} \qquad (2.1)$$

$$\vec{J} = \kappa \vec{E}$$

where $Z_0 = c\mu_0 = (c\varepsilon_0)^{-1} = 376.73\ \Omega$ is the impedance of free space, κ is the conductivity, $\vec{J}$ is the bias current, c is the velocity of light, x is the longitudinal coordinate.

For discretisation of this 1D problem we distinguish two regions: vacuum and conductor. We assume that the time step $\Delta\tau$ is constant and is the same for both regions, while the discrete mesh spacing Δx is also constant but different for each region. As shown in later analysis the different space steps in vacuum and conductor are required to satisfy the stability conditions of numerical schemes. To develop the numerical schemes, the continuous space-time dependence of the electromagnetic field $u(x, \tau) \equiv \{E, H\}(x, \tau)$ will hereinafter be substituted by the relevant

5

quantity $u(x_i, \tau_n)$ in discrete space-time coordinates $x_i = i \cdot \Delta x$, $\tau_n = n \cdot \Delta \tau$ with i, n integer numbers. The relevant discretized solution at the mesh point i and time level n will be represented as u_i^n. Note that in this definition n is a mere superscript, rather than an exponent. In all regions the electric and magnetic fields on discrete space are shifted by half a space step from each other. To be shown in this Chapter is that if the discrete electric and magnetic fields are defined at the same time level the resulting numerical scheme is implicit, while for an explicit scheme the time level of the magnetic field is shifted by a half-time step from the electric one.

2.1 1D Numerical Scheme in Vacuum

The integral Maxwell's equations (2.1) for the 1D continuous electromagnetic fields problem in vacuum region ($\kappa = 0$) are simplified to

$$\oint \vec{H} d\vec{l} = \frac{1}{Z_0} \iint_S \frac{\partial \vec{E}}{\partial \tau} d\vec{s}$$

$$\oint \vec{E} d\vec{l} = -Z_0 \iint_S \frac{\partial \vec{H}}{\partial \tau} d\vec{s}$$

(2.2)

To describe the electromagnetic fields in finite time and space, the equations (2.2) should be added to the initial (time) and boundary (space) conditions. We suppose that boundaries of the vacuum region of interest satisfy the perfect electric (PEC) boundary conditions, i.e. the tangential component of the electric field is zero on boundaries KK' ($x = -L$) and OO' ($x = 0$), as shown in Fig.2. To be assumed as the initial conditions for the problem are the results of analytical or numerical solutions.

2.1.1 Space Discretization

For discretization of electromagnetic field in one-dimensional space we define normal and dual uniform grids in the space for electric and magnetic fields respectively. The distance between the two closest nodes in both grids is the same and is termed space step Δx_0. The dual grid is shifted by half a space step with regard to the normal grid. The normal grid is chosen in the way that it cover the boundary points as well. By introducing integer variable i the coordinates of the nodes of the grids can be expressed via space step as $i \cdot \Delta x_0$ and $(i + 0.5) \cdot \Delta x_0$ for normal and dual grids respectively. Now we define the electric field e_i on the nodes of normal grid and magnetic one $h_{i+1/2}$ on nodes of dual grid. The scheme of the discretization is shown in Figure 2. Here the index i for the electric field and index $(i + 1/2)$ for the magnetic fields represent the space points where the fields are defined.
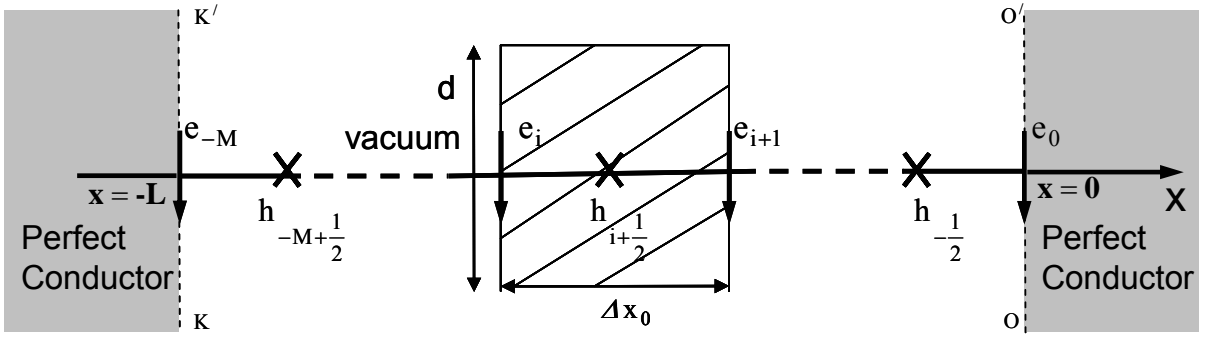
Figure 2. *A schematic view of the electromagnetic field in the discrete space of a vacuum region.*

According to Figure 2 the space discretization of the left and right parts of the second equation in (2.2) will read as

$$\oint \vec{E}\,d\vec{l} \approx (e_{i+1} - e_i)d$$

$$-Z_0 \frac{\partial}{\partial \tau} \iint \vec{H}\,d\vec{s} \approx Z_0 \frac{\partial}{\partial \tau} h_{i+\frac{1}{2}} \Delta x_0 \cdot d \qquad \text{with } -M < i < 0 \qquad (2.3)$$

where Δx_0 is the discrete space step in vacuum and i, M are integers. The integer M is defined as the number of discrete points of an electric field in space, i.e. the number of normal grid nodes. Thus, the number of discrete points for a magnetic field (the number of dual grid nodes) will be $M-1$ (Fig.2). Equaling both equations in (2.3) we get

$$-Z_0 \frac{\partial}{\partial \tau} h_{i+\frac{1}{2}} \Delta x_0 = e_{i+1} - e_i \qquad (2.4)$$

This equation could also be easily obtained from the 1D differential Maxwell equations (2.1) using the central difference method for the approximation of the space derivative of electromagnetic fields.
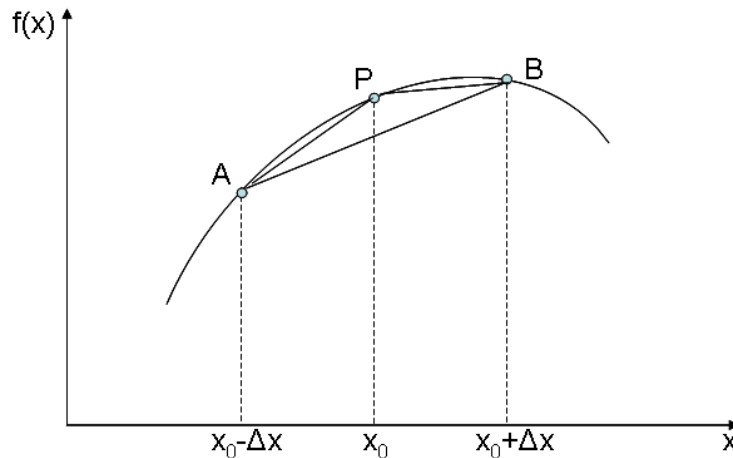
Figure 3. *Estimates for the derivative of f(x) at point P using central differences.*

In the central differences method the derivative of any continuous function $f(x)$ at point P is approximated as (Fig.3)

$$\left. \frac{df(x)}{dx} \right|_{x=x_0} \approx \frac{f(x + \Delta x) - f(x - \Delta x)}{2\Delta x} + o(\Delta x^2) \tag{2.5}$$

The order of approximation can easily be proven by using Taylor expansion [54]. Since this approximation has the second-order accuracy with respect to Δx, we expect that the final numerical scheme will have the same order of accuracy [55, 56] when the geometric mesh coincides with boundary interface. Otherwise an additional numerical error added from approximation of the boundary interface that can compromise the accuracy of calculation.

Now we discretize the first equation in formula (2.2).

$$\oint \vec{H} \, d\vec{l} = \frac{1}{Z_0} \iint_S \frac{\partial \vec{E}}{\partial \tau} \, d\vec{s} \tag{2.6}$$
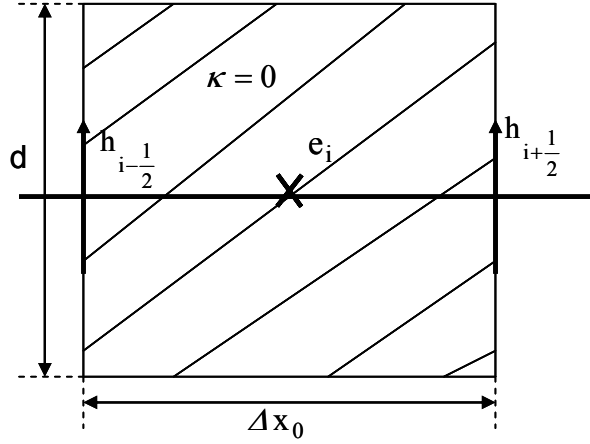
Figure 4. *The geometric view of the i th cell in vacuum.*

According to the Figure 4, the left- and right-hand sides of this Equation will read as

$$\oint \vec{H} \, d\vec{l} \approx (h_{i+\frac{1}{2}} - h_{i-\frac{1}{2}})d$$

$$\frac{1}{Z_0} \iint \frac{\partial}{\partial \tau} \vec{E} d\vec{s} \approx \frac{1}{Z_0} \frac{\partial}{\partial \tau} e_i \, \Delta x_0 \cdot d \qquad \text{with } -M < i < 0 \tag{2.7}$$

Substituting (2.7) to (2.6) we get

$$\frac{1}{Z_0} \frac{\partial}{\partial \tau} e_i = \frac{1}{\Delta x_0} \left(h_{i+\frac{1}{2}} - h_{i-\frac{1}{2}} \right) \tag{2.8}$$

Finally the time continuous and space discretized, 1D Maxwell's equations (2.2) will read as

$$\frac{\partial}{\partial \tau} h_{i+\frac{1}{2}} = \frac{1}{Z_0} \frac{e_{i+1} - e_i}{\Delta x_0}$$

$$\frac{1}{Z_0} \frac{\partial}{\partial \tau} e_i = \frac{h_{i+\frac{1}{2}} - h_{i-\frac{1}{2}}}{\Delta x_0} \tag{2.9}$$

with PEC boundary conditions $e_0 = e_{-M} \equiv 0$. Introducing the vectors for electric $\widehat{e}$ and magnetic $\widehat{h}$ fields

$$\widehat{e} = \frac{1}{Z_0}\begin{pmatrix} e_{-0} \\ \vdots \\ e_{-M} \end{pmatrix}, \quad \widehat{h} = \begin{pmatrix} h_{-0.5} \\ \vdots \\ h_{-(M+0.5)+1} \end{pmatrix} \tag{2.10}$$

the equations (2.9) can be rewritten in a simple matrix form

$$\frac{\partial}{\partial \tau}\widehat{h} = P_{vacuum}\,\widehat{e}$$

$$\frac{\partial}{\partial \tau}\widehat{e} = P^*_{vacuum}\,\widehat{h} \tag{2.11}$$

In Equation (2.11) P_{vacuum}, P^*_{vacuum} are the matrixes of $[(M-1) \times M]$, $[M \times (M-1)]$ dimensions respectively matching the discrete operators of derivative by space for electric and magnetic fields

$$P_{vacuum} = \frac{1}{\Delta x_0}\begin{pmatrix} -1 & 1 & 0 & \cdots & 0 \\ 0 & -1 & 1 & \cdots & 0 \\ \vdots & \vdots & \ddots & \ddots & \vdots \\ 0 & 0 & \cdots & -1 & 1 \end{pmatrix}, \quad P^*_{vacuum} = \frac{1}{\Delta x_0}\begin{pmatrix} -1 & 0 & 0 & \cdots & 0 \\ 1 & -1 & 0 & \cdots & 0 \\ 0 & 1 & -1 & \cdots & 0 \\ 0 & 0 & \ddots & \ddots & \vdots \\ \vdots & \vdots & \vdots & 1 & -1 \\ 0 & 0 & \cdots & 0 & 1 \end{pmatrix} \tag{2.12}$$

As follows from (2.12), the 1D derivative operators on primary P_{vacuum} and dual P^*_{vacuum} grids have the property of the generalized symmetry, i.e. $P^*_{vacuum} = P^T_{vacuum}$.

2.1.2 Time Discretization

In this section we introduce the discretization of continuous time variable. For the time derivative we will use the central difference approximation (2.5) with the discrete time step $\Delta \tau$. We define the integer variable n for the time level description that will indicate the real time $\tau_n = n \cdot \Delta \tau$.

We will discuss two types of EM field time discretization that lead to implicit and explicit numerical schemes respectively.

a. Implicit 1D numerical scheme

One possibility for time discretization is to define the electric $\widehat{e}$ and magnetic $\widehat{h}$ fields at the same time level n. In this case we need to apply the linear interpolation describing EM fields at the time level $n + 0.5$ as

$$\widehat{h}^{n+\frac{1}{2}} = \frac{\widehat{h}^{n+1} + \widehat{h}^n}{2} \quad \widehat{e}^{n+\frac{1}{2}} = \frac{\widehat{e}^{n+1} + \widehat{e}^n}{2} \tag{2.13}$$

9

Using central difference approximation for time derivatives the discretized form of EM field equations (2.9) will read as

$$h_{i+\frac{1}{2}}^{n+1} = h_{i+\frac{1}{2}}^{n} + \frac{\Delta\tau}{\Delta x_0} \frac{1}{Z_0} \left[\frac{e_{i+1}^{n+1} + e_{i+1}^{n}}{2} - \frac{e_i^{n+1} + e_i^{n}}{2} \right]$$

$$e_i^{n+1} = e_i^{n} + \frac{\Delta\tau}{\Delta x_0} Z_0 \left[\frac{h_{i+\frac{1}{2}}^{n+1} + h_{i+\frac{1}{2}}^{n}}{2} - \frac{h_{i-\frac{1}{2}}^{n+1} + h_{i-\frac{1}{2}}^{n}}{2} \right] \tag{2.14}$$

or in matrix form

$$\widehat{h}^{n+1} = \widehat{h}^{n} + \Delta\tau\, P_{vacuum} \frac{\widehat{e}^{n+1} + \widehat{e}^{n}}{2}$$

$$\widehat{e}^{n+1} = \widehat{e}^{n} + \Delta\tau\, P_{vacuum}^{*} \frac{\widehat{h}^{n+1} + \widehat{h}^{n}}{2} \tag{2.15}$$

The equations (2.15) may be written as follows:

$$\widehat{h}^{\#} = \widehat{h}^{n} + \frac{\Delta\tau}{2} P_{vacuum}\, \widehat{e}^{n}$$

$$W_0 \left[\widehat{e}^{n+1} - \widehat{e}^{n} \right] = \Delta\tau\, P_{vacuum}^{*}\, \widehat{h}^{\#}$$

$$\widehat{h}^{n+1} = \widehat{h}^{\#} + \frac{\Delta\tau}{2} P_{vacuum}\, \widehat{e}^{n+1} \tag{2.16}$$

with three-diagonal matrix W_0 given as

$$W_0 = I - \frac{\Delta\tau^2}{4} P_{vacuum}^{*} P_{vacuum} \tag{2.17}$$

where I is the unit matrix.
As seen in this case the numerical scheme is implicit.

b. Explicit 1D Numerical Scheme

Another option for time discretization is to define the electric $\widehat{e}$ and magnetic $\widehat{h}$ fields at different time levels n and $n+0.5$ respectively. Using central difference approximation for time derivatives the discretized form of EM field equations (2.9) will read as

$$h_{i+\frac{1}{2}}^{n+\frac{1}{2}} = h_{i+\frac{1}{2}}^{n-\frac{1}{2}} + \frac{\Delta\tau}{\Delta x_0} \frac{1}{Z_0} \left[e_{i+1}^{n} - e_i^{n} \right]$$

$$e_i^{n+1} = e_i^{n} + \frac{\Delta\tau}{\Delta x_0} Z_0 \left[h_{i+\frac{1}{2}}^{n+\frac{1}{2}} - h_{i-\frac{1}{2}}^{n+\frac{1}{2}} \right] \tag{2.18}$$

or in matrix form

$$\widehat{h}^{\,n+\frac{1}{2}} = \widehat{h}^{\,n-\frac{1}{2}} + \Delta\tau\, P_{vacuum}\,\widehat{e}^{\,n}$$

$$\widehat{e}^{\,n+1} = \widehat{e}^{\,n} + \Delta\tau\, P^{*}_{vacuum}\,\widehat{h}^{\,n+\frac{1}{2}}$$

(2.19)

As seen from the field update equations (2.18) and (2.19) the numerical scheme is explicit.

The important issue in numerical modeling of the Maxwell equations is the stability analyses of the numerical schemes, to be discussed in the next section.

2.1.3 Stability of the Scheme

In this chapter we will discuss the stability and convergence of the above-introduced schemes. First we introduce the general theory of stability analyses [54, 57-59].

Consider a system satisfying $\dfrac{d\vec{U}}{dt} = L\,\vec{U}$, where L is a linear differential operator and $\vec{U}(\vec{r},t)$ is a state vector known at $t=0$, i.e. $\vec{U}(\vec{r},0) = \vec{U}_{0}$. The discretization of such a system in time will bring us to the following equation in difference form

$$\widehat{U}^{\,n+1} = G(\Delta x, \Delta t)\,\widehat{U}^{\,n}$$

(2.20)

where G is called the amplification matrix of the difference scheme, $\widehat{U}$ is a discretized vector in the space. The time level is given as a superscript.

In general when the eigenvectors of amplification matrix G make the basis, the solution can be expressed in terms of eigenvector expansion. In particular, such a basis always exists when the matrix G is self-conjugated or similar to the symmetric matrix [55, 56]. In this chapter we assume that the eigenvectors $\widehat{\psi}^{(v)}$ of the amplification matrix G make up a complete basis for the linear problem (2.20). The initial state vector expansion over the eigenvectors $\widehat{\psi}^{(v)}$ then will read as

$$\widehat{U}^{\,0} = \sum_{v} \widehat{U}^{\,0}_{v}\,\widehat{\psi}^{(v)}$$

(2.21)

where $\widehat{U}^{\,0}_{v}$ are the expansion amplitudes at time step zero.

From equations (2.20) and (2.21) the state vector $\widehat{U}^{\,n}$ at time level *n* can be presented as

$$\widehat{U}^{\,n} = (G)^{n}\,\widehat{U}^{\,0} = (G)^{n}\sum_{v}\widehat{U}^{\,0}_{v}\,\widehat{\psi}^{(v)}$$

(2.22)

The eigenvectors $\widehat{\psi}^{(v)}$ of amplification matrix G satisfy the following equation

$$G\,\widehat{\psi}^{(v)} = g_{v}\,\widehat{\psi}^{(v)}$$

(2.23)

where g_{v} are the eigenvalues of amplification matrix G.

Using the state vector expansion (2.22) we get

$$\widehat{U}^{\,n} = \sum_{v}\widehat{U}^{\,0}_{v}\left(g_{v}\right)^{n}\widehat{\psi}^{(v)}$$

(2.24)

As seen from the presentation (2.24), the discrete model $\widehat{U}^n$ is stable when the following condition to eigenvalues are fulfilled

$$|g_\nu| \le 1 \qquad (2.25)$$

We will apply the above stability theory to the analysis of the numerical algorithms for plane wave in vacuum described in the previous section. The results will be then valid for modeling the source-free 1D electromagnetic problems, since any EM fields in vacuum can be expressed via the superposition of plane waves.

a. Stability of 1D Implicit Scheme in Free Space

The implicit numerical scheme in original form (2.14) read as

$$h_{i+\frac{1}{2}}^{n+1} = h_{i+\frac{1}{2}}^{n} + \frac{\Delta\tau}{\Delta x_0}\frac{1}{Z_0}\left[\frac{e_{i+1}^{n+1} + e_{i+1}^{n}}{2} - \frac{e_{i}^{n+1} + e_{i}^{n}}{2}\right]$$

$$e_{i}^{n+1} = e_{i}^{n} + \frac{\Delta\tau}{\Delta x_0}Z_0\left[\frac{h_{i+\frac{1}{2}}^{n+1} + h_{i+\frac{1}{2}}^{n}}{2} - \frac{h_{i-\frac{1}{2}}^{n+1} + h_{i-\frac{1}{2}}^{n}}{2}\right] \qquad (2.26)$$

For the plane wave we have the following relations between the two closest discrete points in space

$$h_{i+\frac{1}{2}}^{n} = h_{i-\frac{1}{2}}^{n}\, e^{jk\Delta x_0}$$

$$e_{i+1}^{n} = e_{i}^{n}\, e^{jk\Delta x_0} \qquad (2.27)$$

where k is the wave number.
Using these relations the numerical scheme (2.26) is modified to

$$e_{i}^{n+1} - e_{i}^{n} = Z_0\alpha\left[e^{jk\Delta x_0} - 1\right]\frac{h_{i-\frac{1}{2}}^{n+1} + h_{i-\frac{1}{2}}^{n}}{2}$$

$$h_{i-\frac{1}{2}}^{n+1} - h_{i-\frac{1}{2}}^{n} = \frac{1}{Z_0}\alpha\left[1 - e^{-jk\Delta x_0}\right]\frac{e_{i}^{n+1} + e_{i}^{n}}{2} \qquad (2.28)$$

where $\alpha = \Delta\tau/\Delta x_0$.
The updated equations (2.28) can be presented as

$$h_{i-\frac{1}{2}}^{n+1} = \frac{F_2}{F_1}\, h_{i-\frac{1}{2}}^{n} + \frac{1}{Z_0}\frac{\alpha}{F_1}\left(1 - e^{-jk\Delta x_0}\right)e_{i}^{n} \qquad F_{1,2} = 1 \pm \vartheta$$

with

$$e_{i}^{n+1} = \frac{F_2}{F_1}\, e_{i}^{n} + Z_0\frac{\alpha}{F_1}\left(e^{jk\Delta x_0} - 1\right)h_{i-\frac{1}{2}}^{n} \qquad \vartheta = \alpha^2\sin^2\left(k\frac{\Delta x_0}{2}\right) \qquad (2.29)$$

To get (2.29) the following trigonometric relation is used

$$\left(1 - e^{-jk\Delta x_0}\right)\left(e^{jk\Delta x_0} - 1\right) = -4\sin^2\left(k\frac{\Delta x_0}{2}\right) \tag{2.30}$$

Following (2.20) the amplification matrix G for vector $\hat{U}^n = \begin{pmatrix} e_i^n \\ h_{i-0.5}^n \end{pmatrix}$ will be given by

$$G = \begin{pmatrix} \dfrac{F_2}{F_1} & Z_0\dfrac{\alpha}{F_1}\left(e^{jk\Delta x_0} - 1\right) \\ \dfrac{1}{Z_0}\dfrac{\alpha}{F_1}\left(1 - e^{-jk\Delta x_0}\right) & \dfrac{F_2}{F_1} \end{pmatrix} \tag{2.31}$$

The eigenvalues g_ν of amplification matrix G are given by $\det(G - g\,I) = 0$ (I - unit matrix) that read as

$$\det(G - g\,I) = \begin{vmatrix} \dfrac{F_2}{F_1} - g & \dfrac{\alpha}{F_1}\left(e^{jk\Delta x_0} - 1\right) \\ \dfrac{\alpha}{F_1}\left(1 - e^{-jk\Delta x_0}\right) & \dfrac{F_2}{F_1} - g \end{vmatrix} = \left(\dfrac{F_2}{F_1} - g\right)^2 + 4\dfrac{\vartheta}{F_1^2} = 0 \tag{2.32}$$

The eigenvalues $g_{1,2}$ of amplification matrix G are then given by

$$g_{1,2} = \frac{1 - \vartheta \pm 2j\sqrt{\vartheta}}{1 + \vartheta} \tag{2.33}$$

As is seen the eigenvalues are complex with the modules equal to unity.

$$|g|^2 = g^* g = \frac{(1 - \vartheta)^2 + 4\vartheta}{(1 + \vartheta)^2} = 1 \tag{2.34}$$

According to the stability criteria (2.25) it follows that the 1D implicit scheme is unconditionally stable, i.e. in the numerical scheme the time and space steps can be chosen independently.

b. Stability of Explicit Scheme in Free Space

For the explicit scheme (2.18) using the relations (2.27) for plane wave we get

$$h_{i-\frac{1}{2}}^{n+\frac{1}{2}} = h_{i-\frac{1}{2}}^{n-\frac{1}{2}} + \frac{1}{Z_0}\alpha\left[1 - e^{-jk\Delta x_0}\right]e_i^n$$

$$e_i^{n+1} = e_i^n + Z_0\alpha\left[e^{jk\Delta x_0} - 1\right]h_{i-\frac{1}{2}}^{n+\frac{1}{2}} \tag{2.35}$$

Introducing the vector $\hat{U}^n = \begin{pmatrix} e_i^n \\ h_{i-0.5}^{n-0.5} \end{pmatrix}$ the amplification matrix G will read as

$$G = \begin{pmatrix} 1 - 4\,\alpha^2 \sin^2\left(k\,\dfrac{\Delta x_0}{2}\right) & Z_0\,\alpha\left(e^{j k \Delta x_0} - 1\right) \\ \dfrac{1}{Z_0}\,\alpha\left(1 - e^{-j k \Delta x_0}\right) & 1 \end{pmatrix}$$ (2.36)

The eigenvalues $g_{1,2}$ of the amplification matrix G for explicit scheme will then be derived as

$$g_{1,2} = 1 - 2\vartheta \pm 2\sqrt{\vartheta(\vartheta - 1)} \quad \text{with} \quad \begin{aligned} \vartheta &\equiv \alpha^2 \sin^2\left(k\,\frac{\Delta x_0}{2}\right) \\ \alpha &\equiv \frac{\Delta \tau}{\Delta x_0} \end{aligned}$$ (2.37)

For $\vartheta < 1$ the eigenvalues $g_{1,2}$ are complex and the stability condition (2.25) is fulfilled since $|g| = 1$. In the case of real eigenvalues ($\vartheta \geq 1$), the stability condition is satisfied for $\vartheta = 1$. Summarizing the cases of real and complex eigenvalues, the stability condition for explicit scheme is read as

$$\vartheta \leq 1$$ (2.38)

In terms of space and time steps we get the following stability condition

$$\left(\frac{\Delta \tau}{\Delta x_0}\right)^2 \sin^2\left(k\,\frac{\Delta x_0}{2}\right) \leq 1$$ (2.39)

Since the sinus function for real arguments is always smaller or equal to one the final stability condition for explicit scheme is read as

$$\Delta \tau \leq \Delta x_0$$ (2.40)

As seen from (2.37), the stability condition for explicit scheme also implies the complex eigenvalues for amplification matrix G.

2.1.4 Numerical Dispersion Analyses

The important issues in numerical modeling are the numerical scheme accuracy studies [16, 19, 34]. In this section the dispersion properties for the implicit and explicit numerical schemes in vacuum will be discussed. For the plan waves in vacuum the discrete relations (2.27) in space should be added with the following relations for closest discrete time points

$$h_{i+\frac{1}{2}}^{n+1} = h_{i+\frac{1}{2}}^{n}\,e^{j \Omega \Delta \tau}$$

$$e_i^{n+1} = e_i^{n}\,e^{j \Omega \Delta \tau}$$ (2.41)

where in our notations Ω is normalized frequency ($\Omega = \omega/c$, ω is frequency, c is velocity of light). Note, that the dispersion relation of the continuous plane wave in vacuum is given by $\Omega = k$, i.e. the phase velocity in vacuum is equal to velocity of light [15, 60].

a. Numerical Dispersion of the Implicit Scheme

Using the relations (2.41) the updated equations (2.28) will read as

$$\left[e^{j\Omega\Delta\tau}-1\right]e_i^n = \frac{Z_0\alpha}{2}\left[e^{jk\Delta x_0}-1\right]\left[e^{j\Omega\Delta\tau}+1\right]h_{i-\frac{1}{2}}^n$$

$$\text{with } \alpha = \Delta\tau/\Delta x_0 \qquad (2.42)$$

$$Z_0\left[e^{j\Omega\Delta\tau}-1\right]h_{i-\frac{1}{2}}^n = \left[1-e^{-jk\Delta x_0}\right]\left[e^{j\Omega\Delta\tau}+1\right]\alpha\frac{e_i^n}{2}$$

Using the trigonometric relations

$$e^{j2x}-1 = 2je^{jx}\sin(x)$$
$$e^{j2x}+1 = 2e^{jx}\cos(x) \qquad (2.43)$$
$$\left(e^{j2x}-1\right)\left(1-e^{-j2x}\right) = -4\sin^2(x)$$

we get the following dispersion equation:

$$\text{tg}^2\left(\Omega\frac{\Delta\tau}{2}\right) = \left(\frac{\Delta\tau}{\Delta x_0}\right)^2\sin^2\left(k\frac{\Delta x_0}{2}\right) \qquad (2.44)$$

From this dispersion equation we find the numerical phase v_{ph} and group v_g velocities (normalized to speed of light) of the electromagnetic wave

$$v_{ph} = \frac{\Omega}{k} = \frac{2}{k\Delta\tau}\text{arctg}\left[\frac{\Delta\tau}{\Delta x_0}\sin\left(k\frac{\Delta x_0}{2}\right)\right]$$

$$v_g = \frac{d\Omega}{dk} = \frac{\cos\left(k\frac{\Delta x_0}{2}\right)}{1+\left(\frac{\Delta\tau}{\Delta x_0}\right)^2\sin^2\left(k\frac{\Delta x_0}{2}\right)} \qquad (2.45)$$

As seen from the dispersion relation, the wave number k and normalized frequency Ω are real for any time and space steps, i.e. the scheme is unconditionally stable in free space. On the other hand, as follows from (2.44) and (2.45), the implicit 1D scheme for any space Δx_0 and time $\Delta\tau$ steps has the numerical dispersion, i.e. the phase and the group velocities differs from the velocity of light $\Omega \neq k$.

b. Numerical Dispersion of the Explicit Scheme

For the explicit numerical scheme (2.18) the dispersion equation can be derived with analogy to implicit one [54]

$$\sin^2\left(\Omega\frac{\Delta\tau}{2}\right) = \left(\frac{\Delta\tau}{\Delta x_0}\right)^2\sin^2\left(k\frac{\Delta x_0}{2}\right) \qquad (2.46)$$

As seen in this case, the wave number k and Ω are real only when $\Delta\tau \le \Delta x_0$ and the stability condition is satisfied. From dispersion equation (2.46) it follows that for the equal time and space steps the numerical scheme is non-dispersive, i.e. the numerical phase velocity is equal to velocity of light $\Omega = k$. Thus the dispersion free condition for explicit scheme is $\Delta\tau = \Delta x_0$, which is in agreement with the stability condition (2.40). From dispersion equation (2.46) the expressions for the EM wave numerical phase and group velocities normalized to speed of light read as

$$v_{ph} = \frac{\Omega}{k} = \frac{2}{k\,\Delta\tau}\arcsin\left[\frac{\Delta\tau}{\Delta x_0}\sin\left(k\frac{\Delta x_0}{2}\right)\right]$$

$$v_g = \frac{d\Omega}{dk} = \frac{\cos\left(k\dfrac{\Delta x_0}{2}\right)}{\sqrt{1-\left(\dfrac{\Delta\tau}{\Delta x_0}\right)^2\sin^2\left(k\dfrac{\Delta x_0}{2}\right)}} \qquad (2.47)$$

Thus, in dispersion free scheme the numerical normalized phase and group velocities are equal to one and coincides with the continuous wave phase and group velocities, i.e. in vacuum are equal to the speed of light. Figure 5 illustrates the normalized numerical phase and group velocities versus variable $0.5k\,\Delta x_0$ according to formulas (2.45) and (2.47). In this example the discrete time step is taken to be half of the space step $\Delta\tau = 0.5\ \Delta x_0$.
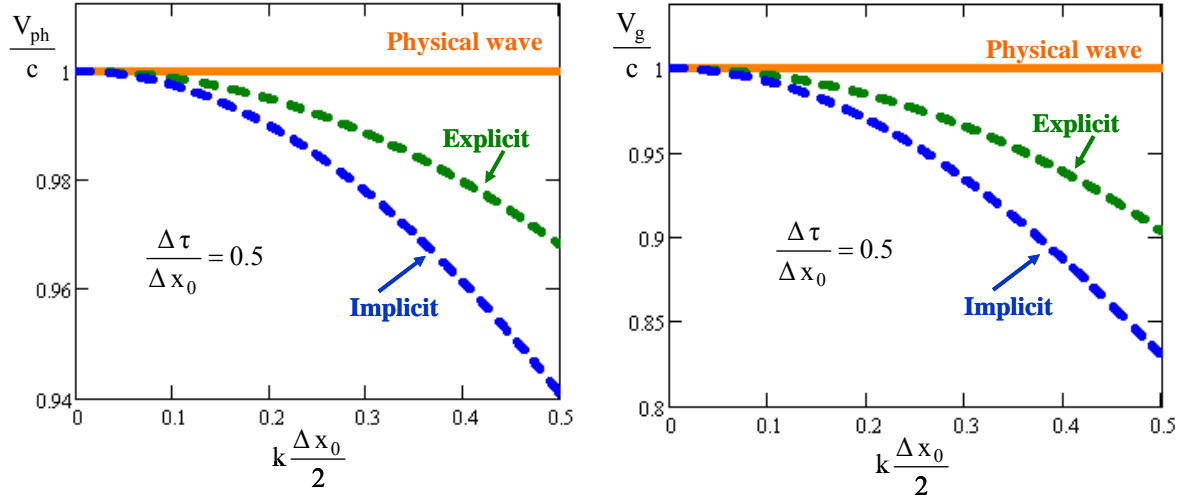
Figure 5. *Numerical phase and group velocities of the implicit (blue dashed) and the explicit (green dashed) schemes versus* $0.5k\,\Delta x_0$. *The physical velocities are given by solid line (orange).*

As we see from the figure for given wave number k, the numerical dispersion of the schemes (explicit and implicit) are suppressed when the following condition is fulfilled

$$k\frac{\Delta x_0}{2} \le \frac{1}{4} \qquad (2.48)$$

Thus, in the numerical modeling of 1D multi-wave problem, the numerical dispersion error will be less than 5% for the discrete space step $\Delta x_0 \le (2k_{max})^{-1}$.

2.2 1D Numerical Scheme in Conductor

In this section we introduce the continuous electromagnetic problem in homogeneous metallic media with finite conductivity κ. The 1D integral Maxwell's equations (2.1) will read as

$$\oint \vec{H}\,d\vec{l} = \iint_S \left[\kappa \vec{E} + \frac{1}{Z_0} \frac{\partial \vec{E}}{\partial \tau} \right] d\vec{s}$$

$$\oint \vec{E}\,d\vec{l} = -Z_0 \iint_S \frac{\partial \vec{H}}{\partial \tau}\,d\vec{s}$$

(2.48)

With proper boundary conditions and initial values of the electromagnetic fields the problem becomes closed. To describe the numerical scheme for this problem, we shall start with a perfect electric (PEC) boundary condition, i.e. the electric field being zero on boundaries that corresponds to the space points $x = 0$ and $x = L_c$, respectively (fig.6).

2.2.1 Space discretization

In analogy with the plane wave in vacuum, for discretization of electromagnetic field in one-dimensional space, we define the normal and dual uniform grids in space for electric and magnetic fields respectively with the space step Δx. The dual grid is shifted by a half-space step relative to the normal grid. The normal grid is chosen in the way that it cover the boundary points. Similar to the vacuum case (section 2.1), in conductor region the same notations for field description in the discrete space are used. The discretization is graphically shown in Figure 6. As seen from the figure, all notations for field description in the discrete space are kept except for the number of discrete points M that is different in this case being replaced by integer number N .
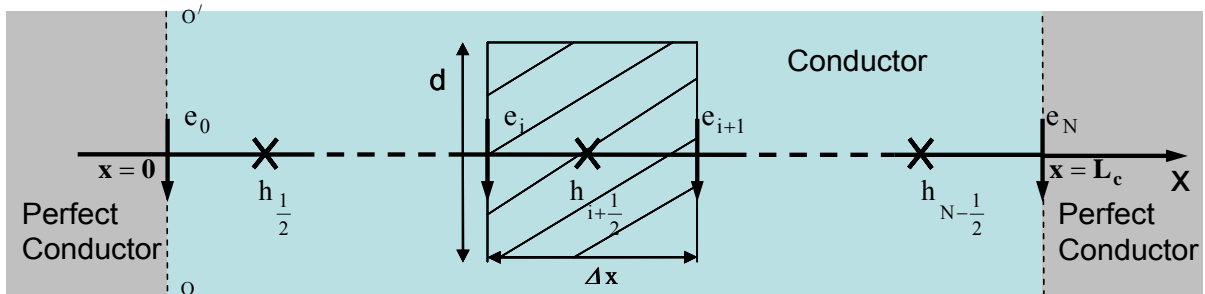
Figure 6. *Electromagnetic field schematic view in discrete space of conductor region.*

Now, according to figure 6, the discretization of the second equation in formula (2.48) will read as

$$\oint \vec{E}\,d\vec{l} \approx (e_{i+1} - e_i)d$$

$$-Z_0 \frac{\partial}{\partial \tau} \iint \vec{H}\,d\vec{s} \approx Z_0 \frac{\partial}{\partial \tau} h_{i+\frac{1}{2}} \Delta x \cdot d \qquad \text{with } 0 < i < N$$

(2.49)

Equaling both equations we get

$$Z_0 \frac{\partial}{\partial \tau} h_{i+\frac{1}{2}} \Delta x = (e_{i+1} - e_i)$$

(2.50)
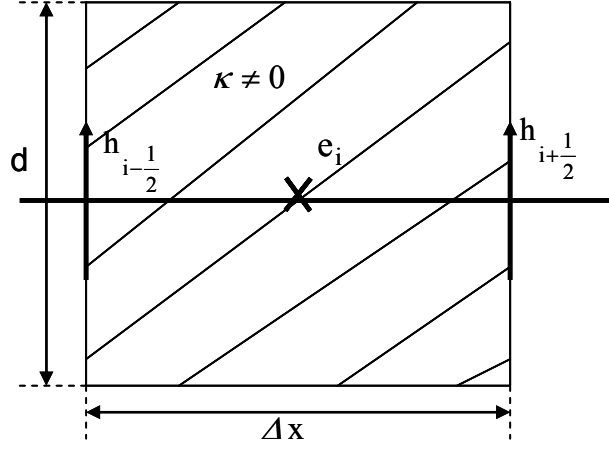
Figure 7. *The geometric view of the i th cell in conductor.*

According to figure 6, the space discretization of right and left sides of the first equation in formula (2.48) will read as

$$\oint \vec{H} \, d\vec{l} \approx (h_{i+\frac{1}{2}} - h_{i-\frac{1}{2}})d$$

$$\iint \left(\kappa \vec{E} + \frac{1}{Z_0} \frac{\partial}{\partial \tau} \vec{E} \right) d\vec{s} \approx \left(\kappa e_i + \frac{1}{Z_0} \frac{\partial}{\partial \tau} e_i \right) \Delta x \cdot d \qquad \text{with } 0 < i < N \qquad (2.51)$$

The space discretized first equation in (2.48) is then given by

$$\frac{1}{Z_0} \frac{\partial}{\partial \tau} \tau e_i + \kappa e_i = \frac{1}{\Delta x} \left(h_{i+\frac{1}{2}} - h_{i-\frac{1}{2}} \right) \qquad (2.52)$$

Finally the space discretized and time continuous 1D Maxwells equation for conductive media will reads as

$$Z_0 \frac{\partial}{\partial \tau} h_{i+\frac{1}{2}} \Delta x = (e_{i+1} - e_i)$$

$$\frac{1}{Z_0} \frac{\partial}{\partial \tau} e_i + \kappa e_i = \frac{1}{\Delta x} \left(h_{i+\frac{1}{2}} - h_{i-\frac{1}{2}} \right) \qquad (2.53)$$

with PEC boundary conditions $e_0 = e_N \equiv 0$ at any time value the problem is closed. Introducing the vectors of electric $\widehat{e}$ and magnetic $\widehat{h}$ fields in discrete space

$$\widehat{e} = \frac{1}{Z_0} \begin{pmatrix} e_0 \\ \vdots \\ e_N \end{pmatrix}, \quad \widehat{h} = \begin{pmatrix} h_{0.5} \\ \vdots \\ h_{N-0.5} \end{pmatrix} \qquad (2.54)$$

we may rewrite the update equations (2.53) in matrix form as

$$\frac{\partial}{\partial \tau} \widehat{h} = P \, \widehat{e}$$

$$\frac{\partial}{\partial \tau} \widehat{e} + \widetilde{\kappa} \, \widehat{e} = P^* \, \widehat{h} \qquad \text{with } \widetilde{\kappa} = \kappa Z_0 \qquad (2.55)$$

18

Here the discrete space derivative operators P, P^* have sizes $[(N-1)\times N]$ and $[N\times(N-1)]$ respectively and are given as

$$P = \frac{1}{\Delta x}\begin{pmatrix} -1 & 1 & 0 & \cdots & 0 \\ 0 & -1 & 1 & \cdots & 0 \\ \vdots & \vdots & \ddots & \ddots & \vdots \\ 0 & 0 & \cdots & -1 & 1 \end{pmatrix} \quad P^* = \frac{1}{\Delta x}\begin{pmatrix} -1 & 0 & 0 & \cdots & 0 \\ 1 & -1 & 0 & \cdots & 0 \\ 0 & 1 & -1 & \cdots & 0 \\ 0 & 0 & \ddots & \ddots & \vdots \\ \vdots & \vdots & \vdots & 1 & -1 \\ 0 & 0 & \cdots & 0 & 1 \end{pmatrix} \quad (2.56)$$

As for the vacuum case, here also the property of generalized symmetry for the discrete derivative operators P and P^* is preserved ($P^* = P^T$).

2.2.2 Time Discretization

In this section we will introduce the time discretization of the above numerical scheme given in matrix form (2.55). Similar to the vacuum scheme in conductor, we will use the upper index n for discrete time level description. Let us discretize the second equation of formula (2.55)

$$\frac{\partial}{\partial \tau}\widehat{e} + \widetilde{\kappa}\,\widehat{e} = P^* \widehat{h} \qquad (2.57)$$

Assuming that the difference of magnetic fields between two space closest points is constant ($P^* \widehat{h} = const$) the differential equation (2.57) over time variable can be solved analytically. The general solution is just the sum of homogeneous and partial solutions and reads as

$$\widehat{e}(\tau) = A\,e^{-\widetilde{\kappa}\tau} + B \qquad (2.58)$$

where A and B are unknown constants.
The first part of this equation is relevant to homogeneous solution and second – to partial solution. Substituting (2.58) into (2.57), the constant B is equal to

$$B = \frac{1}{\widetilde{\kappa}}\,P^* \widehat{h} \qquad (2.59)$$

The constant A can be found from the field initial value at time $\tau = 0$.

$$A = \widehat{e}(\tau = 0) - B \qquad (2.60)$$

Finally, the solution of differential equation (2.57) will read as

$$\widehat{e}(\tau) = \widehat{e}(\tau = 0)\,e^{-\widetilde{\kappa}\tau} + \frac{1}{\widetilde{\kappa}}\left(1 - e^{-\widetilde{\kappa}\tau}\right)P^* \widehat{h} \qquad (2.61)$$

Assuming that the electric field is known at time step n, the equation (2.61) gives the electric field at next time step $n+1$

$$\hat{e}^{n+1} = \hat{e}^n \, e^{-\tilde{\kappa}\Delta\tau} + \frac{1}{\tilde{\kappa}}\left(1 - e^{-\tilde{\kappa}\Delta\tau}\right) P^* \, \hat{h}^{n+\frac{1}{2}} \qquad (2.62)$$

We assume that the discrete derivative of magnetic field remains constant within the time $\Delta\tau$. Using central difference approximations for time derivative in the first equation of (2.55) we get

$$\frac{\hat{h}^{n+\frac{1}{2}} - \hat{h}^{n-\frac{1}{2}}}{\Delta\tau} = P\,\hat{e}^n \qquad (2.63)$$

Thus, the equations (2.62) and (2.63) describe the numerical scheme for EM fields time evolution in conductor

$$\hat{h}^{n+\frac{1}{2}} = \hat{h}^{n-\frac{1}{2}} + \Delta\tau\, P\,\hat{e}^n$$

$$\hat{e}^{n+1} = \hat{e}^n \, a + b\, P^* \, \hat{h}^{n+\frac{1}{2}} \qquad (2.64)$$

with constant coefficients

$$a = e^{-\tilde{\kappa}\Delta\tau}$$

$$b = \frac{1}{\tilde{\kappa}}\left(1 - a\right) \qquad (2.65)$$

It is seen that by defining the electric and magnetic fields on discrete time axis at time levels n and $n+0.5$ respectively the field update equations (2.64) are explicit. Thus, the relevant 1D numerical scheme (2.64) is termed explicit and in the original form reads as

$$h_{i+\frac{1}{2}}^{n+1} - h_{i+\frac{1}{2}}^{n} = \frac{\Delta\tau}{Z_0\,\Delta x}(e_{i+1}^{n+\frac{1}{2}} - e_i^{n+\frac{1}{2}})$$

$$e_i^{n+1} = e_i^n \, a + \frac{Z_0}{\Delta x}\, b \left(h_{i+\frac{1}{2}}^{n+\frac{1}{2}} - h_{i-\frac{1}{2}}^{n+\frac{1}{2}} \right) \qquad (2.66)$$

If the electric and magnetic fields are defined on discrete time axis at the same time level, the update equations (2.64) will read as

$$\hat{h}^{n+1} = \hat{h}^n + \Delta\tau\, P\,\frac{\hat{e}^{n+1} + \hat{e}^n}{2}$$

$$\hat{e}^{n+1} = \hat{e}^n \, a + b\, P^* \, \frac{\hat{h}^{n+1} + \hat{h}^n}{2} \qquad (2.67)$$

where the linear interpolation is used to define the fields at time level $n+0.5$. After some evaluations we may rewrite the equations (2.67) in the following matrix form:

$$\widehat{h}^{\#} = \widehat{h}^{n} + \frac{\Delta \tau}{2} P \widehat{e}^{n}$$

$$W_c (\widehat{e}^{n+1} - \widehat{e}^{n}) = \widehat{e}^{n} (a-1) + b P^{*} \widehat{h}^{\#} \qquad (2.68)$$

$$\widehat{h}^{n+1} = \widehat{h}^{\#} + \frac{\Delta \tau}{2} P \widehat{e}^{n+1}$$

with three diagonal matrix

$$W_c = I - \frac{\Delta \tau}{4} b P^{*} P \qquad (2.69)$$

where I is the unit diagonal matrix. As we see, the updates of EM fields are done implicitly and the relevant numerical scheme (2.69) is termed *implicit*. In the original form the implicit scheme will read as

$$h_{i+\frac{1}{2}}^{n+1} - h_{i+\frac{1}{2}}^{n} = \frac{\Delta \tau}{Z_0 \Delta x} \left(\frac{e_{i+1}^{n+1} + e_{i+1}^{n}}{2} - \frac{e_i^{n+\frac{1}{2}} + e_i^{n}}{2} \right)$$

$$e_i^{n+1} = e_i^{n} a + \frac{Z_0}{\Delta x} b \left(\frac{h_{i+\frac{1}{2}}^{n+1} + h_{i+\frac{1}{2}}^{n}}{2} - \frac{h_{i-\frac{1}{2}}^{n+1} + h_{i-\frac{1}{2}}^{n}}{2} \right) \qquad (2.70)$$

In the next section the stability of explicit (2.66) and implicit (2.70) 1D numerical schemes for conductive media is studied.

2.2.3 Stability Study

Similar to the numerical schemes in vacuum, we consider the stability of the numerical schemes in conductor by Fourier analyses. The relations (2.27) for the plane wave between two closest discrete points in space are valid for conductor but with the space step Δx

$$h_{i+\frac{1}{2}} = h_{i-\frac{1}{2}} e^{jk\Delta x}$$

$$e_{i+1} = e_i e^{jk\Delta x} \qquad (2.71)$$

Note that we have omitted the time level indexes, since the relations are not dependent on time.

We will perform the stability studies for the implicit and explicit numerical schemes using stability theory as described in section 2.1.3.

a. Stability of the Implicit Scheme

Using the relations (2.71), the implicit numerical scheme (2.70) in conductor will read as

$$e^{jk\Delta x}\left[h^{n+1}_{i-\frac{1}{2}}-h^{n}_{i-\frac{1}{2}}\right]=\frac{1}{Z_0}\alpha\left[e^{jk\Delta x}-1\right]\frac{e^{n+1}_i+e^n_i}{2}$$

$$e^{n+1}_i=e^n_i\,a+Z_0\,b'\left(e^{jk\Delta x}-1\right)\frac{h^{n+1}_{i-\frac{1}{2}}+h^{n}_{i-\frac{1}{2}}}{2} \tag{2.72}$$

where

$$\alpha=\frac{\Delta\tau}{\Delta x},\quad b'=\frac{b}{\Delta x} \tag{2.73}$$

Using the trigonometric relation (2.30), the update equations (2.72) will read as

$$e^{n+1}_i=\frac{a-\vartheta}{1+\vartheta}\,e^n_i+Z_0\,\frac{b'}{1+\vartheta}\left(e^{jk\Delta x}-1\right)h^n_i$$

$$h^{n+1}_i=\frac{1-\vartheta}{1+\vartheta}\,h^n_i+\frac{1}{Z_0}\frac{\alpha}{1+\vartheta}\left(1-e^{-jk\Delta x}\right)\frac{a+1}{2}\,e^n_i \qquad \text{with } \vartheta=\alpha\,b'\sin^2\left(k\frac{\Delta x}{2}\right) \tag{2.74}$$

According to equation (2.20) for vector $U^n=\begin{pmatrix}e^n_i\\ h^n_{i-0.5}\end{pmatrix}$, the amplification matrix G is then given by

$$G=\begin{pmatrix}\dfrac{a-\vartheta}{1+\vartheta} & Z_0\dfrac{b'}{1+\vartheta}\left(e^{jk\Delta x}-1\right)\\[4mm] \dfrac{1}{Z_0}\dfrac{\alpha}{1+\vartheta}\left(1-e^{-jk\Delta x}\right)\dfrac{a+1}{2} & \dfrac{1-\vartheta}{1+\vartheta}\end{pmatrix} \tag{2.75}$$

The eigenvalues $g_{1,2}$ of amplification matrix G can be determined by setting to zero the determinant of the matrix $(G-gI)$

$$\det(G-gI)=\begin{vmatrix}\dfrac{a-\vartheta}{1+\vartheta}-g & Z_0\dfrac{b'}{1+\vartheta}\left(e^{jk\Delta x}-1\right)\\[4mm] \dfrac{1}{Z_0}\dfrac{\alpha}{1+\vartheta}\left(1-e^{-jk\Delta x}\right)\dfrac{a+1}{2} & \dfrac{1-\vartheta}{1+\vartheta}-g\end{vmatrix}=0 \tag{2.76}$$

that will read as

$$\left(\frac{a-\vartheta}{1+\vartheta}-g\right)\left(\frac{1-\vartheta}{1+\vartheta}-g\right)+2(a+1)\frac{\vartheta}{(1+\vartheta)^2}=0 \tag{2.77}$$

Simplification gives

$$\left\{1-\vartheta-(1+\vartheta)\,g\right\}^2+(a-1)\left\{1-\vartheta-(1+\vartheta)\,g\right\}+2(a+1)\vartheta=0 \tag{2.78}$$

And for eigenvalues $g_{1,2}$ we get

$$g_{1,2} = \frac{2(1-\vartheta)+(a-1)\pm\sqrt{(a-1)^2-8(a+1)\vartheta}}{2(1+\vartheta)} \qquad (2.79)$$

For complex eigenvalues $\vartheta \ge \dfrac{(1-a)^2}{8(1+a)}$, and taking into account that $0 \le a \le 1$ and $\vartheta \ge 0$ the modules satisfy the relation

$$|g|^2 = |g_1 \cdot g_2| = \left|\frac{a+\vartheta}{1+\vartheta}\right| \le 1 \qquad (2.80)$$

and the stability condition is satisfied.

For real eigenvalues we have $\vartheta \le \dfrac{(1-a)^2}{8(1+a)}$. Taking into account that the max of squared root is achieved for $\vartheta = 0$ it is easy to show that the stability condition $|g_{1,2}| \le 1$ is satisfied. Thus we get that the implicit numerical scheme in conductor is unconditionally stable.

b. Stability of the Explicit Scheme

Further we shall analyze the stability of the explicit numerical scheme (2.66). Again using the property (2.71) for plane waves, the field updated equations will read as

$$h_{i+\frac{1}{2}}^{n+\frac{1}{2}} = h_{i+\frac{1}{2}}^{n-\frac{1}{2}} + \frac{1}{Z_0}\alpha\left[e^{jk\Delta x}-1\right]e_i^n$$

$$e_i^{n+1} = e_i^n\, a + Z_0\, b'\left(1-e^{-jk\Delta x}\right)h_{i+\frac{1}{2}}^{n+\frac{1}{2}} \qquad (2.81)$$

with $\alpha = \Delta\tau/\Delta x$.

Again using trigonometric relations (2.30), the equations (2.81) will be modified to

$$h_{i+\frac{1}{2}}^{n+\frac{1}{2}} = h_{i+\frac{1}{2}}^{n-\frac{1}{2}} + \frac{1}{Z_0}\alpha\left[e^{jk\Delta x}-1\right]e_i^n$$

$$e_i^{n+1} = \left[a-\vartheta\right]e_i^n + Z_0\, b'\left(1-e^{-jk\Delta x}\right)h_{i+\frac{1}{2}}^{n-\frac{1}{2}} \qquad \text{with } \vartheta = 4\,\alpha\, b'\sin^2\left(k\frac{\Delta x}{2}\right) \qquad (2.82)$$

According to (2.20) for vector $U^n = \begin{pmatrix} e_i^n \\ h_{i+\frac{1}{2}}^{n-\frac{1}{2}} \end{pmatrix}$, the amplification matrix G will be given as

$$G = \begin{pmatrix} a-\vartheta & Z_0\, b'\left(1-e^{-jk\Delta x}\right) \\ \dfrac{1}{Z_0}\alpha\left(e^{jk\Delta x}-1\right) & 1 \end{pmatrix} \qquad (2.83)$$

The eigenvalues $g_{1,2}$ of the amplification matrix G are given by

$$\det(G - gI) = \begin{vmatrix} a - \vartheta - g & Z_0\, b\left(1 - e^{-jk\Delta x}\right) \\ \dfrac{1}{Z_0}\alpha\left(e^{jk\Delta x} - 1\right) & 1 - g \end{vmatrix} = 0 \tag{2.84}$$

that reads as

$$g^2 - \left(1 + a - \vartheta\right)g + a = 0 \tag{2.85}$$

And the solution for eigenvalues $g_{1,2}$ is

$$g_{1,2} = \frac{\left(1 + a - \vartheta\right) \pm \sqrt{\left(1 + a - \vartheta\right)^2 - 4a}}{2} \tag{2.86}$$

For the complex eigenvalues we get

$$\left|g\right|^2 = \left|a\right| \le 1 \tag{2.87}$$

That is always fulfilled since $0 \le a \le 1$.

Denoting $x \equiv 1 + a - \vartheta$, for the real eigenvalues ($x^2 > 4a$) the stability conditions $\left|g_{1,2}\right| \le 1$ are converted to the following set of inequalities:

$$\left|g_{1,2}\right| \le 1 : \begin{array}{l} \sqrt{x^2 - 4a} \le 2 - x \\ \sqrt{x^2 - 4a} \ge -2 - x \\ \sqrt{x^2 - 4a} \ge -2 + x \\ \sqrt{x^2 - 4a} \le 2 + x \end{array} \tag{2.88}$$

The initial three inequalities are satisfied for any real eigenvalues ($x \ge 2\sqrt{a}$, $x \le -2\sqrt{a}$) as $\vartheta \ge 0$. The last inequality is satisfied for $x \ge 2\sqrt{a}$.

For $x \le -2\sqrt{a}$ the last inequality implies the condition $x \le -(1 + a)$. In terms of a, ϑ, for $\vartheta \ge \left(1 - \sqrt{a}\right)^2$ the stability condition is then read as

$$\frac{\vartheta}{1 + a} \le 2 \tag{2.89}$$

Substituting the variable ϑ from (2.82) into (2.89) we get

$$4\frac{\Delta\tau}{\tilde{\kappa}\,\Delta x^2}\frac{1 - a}{1 + a}\sin^2\left(k\frac{\Delta x}{2}\right) \le 2 \;\; \text{with} \;\; \begin{array}{l} \tilde{\kappa} \equiv \kappa\, Z_0 \\ a = e^{-\tilde{\kappa}\Delta\tau} \end{array} \tag{2.90}$$

Using the following trigonometric relation

$$\frac{1 - a}{1 + a} = \tanh\left(\frac{\tilde{\kappa}\,\Delta\tau}{2}\right) \tag{2.91}$$

we may rewrite (2.90) as follows:

24

$$2 \frac{\Delta\tau}{\widetilde{\kappa}\,\Delta x^2} \sin^2\!\left(k\,\frac{\Delta x}{2}\right) \tanh\!\left(\frac{\widetilde{\kappa}\,\Delta\tau}{2}\right) \le 1 \tag{2.92}$$

Since $\sin^2\!\left(k\,\dfrac{\Delta x}{2}\right) \le 1$, this inequality is modified to

$$\frac{2\,\Delta\tau}{\widetilde{\kappa}\,\Delta x^2} \tanh\!\left(\frac{\widetilde{\kappa}\,\Delta\tau}{2}\right) \le 1 \tag{2.94}$$

Finally the stability condition for the conductor region will read

$$\Delta x^2 \ge \frac{2\,\Delta\tau}{\widetilde{\kappa}} \tanh\!\left(\frac{\widetilde{\kappa}\,\Delta\tau}{2}\right) \tag{2.95}$$

Taking into account that the hyperbolic tangents for real and positive arguments are always smaller or equal to one, the stability condition (2.95) could be simplified to

$$\Delta x \ge \sqrt{\frac{2\,\Delta\tau}{\widetilde{\kappa}}} \tag{2.96}$$

The stability conditions (2.95) and (2.96) in the conductor region coincides with the conditions derived in Ref. [61].

2.3 Hybrid 1D Numerical Scheme for IBC Modeling in Time Domain

In this section we will introduce the hybrid scheme, which will model the impedance boundary condition in time domain. For that purpose we consider a 1D electromagnetic problem in vacuum, which is supplied with perfect conductor on one side $x = -L$ and metal with finite conductivity on the other side $x = 0$ (Fig.8).
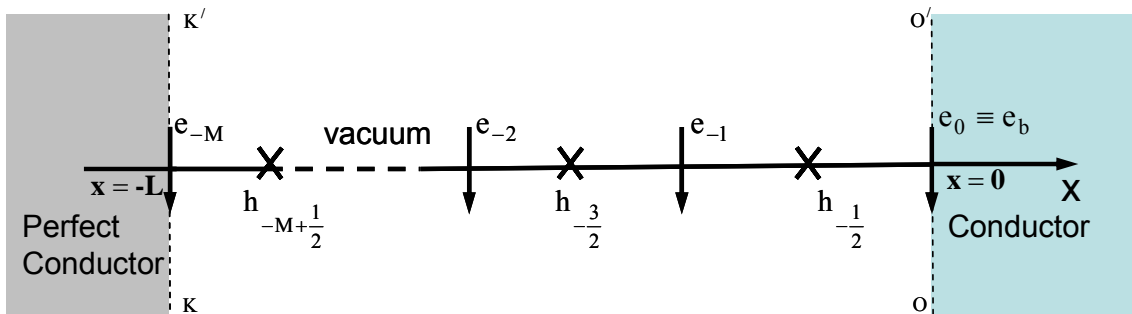
Figure 8. *Electromagnetic field schematic view in discrete space of vacuum region with metallic boundary on one side and PEC on the other side.*

The boundary electric field e_b in frequency domain can be found from the impedance boundary condition (IBC), which is equivalent to modeling the problem in time domain. To model the finite conductivity in time domain, first we will discuss a numerical scheme in conductor assuming that one of boundary is changed to vacuum and the magnetic field $h_{-0.5}$ in vacuum is given. Graphically the space discretization of such a problem is shown in Figure 9.
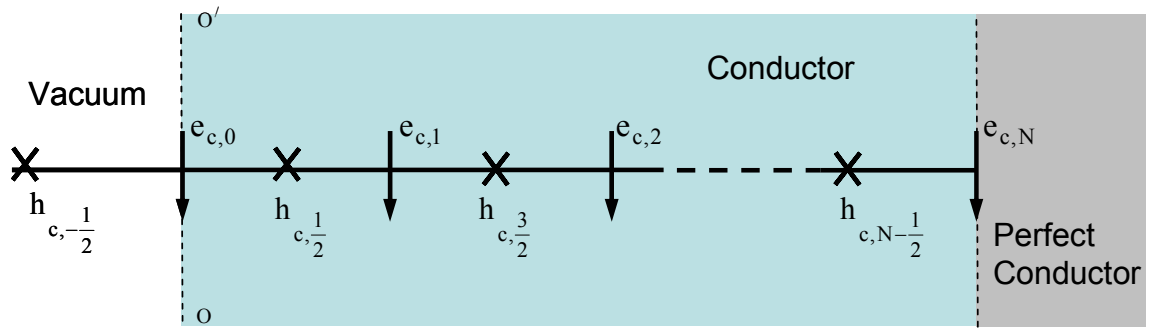
Figure 9. *Electromagnetic field schematic view in discrete space of conductor region with free space boundary.*

The electric field update on vacuum-conductor boundary cell $x = 0$ is schematically shown in Figure 10.
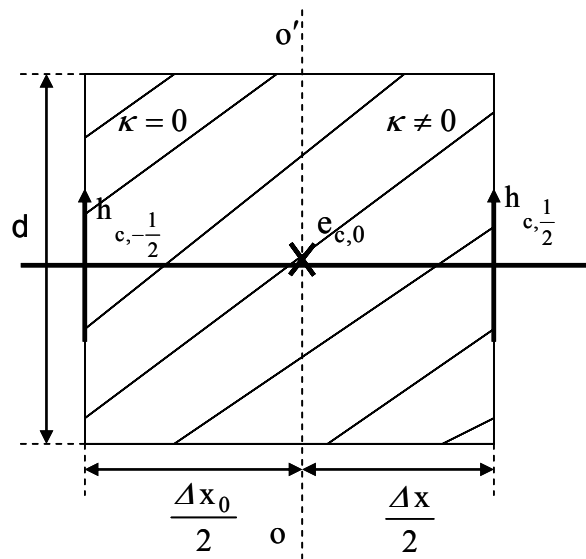
Figure 10. *Geometric view of the vacuum-conductor boundary cell.*

As we can see from Figures 9 and 10, the boundary cell needs special consideration, because one part of the region is filled with metal $\kappa \neq 0$ and the other part with vacuum $\kappa = 0$. In addition, in this case two different space steps appear in one cell that are chosen from algorithm stability considerations discussed in the previous two sections. For the boundary cell the surface integral of electric field in first equation of (2.1) will be modified to

$$\iint \left(\kappa \vec{E} + \frac{1}{Z_0} \frac{\partial}{\partial \tau} \vec{E} \right) d\vec{s} \approx \frac{1}{Z_0} \frac{\partial e_{c,0}}{\partial \tau} \frac{\Delta x_0}{2} d + \left(\kappa e_{c,0} + \frac{1}{Z_0} \frac{\partial e_{c,0}}{\partial \tau} \right) \frac{\Delta x}{2} \cdot d \qquad (2.97)$$

After some simplifications we get the following differential equation

$$\frac{\Delta x + \Delta x_0}{\Delta x} \frac{1}{Z_0} \frac{\partial e_{c,0}}{\partial \tau} + \kappa e_{c,0} = \frac{2}{\Delta x} \left(h_{c,\frac{1}{2}} - h_{c,-\frac{1}{2}} \right) \qquad (2.98)$$

Solving this differential equation in the same manner as in the previous case and assuming the right-hand side constant we get

26

$$e_{c,0}(\tau) = e_{c,0}(\tau=0)\, e^{-\kappa Z_0 \frac{\Delta x}{\Delta x+\Delta x_0}\Delta\tau} + \frac{2}{\kappa Z_0\,\Delta x}\left(1-e^{-\kappa Z_0 \frac{\Delta x}{\Delta x+\Delta x_0}\Delta\tau}\right)\left(h_{c,\frac{1}{2}} - h_{c,-\frac{1}{2}}\right) \quad (2.99)$$

And the electric field update in discrete form will read as

$$e_{c,0}^{n+1} = e_{c,0}^{n}\, a' + \frac{2}{\widetilde{\kappa}\,\Delta x}(1-a')\left(h_{c,\frac{1}{2}}^{n+\frac{1}{2}} - h_{c,-\frac{1}{2}}^{n+\frac{1}{2}}\right) \quad (2.100)$$

with

$$a' = e^{-\widetilde{\kappa}\frac{\Delta x}{\Delta x+\Delta x_0}\Delta\tau}$$
$$\widetilde{\kappa} = \kappa Z_0 \quad (2.101)$$

Note that the magnetic field is shifted by a half-time step in respect with electric field.

a. The Explicit Hybrid Numerical Scheme

Using the explicit numerical schemes for vacuum (2.19) and conductor (2.64) regions the hybrid scheme can be written in the following matrix form:

$$\begin{cases}
\widehat{e}^{\,n} = \widehat{e}^{\,n-1} + \Delta\tau\, P^{*}_{vacuum}\,\widehat{h}^{\,n-\frac{1}{2}} \\[2mm]
--- \text{field updates in conductive region with entry } h_{c,-\frac{1}{2}}^{n-\frac{1}{2}} \equiv h_{-\frac{1}{2}}^{n-\frac{1}{2}} --- \\[2mm]
\widehat{e}_{c}^{\,n} = \widehat{e}_{c}^{\,n-1}\,\widehat{a} + \widehat{b}\,P^{*}\,\widehat{h}_{c}^{\,n-\frac{1}{2}} \\[2mm]
\widehat{h}_{c}^{\,n+\frac{1}{2}} = \widehat{h}_{c}^{\,n-\frac{1}{2}} + \Delta\tau\,P\,\widehat{e}_{c}^{\,n} \\[1mm]
---------------------------------- \\[1mm]
e_{0}^{n} \equiv e_{c,0}^{n} \\[2mm]
\widehat{h}^{\,n+\frac{1}{2}} = \widehat{h}^{\,n-\frac{1}{2}} + \Delta\tau\,P_{vacuum}\,\widehat{e}^{\,n}
\end{cases} \quad (2.102)$$

Here $\widehat{a}$ and $\widehat{b}$ are the diagonal matrixes with entries

$$\widehat{a}_{0,0} = e^{-\widetilde{\kappa}\Delta\tau\frac{\Delta x}{\Delta x+\Delta x_0}} \quad \widehat{a}_{i,i} = e^{-\widetilde{\kappa}\Delta\tau}$$
$$\widehat{b}_{0,0} = \frac{2}{\widetilde{\kappa}}(1-\widehat{a}_{0,0}) \quad \widehat{b}_{i,i} = \frac{1}{\widetilde{\kappa}}(1-\widehat{a}_{i,i}) \quad \text{for } i\ge 1 \quad (2.103)$$

Note that we kept the main notations of the numerical schemes in vacuum and conductive regions for the discrete space and time descriptions. The update equation (2.102) also includes the boundary electric field update in the numerical scheme of conductive region that can be seen from matrix (2.103) elements. Assuming that discrete electric and magnetic field values are known at time levels $n-1$ and $n-0.5$ respectively, the update equations (2.102) give the field values at next time level, i.e. the values at time level n for electric and $n+0.5$ for magnetic fields.

First we update the electric field in vacuum region using the field values at the previous time level. Then using the boundary magnetic field value as an input for the numerical scheme in conductive region we get the tangential electric field on boundary surface in output, which is used to update the magnetic field in vacuum region. So the hybrid numerical scheme (2.102) models the IBC boundary condition in time domain explicitly. We should keep in mind also that the modeled length of the conductive region in time domain should be taken so that it remains much bigger than the skin-depth of the considered electromagnetic problem, i.e. the field value at the second boundary interface of the conductive region could be taken zero.

b. The Implicit Hybrid Numerical Scheme

When the discrete electric and magnetic fields are defined at the same time level, the hybrid numerical scheme reads as

$$
\begin{cases}
\widehat{h}^{\#} = \widehat{h}^{n} + \dfrac{\Delta\tau}{2} P_{vacuum}\,\widehat{e}^{n} \\[2mm]
W_{0}\left[\widehat{e}^{n+1} - \widehat{e}^{n}\right] = \Delta\tau\, P_{vacuum}^{*}\,\widehat{h}^{\#} \\[2mm]
---\text{field updates in conductive region with entry } h_{c,-\frac{1}{2}}^{n} = h_{-\frac{1}{2}}^{n} --- \\[2mm]
\widehat{h}_{c}^{\#} = \widehat{h}_{c}^{n} + \dfrac{\Delta\tau}{2} P\,\widehat{e}_{c}^{n} \\[2mm]
W_{c}(\widehat{e}_{c}^{n+1} - \widehat{e}_{c}^{n}) = (\widehat{a} - \widehat{I}_{c})\widehat{e}_{c}^{n} + \widehat{b}\,P^{*}\,\widehat{h}_{c}^{\#} \\[2mm]
\widehat{h}_{c}^{n+1} = \widehat{h}_{c}^{\#} + \dfrac{\Delta\tau}{2} P\,\widehat{e}_{c}^{n+1} \\[2mm]
------------------------------------ \\[2mm]
e_{0}^{n+1} = e_{c,0}^{n+1} \\[2mm]
\widehat{h}^{n+1} = \widehat{h}^{\#} + \dfrac{\Delta\tau}{2} P_{vacuum}\,\widehat{e}^{n+1}
\end{cases}
\tag{2.104}
$$

where the implicit numerical schemes for vacuum (2.16) and conductive (2.68) regions are used. The diagonal matrixes $\widehat{a}$ and $\widehat{b}$ are defined in (2.103) and three-diagonal matrixes W_{0}, W_{c} are determined as

$$
W_{0} = I - \frac{\Delta\tau^{2}}{4} P_{vacuum}^{*} P_{vacuum}
$$

$$
W_{c} = I_{c} - \frac{\Delta\tau}{4}\widehat{b}\,P^{*}P
\tag{2.105}
$$

with I and I_{c} unit diagonal matrixes for vacuum and conductive schemes respectively.

As we see, the hybrid numerical scheme (2.104) is fully implicit for both regions. Described implicit numerical scheme models the IBC boundary condition in time domain.

2.3.1 Stability of the Hybrid Numerical Scheme

A critical aspect of any numerical scheme is the stability of the scheme. Both explicit and implicit numerical schemes in vacuum and in conductor are stable as long as they fulfill their stability conditions. However, this does not guarantee stability for hybrid scheme since coupling of two stable schemes might result in an unstable scheme. For that reason in this section we will investigate the local stability of boundary field update using the general stability theory given in section 2.1.3. The study again will be performed for plane waves.

a. Stability of Explicit Hybrid Scheme

For the boundary field updates in original form we have to distinguish two pairs of equations, one with magnetic field update in conductive region

$$h_{c,\frac{1}{2}}^{n+\frac{1}{2}} = h_{c,\frac{1}{2}}^{n-\frac{1}{2}} + \frac{1}{Z_0}\frac{\Delta\tau}{\Delta x}\left(e_{c,1}^n - e_{c,0}^n\right)$$

$$e_{c,0}^{n+1} = e_{c,0}^n\, a' + Z_0\frac{2}{\widetilde{\kappa}\Delta x}\left(1-a'\right)\left(h_{c,\frac{1}{2}}^{n+\frac{1}{2}} - h_{c,-\frac{1}{2}}^{n+\frac{1}{2}}\right)$$

(2.106a)

and the other one in vacuum region

$$h_{c,-\frac{1}{2}}^{n+\frac{1}{2}} = h_{c,-\frac{1}{2}}^{n-\frac{1}{2}} + \frac{1}{Z_0}\frac{\Delta\tau}{\Delta x_0}\left(e_{c,0}^n - e_{-1}^n\right)$$

$$e_{c,0}^{n+1} = e_{c,0}^n\, a' + Z_0\frac{2}{\widetilde{\kappa}\Delta x}\left(1-a'\right)\left(h_{c,\frac{1}{2}}^{n+\frac{1}{2}} - h_{c,-\frac{1}{2}}^{n+\frac{1}{2}}\right)$$

(2.106b)

Each of the magnetic field updates in equations (2.106) are stable within the stability condition for vacuum and conductive regions respectively, but the boundary electric field update equation in the general hybrid scheme may become unstable through the boundary. Therefore, we should investigate the stability of field updates in boundary cells.
Using the following relations of space description for the plane wave

$$e_{-1} = e_{c,0}\, e^{-jk\Delta x_0} \qquad\qquad h_{c,\frac{1}{2}} = h_{c,-\frac{1}{2}}\, e^{jk\frac{\Delta x+\Delta x_0}{2}}$$
$$e_{c,1} = e_{c,0}\, e^{jk\Delta x}$$

(2.107)

and omitting the index c, the field update equations (2.106) will read as

$$h_{-\frac{1}{2}}^{n+\frac{1}{2}} = h_{-\frac{1}{2}}^{n-\frac{1}{2}} + \frac{1}{Z_0}\frac{\Delta\tau}{\Delta x}e^{-jk\frac{\Delta x_0}{2}}\left(e^{jk\frac{\Delta x}{2}} - e^{-jk\frac{\Delta x}{2}}\right)e_0^n$$

$$e_0^{n+1} = e_0^n\, a' + Z_0\frac{2}{\widetilde{\kappa}\Delta x}\left(1-a'\right)e^{jk\frac{\Delta x_0}{2}}\left(e^{jk\frac{\Delta x}{2}} - e^{-jk\frac{\Delta x_0}{2}}\right)h_{-\frac{1}{2}}^{n+\frac{1}{2}}$$

(2.108a)

$$h_{-\frac{1}{2}}^{n+\frac{1}{2}} = h_{-\frac{1}{2}}^{n-\frac{1}{2}} + \frac{1}{Z_0} \frac{\Delta \tau}{\Delta x_0} e^{-jk\frac{\Delta x_0}{2}} \left(e^{jk\frac{\Delta x_0}{2}} - e^{-jk\frac{\Delta x_0}{2}} \right) e_0^n$$

$$e_0^{n+1} = e_0^n \, a' + Z_0 \frac{2}{\tilde{\kappa} \Delta x} (1-a') e^{jk\frac{\Delta x_0}{2}} \left(e^{jk\frac{\Delta x}{2}} - e^{-jk\frac{\Delta x_0}{2}} \right) h_{-\frac{1}{2}}^{n+\frac{1}{2}} \qquad (2.108b)$$

Finally the updated equations read as

$$h_{-\frac{1}{2}}^{n+\frac{1}{2}} = h_{-\frac{1}{2}}^{n-\frac{1}{2}} + \frac{1}{Z_0} \frac{\Delta \tau}{\Delta x} e^{-jk\frac{\Delta x_0}{2}} \left(e^{jk\frac{\Delta x}{2}} - e^{-jk\frac{\Delta x}{2}} \right) e_0^n$$

$$e_0^{n+1} = e_0^n \left(a' - \vartheta_a \right) + Z_0 \frac{2}{\tilde{\kappa} \Delta x} (1-a') e^{jk\frac{\Delta x_0}{2}} \left(e^{jk\frac{\Delta x}{2}} - e^{-jk\frac{\Delta x_0}{2}} \right) h_{-\frac{1}{2}}^{n-\frac{1}{2}} \qquad (2.109a)$$

$$h_{-\frac{1}{2}}^{n+\frac{1}{2}} = h_{-\frac{1}{2}}^{n-\frac{1}{2}} + \frac{1}{Z_0} \frac{\Delta \tau}{\Delta x_0} e^{-jk\frac{\Delta x_0}{2}} \left(e^{jk\frac{\Delta x_0}{2}} - e^{-jk\frac{\Delta x_0}{2}} \right) e_0^n$$

$$e_0^{n+1} = e_0^n \left(a' - \vartheta_b \right) + Z_0 \frac{2}{\tilde{\kappa} \Delta x} (1-a') e^{jk\frac{\Delta x_0}{2}} \left(e^{jk\frac{\Delta x}{2}} - e^{-jk\frac{\Delta x_0}{2}} \right) h_{-\frac{1}{2}}^{n-\frac{1}{2}} \qquad (2.109b)$$

where

$$\vartheta_{a,b} = (1+a)\beta_{a,b} e^{jk\frac{\Delta x - \Delta x_0}{4}}$$

$$\beta_a \equiv \frac{8\Delta \tau}{\tilde{\kappa} \Delta x^2} \, \text{th}\left(\frac{\tilde{\kappa} \Delta \tau}{2} \frac{\Delta x}{\Delta x + \Delta x_0} \right) \sin\left(k \frac{\Delta x}{2} \right) \sin\left(k \frac{\Delta x + \Delta x_0}{4} \right) \qquad (2.110)$$

$$\beta_b \equiv \frac{8\Delta \tau}{\tilde{\kappa} \Delta x \Delta x_0} \, \text{th}\left(\frac{\tilde{\kappa} \Delta \tau}{2} \frac{\Delta x}{\Delta x + \Delta x_0} \right) \sin\left(k \frac{\Delta x_0}{2} \right) \sin\left(k \frac{\Delta x + \Delta x_0}{4} \right)$$

and the following trigonometric relation have been used

$$\frac{1-a'}{1+a'} = \tanh\left(\frac{\tilde{\kappa} \Delta \tau}{2} \frac{\Delta x}{\Delta x + \Delta x_0} \right) \qquad (2.111)$$

According to (2.20) for vector $U^n = \begin{pmatrix} e_0^n \\ h_{-0.5}^{n-0.5} \end{pmatrix}$, the amplification matrixes $G_{a,b}$ are given by

$$G_a = \begin{pmatrix} a' - \vartheta_a & Z_0 \frac{2}{\tilde{\kappa} \Delta x} (1-a') e^{jk\frac{\Delta x_0}{2}} \left(e^{jk\frac{\Delta x}{2}} - e^{-jk\frac{\Delta x_0}{2}} \right) \\ \frac{1}{Z_0} \frac{\Delta \tau}{\Delta x} e^{-jk\frac{\Delta x_0}{2}} \left(e^{jk\frac{\Delta x}{2}} - e^{-jk\frac{\Delta x}{2}} \right) & 1 \end{pmatrix} \qquad (2.112a)$$

$$G_b = \begin{vmatrix} a' - \vartheta_b & Z_0 \dfrac{2}{\tilde{\kappa}\,\Delta x}(1-a')e^{jk\frac{\Delta x_0}{2}}\left(e^{jk\frac{\Delta x}{2}} - e^{-jk\frac{\Delta x_0}{2}}\right) \\[4mm] \dfrac{1}{Z_0}\dfrac{\Delta \tau}{\Delta x_0}e^{-jk\frac{\Delta x_0}{2}}\left(e^{jk\frac{\Delta x_0}{2}} - e^{-jk\frac{\Delta x_0}{2}}\right) & 1 \end{vmatrix} \qquad (2.112b)$$

The eigenvalues $g_{a,b}$ of amplification matrixes $G_{a,b}$ can be obtained by setting to zero the determinant of the matrix $\left(G_{a,b} - g_{a,b}I\right)$

$$\det\!\left(G_{a,b} - g_{a,b}\right) = \left(a' - \vartheta_{a,b} - g_{a,b}\right)\!\left(1 - g_{a,b}\right) + \vartheta_{a,b} = 0 \qquad (2.113)$$

The solutions of this equation read as

$$g_{1,2} = \frac{\left(1 + a' - \vartheta\right) \pm \sqrt{\left(1 + a' - \vartheta\right)^2 - 4a'}}{2} \qquad (2.114)$$

As we see, the eigenvalues are complex since ϑ is complex (2.110). Denoting $z \equiv 1 + a' - \vartheta$ the equation (2.114) can be rewritten as

$$g_{1,2} = \frac{z \pm \sqrt{z^2 - 4a'}}{2} \qquad (2.115)$$

and the stability condition will read as

$$\left| z \pm \sqrt{z^2 - 4a'} \right| \leq 2 \qquad (2.116)$$

For $0 \leq a' < 1$ the inequality solution is given by

$$\frac{\mathrm{Re}(z)^2}{(1+a')^2} + \frac{\mathrm{Im}(z)^2}{(1-a')^2} \leq 1 \qquad (2.117)$$
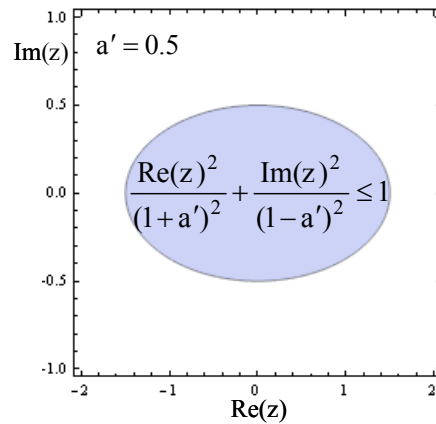
Figure 11. *The stability area for eigenvalues according to inequality (2.116).*

Figure 11 presents an exemplary solution (stable region) of the inequality (2.116) for a particular case of $a' = 0.5$.

31

Denoting $\mu = k\dfrac{\Delta x - \Delta x_0}{4}$ from (2.110) we get

$$\begin{aligned}
\mathrm{Re}\,\vartheta &= (1+a')\beta\cos\mu \\
\mathrm{Im}\,\vartheta &= (1+a')\beta\sin\mu
\end{aligned} \tag{2.118}$$

and the stability condition (2.117) reads as

$$(1-\beta\cos\mu)^2 + \coth^2\left(\frac{\widetilde{\kappa}\,\Delta\tau}{2}\frac{\Delta x}{\Delta x + \Delta x_0}\right)\beta^2\sin^2\mu \le 1 \tag{2.119}$$

Thus we get the following stability condition

$$0 \le \beta \le \tanh^2\left(\frac{\widetilde{\kappa}\,\Delta\tau}{2}\frac{\Delta x}{\Delta x + \Delta x_0}\right)\frac{2\cos\mu}{\sin^2\mu + \tanh^2\left(\dfrac{\widetilde{\kappa}\,\Delta\tau}{2}\dfrac{\Delta x}{\Delta x + \Delta x_0}\right)\cos^2\mu} \tag{2.120}$$

Taking into account

$$\tanh\left(\frac{\widetilde{\kappa}\,\Delta\tau}{2}\frac{\Delta x}{\Delta x + \Delta x_0}\right) \le 1$$

$$\sin^2\mu + \tanh^2\left(\frac{\widetilde{\kappa}\,\Delta\tau}{2}\frac{\Delta x}{\Delta x + \Delta x_0}\right)\cos^2\mu \le 1$$

the conditions (2.120) can be rewritten as

$$0 \le \beta \le 2\tanh^2\left(\frac{\widetilde{\kappa}\,\Delta\tau}{2}\frac{\Delta x}{\Delta x + \Delta x_0}\right)\cos\mu \tag{2.121}$$

Substituting β from equation (2.110) we get

$$\begin{aligned}
\frac{4\Delta\tau}{\widetilde{\kappa}\,\Delta x^2}\sin\left(k\frac{\Delta x}{2}\right)\sin\left(k\frac{\Delta x + \Delta x_0}{4}\right) &\le \cos\left(k\frac{\Delta x - \Delta x_0}{4}\right)\tanh\left(\frac{\widetilde{\kappa}\,\Delta\tau}{2}\frac{\Delta x}{\Delta x + \Delta x_0}\right) \\
\frac{4\Delta\tau}{\widetilde{\kappa}\,\Delta x\,\Delta x_0}\sin\left(k\frac{\Delta x_0}{2}\right)\sin\left(k\frac{\Delta x + \Delta x_0}{4}\right) &\le \cos\left(k\frac{\Delta x - \Delta x_0}{4}\right)\tanh\left(\frac{\widetilde{\kappa}\,\Delta\tau}{2}\frac{\Delta x}{\Delta x + \Delta x_0}\right)
\end{aligned} \tag{2.122}$$

These inequalities always fulfill when the following inequalities are satisfied

$$\frac{4\Delta\tau}{\widetilde{\kappa}\,\Delta x^2}\sin\left(k\frac{\Delta x}{2}\right)\sin\left(k\frac{\Delta x + \Delta x_0}{4}\right) \le \cos\left(k\frac{\Delta x - \Delta x_0}{4}\right)\tanh\left(\frac{\widetilde{\kappa}\,\Delta\tau}{2}\frac{\Delta x}{\Delta x + \Delta x_0}\right) \tag{2.123}$$

$$\Delta x \le \Delta x_0$$

For $k\,\Delta x$ and $k\,\Delta x_0$ smaller than unity the stability conditions (2.123) can be rewritten as

$$\Delta x^2 \geq \frac{\Delta \tau}{\widetilde{\kappa}} \coth\left(\frac{\widetilde{\kappa}\,\Delta \tau}{2}\,\frac{\Delta x}{\Delta x + \Delta x_0}\right) \tag{2.124}$$

$$\Delta x \leq \Delta x_0$$

Usually for high conductive materials ($\kappa > 10^4\,\text{S/m}$) the argument φ of hyperbolic cotangents function is bigger or equal to one, i.e. $\coth(\varphi) \leq 2$, and the condition (2.124) can be modified to

$$\Delta x^2 \geq \frac{2\Delta \tau}{\widetilde{\kappa}} \tag{2.125}$$

$$\Delta x \leq \Delta x_0$$

Finally, with stability conditions of explicit schemes (2.40) for vacuum region and (2.96) for conductive region, the stability conditions of the hybrid explicit numerical scheme will be given by

$$\begin{cases} \Delta \tau \leq \Delta x_0 \quad , \quad \text{for vacuum region} \\[3mm] \Delta x^2 \geq \dfrac{2\Delta \tau}{\widetilde{\kappa}} \quad , \quad \text{for conductive region} \\[3mm] \Delta x \leq \Delta x_0 \end{cases} \tag{2.126}$$

Note that the choice of a stable time step for the hybrid 1D explicit numerical scheme depends only on the discrete space step in the vacuum region and remains the same in the conductive region.

b. Stability of Implicit Hybrid Scheme

Consider the case when discrete electric and magnetic fields are defined at the same time level. According to (2.100) the update equation for boundary electric field contains the magnetic fields in conductor and vacuum regions. Thus, the stability analyses have to be conducted for two sets of update equations with magnetic field in conductor and in vacuum. In particular, in conductor region the update equations will read as

$$h_{c,\frac{1}{2}}^{n+1} = h_{c,\frac{1}{2}}^{n} + \frac{1}{Z_0}\frac{\Delta \tau}{\Delta x}\left(\frac{e_{c,1}^{n+1} + e_{c,1}^{n}}{2} - \frac{e_{c,0}^{n+1} + e_{c,0}^{n}}{2}\right)$$

$$e_{c,0}^{n+1} = e_{c,0}^{n}\,a' + Z_0\,\frac{2}{\widetilde{\kappa}\,\Delta x}\,(1-a')\left(\frac{h_{c,\frac{1}{2}}^{n+1} + h_{c,\frac{1}{2}}^{n}}{2} - \frac{h_{c,-\frac{1}{2}}^{n+1} + h_{c,-\frac{1}{2}}^{n}}{2}\right) \tag{2.127a}$$

In vacuum region:

$$h_{c,-\frac{1}{2}}^{n+1} = h_{c,-\frac{1}{2}}^{n} + \frac{1}{Z_0}\frac{\Delta \tau}{\Delta x_0}\left(\frac{e_{c,0}^{n+1} + e_{c,0}^{n}}{2} - \frac{e_{-1}^{n+1} + e_{-1}^{n}}{2}\right)$$

$$e_{c,0}^{n+1} = e_{c,0}^{n}\,a' + Z_0\,\frac{2}{\widetilde{\kappa}\,\Delta x}\,(1-a')\left(\frac{h_{c,\frac{1}{2}}^{n+1} + h_{c,\frac{1}{2}}^{n}}{2} - \frac{h_{c,-\frac{1}{2}}^{n+1} + h_{c,-\frac{1}{2}}^{n}}{2}\right) \tag{2.127b}$$

Each of the magnetic field updates in equations (2.127) are unconditionally stable, but with boundary electric field update equation in the general hybrid scheme instability may occur coming from the boundary. Thus we should investigate the stability of field updates in boundary cells. Following the procedure, same as for the explicit hybrid numerical scheme for field update equations, we get

$$
h^{n+1}_{-\frac{1}{2}} = h^{n}_{-\frac{1}{2}} + \frac{1}{Z_0}\frac{\Delta\tau}{\Delta x}e^{-jk\frac{\Delta x_0}{2}}\left(e^{jk\frac{\Delta x}{2}} - e^{-jk\frac{\Delta x}{2}}\right)\frac{e^{n+1}_0 + e^{n}_0}{2}
$$

$$
e^{n+1}_0 = e^{n}_0\,a' + Z_0\frac{2}{\tilde{\kappa}\Delta x}(1-a')e^{jk\frac{\Delta x_0}{2}}\left(e^{jk\frac{\Delta x}{2}} - e^{-jk\frac{\Delta x_0}{2}}\right)\frac{h^{n+1}_{-\frac{1}{2}} + h^{n}_{-\frac{1}{2}}}{2}
$$

(2.128a)

$$
h^{n+1}_{-\frac{1}{2}} = h^{n}_{-\frac{1}{2}} + \frac{1}{Z_0}\frac{\Delta\tau}{\Delta x_0}e^{-jk\frac{\Delta x_0}{2}}\left(e^{jk\frac{\Delta x_0}{2}} - e^{-jk\frac{\Delta x_0}{2}}\right)\frac{e^{n+1}_0 + e^{n}_0}{2}
$$

$$
e^{n+1}_0 = e^{n}_0\,a' + Z_0\frac{2}{\tilde{\kappa}\Delta x}(1-a')e^{jk\frac{\Delta x_0}{2}}\left(e^{jk\frac{\Delta x}{2}} - e^{-jk\frac{\Delta x_0}{2}}\right)\frac{h^{n+1}_{-\frac{1}{2}} + h^{n}_{-\frac{1}{2}}}{2}
$$

(2.128b)

where we have omitted the index c.
Finally the update equations will take the following view:

$$
h^{n+1}_{-\frac{1}{2}} = h^{n}_{-\frac{1}{2}}\frac{1-\vartheta_a}{1+\vartheta_a} + \frac{1}{Z_0}\frac{1}{1+\vartheta_a}\frac{\Delta\tau}{\Delta x}\frac{a'+1}{2}e^{-jk\frac{\Delta x_0}{2}}\left(e^{jk\frac{\Delta x}{2}} - e^{-jk\frac{\Delta x}{2}}\right)e^{n}_0
$$

$$
e^{n+1}_0 = e^{n}_0\frac{a'-\vartheta_a}{1+\vartheta_a} + Z_0\frac{1}{1+\vartheta_a}\frac{2}{\tilde{\kappa}\Delta x}(1-a')e^{jk\frac{\Delta x_0}{2}}\left(e^{jk\frac{\Delta x}{2}} - e^{-jk\frac{\Delta x_0}{2}}\right)h^{n}_{-\frac{1}{2}}
$$

(2.129a)

$$
h^{n+1}_{-\frac{1}{2}} = h^{n}_{-\frac{1}{2}}\frac{1-\vartheta_b}{1+\vartheta_b} + \frac{1}{Z_0}\frac{1}{1+\vartheta_b}\frac{\Delta\tau}{\Delta x_0}\frac{a'+1}{2}e^{-jk\frac{\Delta x_0}{2}}\left(e^{jk\frac{\Delta x_0}{2}} - e^{-jk\frac{\Delta x_0}{2}}\right)e^{n}_0
$$

$$
e^{n+1}_0 = e^{n}_0\frac{a'-\vartheta_b}{1+\vartheta_b} + Z_0\frac{1}{1+\vartheta_b}\frac{2}{\tilde{\kappa}\Delta x}(1-a')e^{jk\frac{\Delta x_0}{2}}\left(e^{jk\frac{\Delta x}{2}} - e^{-jk\frac{\Delta x_0}{2}}\right)h^{n}_{-\frac{1}{2}}
$$

(2.129b)

with

$$
\vartheta_{a,b} = (1+a')\beta_{a,b}e^{jk\frac{\Delta x - \Delta x_0}{4}}
$$

$$
\beta_a \equiv \frac{2\Delta\tau}{\tilde{\kappa}\Delta x^2}\tanh\left(\frac{\tilde{\kappa}\Delta\tau}{2}\frac{\Delta x}{\Delta x + \Delta x_0}\right)\sin\left(k\frac{\Delta x}{2}\right)\sin\left(k\frac{\Delta x + \Delta x_0}{4}\right)
$$

(2.130)

$$
\beta_b \equiv \frac{2\Delta\tau}{\tilde{\kappa}\Delta x\Delta x_0}\tanh\left(\frac{\tilde{\kappa}\Delta\tau}{2}\frac{\Delta x}{\Delta x + \Delta x_0}\right)\sin\left(k\frac{\Delta x_0}{2}\right)\sin\left(k\frac{\Delta x + \Delta x_0}{4}\right)
$$

where the trigonometric relations (2.111) have been used.

According to (2.20) for vector $U^n = \begin{pmatrix} e^{n}_0 \\ h^{n}_{-0.5} \end{pmatrix}$ the amplification matrixes $G_{a,b}$ will be

$$G_a = \begin{pmatrix} \dfrac{a' - \vartheta_a}{1 + \vartheta_a} & Z_0 \dfrac{1}{1 + \vartheta_a} \dfrac{2}{\tilde{\kappa}\,\Delta x}(1 - a')e^{jk\frac{\Delta x_0}{2}}\left(e^{jk\frac{\Delta x}{2}} - e^{-jk\frac{\Delta x_0}{2}}\right) \\ \dfrac{1}{Z_0} \dfrac{1}{1 + \vartheta_a} \dfrac{\Delta\tau}{\Delta x} \dfrac{a' + 1}{2} e^{-jk\frac{\Delta x_0}{2}}\left(e^{jk\frac{\Delta x}{2}} - e^{-jk\frac{\Delta x}{2}}\right) & \dfrac{1 - \vartheta_a}{1 + \vartheta_a} \end{pmatrix}$$

$$(2.131a)$$

$$G_b = \begin{pmatrix} \dfrac{a' - \vartheta_b}{1 + \vartheta_b} & Z_0 \dfrac{1}{1 + \vartheta_b} \dfrac{2}{\tilde{\kappa}\,\Delta x}(1 - a')e^{jk\frac{\Delta x_0}{2}}\left(e^{jk\frac{\Delta x}{2}} - e^{-jk\frac{\Delta x_0}{2}}\right) \\ \dfrac{1}{Z_0} \dfrac{1}{1 + \vartheta_b} \dfrac{a' + 1}{2} \dfrac{\Delta\tau}{\Delta x_0} e^{-jk\frac{\Delta x_0}{2}}\left(e^{jk\frac{\Delta x_0}{2}} - e^{-jk\frac{\Delta x_0}{2}}\right) & \dfrac{1 - \vartheta_b}{1 + \vartheta_b} \end{pmatrix}$$

$$(2.131b)$$

The eigenvalues $g_{a,b}$ of amplification matrixes $G_{a,b}$ can be determined by setting to zero the determinant of matrix $(G_{a,b} - g_{a,b}I)$

$$\det(G_{a,b} - g_{a,b}I) =$$
$$= \frac{\left\{1 - \vartheta_{a,b} - (1 + \vartheta_{a,b})g_{a,b}\right\}^2 + (a' - 1)\left\{1 - \vartheta_{a,b} - (1 + \vartheta_{a,b})g_{a,b}\right\} + 2(1 + a')\vartheta_{a,b}}{(1 + \vartheta_{a,b})^2} = 0 \quad (2.132)$$

The solution of this equation is

$$1 - \vartheta_{a,b} - (1 + \vartheta_{a,b})g_{a,b} = \frac{(1 - a') \pm \sqrt{(1 - a')^2 - 8(1 + a')\vartheta_{a,b}}}{2} \quad (2.133)$$

And for eigenvalues we get

$$g_{1,2} = \frac{(1 + a') - 2\vartheta \pm \sqrt{(1 - a')^2 - 8(1 + a')\vartheta}}{2(1 + \vartheta)} \quad (2.134)$$

where we again omit the indexes a and b.

It is easy to show that $|g_2| \leq 1$ ("-" in front of squared root). For the first eigenvalue g_1 we have

$$\left| \frac{(1 + a') - 2\vartheta + \sqrt{(1 - a')^2 - 8(1 + a')\vartheta}}{2(1 + \vartheta)} \right| \leq 1 \quad (2.135)$$

The solution is given by inequality

$$\text{Im}(\vartheta)^2 \leq \frac{(1 - a')^2}{2(1 + a')} \text{Re}(\vartheta) \quad (2.136)$$

Note, that for real value ϑ the scheme is stable.
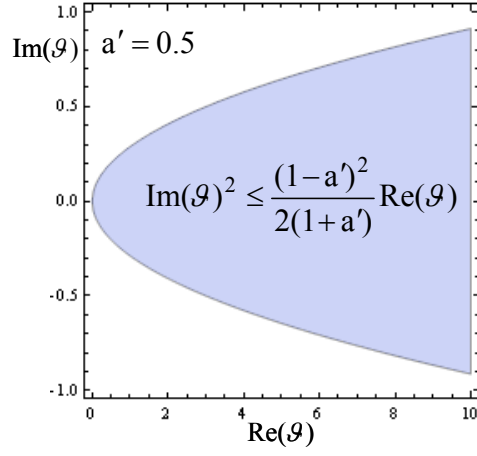
Figure 12. *The stability area for eigenvalues according to inequality (2.135).*

Figure 12 presents the solution of the inequality (2.135) (stable region) for a particular case of $a' = 0.5$.

Denoting $\mu = k \dfrac{\Delta x - \Delta x_0}{4}$ from (2.130) we get

$$
\begin{aligned}
\operatorname{Re}\vartheta &= (1+a')\beta \cos\mu \\
\operatorname{Im}\vartheta &= (1+a')\beta \sin\mu
\end{aligned}
\tag{2.137}
$$

and the stability condition (2.136) reads as

$$
\beta \sin^2\mu \leq \frac{1}{2}\tanh^2\left(\frac{\tilde\kappa\,\Delta\tau}{2}\frac{\Delta x}{\Delta x + \Delta x_0}\right)\cos\mu
\tag{2.138}
$$

Substituting the β from equation (2.130) and taking into account that $\sin^2\mu \leq 1$ we get

$$
\begin{aligned}
\frac{4\,\Delta\tau}{\tilde\kappa\,\Delta x^2}\sin\left(k\frac{\Delta x}{2}\right)\sin\left(k\frac{\Delta x + \Delta x_0}{4}\right) &\leq \cos\left(k\frac{\Delta x - \Delta x_0}{4}\right)\tanh\left(\frac{\tilde\kappa\,\Delta\tau}{2}\frac{\Delta x}{\Delta x + \Delta x_0}\right) \\
\frac{4\,\Delta\tau}{\tilde\kappa\,\Delta x\,\Delta x_0}\sin\left(k\frac{\Delta x_0}{2}\right)\sin\left(k\frac{\Delta x + \Delta x_0}{4}\right) &\leq \cos\left(k\frac{\Delta x - \Delta x_0}{4}\right)\tanh\left(\frac{\tilde\kappa\,\Delta\tau}{2}\frac{\Delta x}{\Delta x + \Delta x_0}\right)
\end{aligned}
\tag{2.139}
$$

These inequalities always fulfill when the following inequalities are satisfied

$$
\begin{aligned}
\frac{4\,\Delta\tau}{\tilde\kappa\,\Delta x^2}\sin\left(k\frac{\Delta x}{2}\right)\sin\left(k\frac{\Delta x + \Delta x_0}{4}\right) &\leq \cos\left(k\frac{\Delta x - \Delta x_0}{4}\right)\tanh\left(\frac{\tilde\kappa\,\Delta\tau}{2}\frac{\Delta x}{\Delta x + \Delta x_0}\right) \\
\Delta x &\leq \Delta x_0
\end{aligned}
\tag{2.140}
$$

When $k\,\Delta x$ and $k\,\Delta x_0$ are smaller than one, the stability conditions (2.140) can be rewritten as

$$
\begin{aligned}
\Delta x^2 &\geq \frac{\Delta\tau}{\tilde\kappa}\coth\left(\frac{\tilde\kappa\,\Delta\tau}{2}\frac{\Delta x}{\Delta x + \Delta x_0}\right) \\
\Delta x &\leq \Delta x_0
\end{aligned}
\tag{2.141}
$$

36

Usually for high conductive materials ($\kappa > 10^4 \, \text{S/m}$) the argument φ of hyperbolic cotangents function is bigger or equal to one, i.e. $\coth(\varphi) \leq 2$, and the condition (2.141) is modified to

$$
\begin{cases}
\Delta x^2 \geq \dfrac{2 \, \Delta \tau}{\widetilde{\kappa}} \\[2mm]
\Delta x \leq \Delta x_0
\end{cases}
\tag{2.142}
$$

Finally the stability condition of the hybrid implicit scheme is completely described by (2.142), since the implicit schemes in free space and conductor are unconditionally stable. Note that the time step and space step in vacuum are condition free for hybrid implicit scheme.

The stability conditions (2.126) and (2.142) for the hybrid explicit and implicit numerical schemes have been verified by numerical tests on the 1D electromagnetic problem for plane wave scattering on metallic surface. The analytical solution of this problem is well known and is given by the following expressions [60]

$$
\begin{aligned}
E_{vacuum}(x,t) &= \text{Re}\left[A\left(e^{jkx} + rs\, e^{-jkx}\right)e^{jk\tau} \right] \\
H_{vacuum}(x,t) &= \text{Re}\left[A\left(e^{jkx} - rs\, e^{-jkx}\right)e^{jk\tau} \right] \\
E_{conductor}(x,t) &= \text{Re}\left[A\left(1 + rs\right)e^{j\xi x}e^{jk\tau} \right] \\
H_{conductor}(x,t) &= \text{Re}\left[A\frac{\xi}{k}\left(1 + rs\right)e^{j\xi x}e^{jk\tau} \right]
\end{aligned}
\tag{2.143}
$$

where the boundary between vacuum and conductor is at $x = 0$ and the following notations have been used

$$
\tau \equiv c\, t
$$

$$
\xi^2 = k^2\left[1 - j\frac{\widetilde{\kappa}}{k}\right]
\tag{2.144}
$$

$$
rs = \frac{k - \xi}{k + \xi}
$$

Coefficient A is defined from the following initial condition

$$
E_{vacuum}(x = 1, t = 0) = 1 \quad \Rightarrow \quad A = \frac{1}{e^{jk} + rs\, e^{-jk}}
$$

One of the important issues in numerical modeling is the convergence property of the numerical schemes that is discussed in the next section.

2.3.2 Convergence Study of the Hybrid Scheme

The numerical schemes derived in previous sections for vacuum and conductive regions have at least second-order convergence [55-59, 62]. The hybrid scheme described in section 2.3 is designed to preserve this property. The hybrid scheme is applied for calculation of 1D electromagnetic problem (2.143) introduced in previous section for different time and space steps. The results are summarized in figure 10 presenting the convergence of the hybrid explicit

and implicit numerical schemes for conductivity $\kappa = 10^3$ S/m. For the calculations the discrete time step is taken to equal half of the space step in vacuum region.
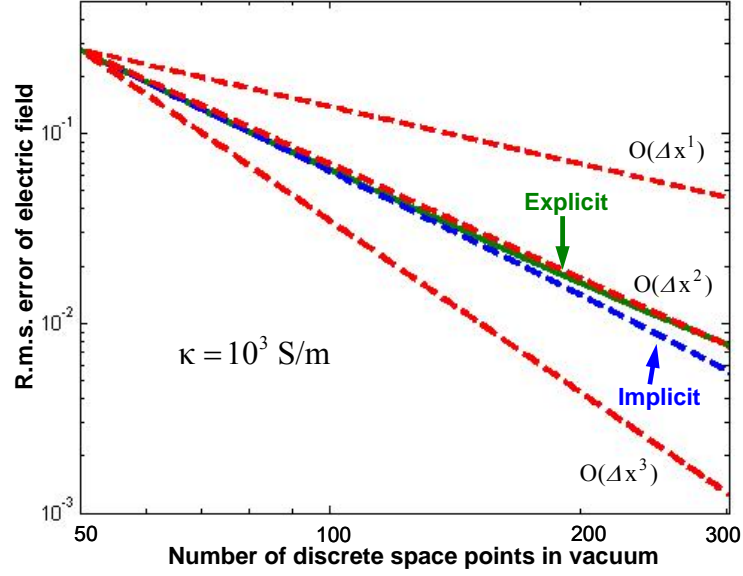
Figure 13*. Convergence of hybrid explicit (green) and implicit (blue dashed) numerical schemes for conductivity $\kappa = 10^3$ S/m. The convergence orders are given by red dashed.*

As the numerical experiments show, for materials with high conductivity $\kappa \geq 10^3$ S/m the convergence of explicit and implicit numerical schemes are preserved (fig.13) even for approximation of boundary cell update coefficient $\widetilde{a}$ by

$$\widetilde{a} = e^{-\frac{\Delta x}{\Delta x + \Delta x_0}\widetilde{\kappa}\Delta\tau} \approx e^{-\frac{1}{2}\widetilde{\kappa}\Delta\tau} \tag{2.145}$$

Figure 14 shows the convergence of the hybrid explicit scheme with and without approximation (2.145) for conductivity $\kappa = 0.1$ S/m.
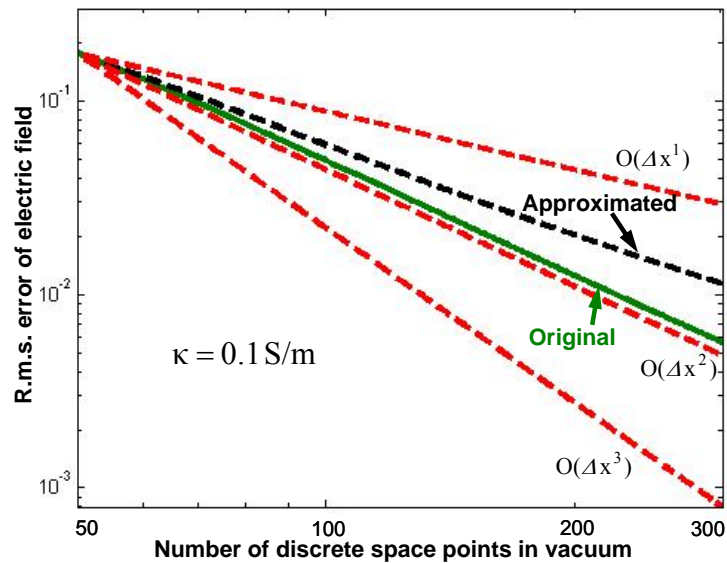
Figure 14*. Convergence of hybrid explicit numerical scheme with (black dashed) and without (green) approximation (2.145) for conductivity $\kappa = 0.1$ S/m. The convergence orders are given by red dashed.*

As we can see from figure 14 the convergence order of the hybrid explicit numerical scheme became worse in case of approximation (2.145). Same behavior on convergence of the scheme was observed for the cases when conductivity of the material is $\kappa < 10^3$ S/m. Thus, to preserve the second-order convergence the approximation (2.145) can be applied for materials with high conductivity $\kappa \geq 10^3$ S/m.

In accelerators usually high conductive materials are used. Therefore, in further 3D hybrid numerical scheme study (Chapter 4) the approximation (2.145) will be used.

2.4 Conclusion

In this chapter the 1D explicit and implicit numerical schemes are introduced for electromagnetic field calculations in metal and in vacuum medias. The stability analyses of these two schemes for both regions are performed. For IBC modeling in time domain the matching of the numerical schemes (explicit and implicit) in the vacuum and in the metal is achieved. The stability analyses of the so-called hybrid (matched) numerical schemes (explicit and implicit) are performed.

From stability study it follows that the implicit hybrid scheme is unconditionally stable on discrete time and space steps in the vacuum region. The stability of explicit hybrid scheme in vacuum region is conditioned by $\Delta\tau \leq \Delta x_0$. In conductor region the stability of both implicit and explicit hybrid schemes is strongly conditioned by space step dependence on time step and space step in vacuum.

The convergences of the hybrid explicit and implicit numerical schemes are studied. It is shown that both numerical schemes have second-order convergence. The numerical experiments on convergence of 1D implicit hybrid scheme show that for high conductive materials $\kappa \geq 10^3$ S/m the boundary electric field update equation can be approximated with usage of equation (2.145).

Chapter 3.

Dispersion-free Numerical Scheme for 3D Electromagnetic Problems with PEC Boundary Conditions

To calculate the wakefields of ultra short bunches in perfectly conducting structures and to prevent the numerical dispersion in longitudinal direction, a longitudinally dispersion-free 3D numerical scheme is proposed in reference [52] that is implemented in the program ECHO. The dispersion-free numerical scheme enables to use a concept of moving mesh frame without loosing the accuracy of calculation.

In this Chapter the overview of the TE/TM ("transverse electric - transverse magnetic") splitting implicit numerical scheme [33, 52, 67] is given. This time-domain numerical scheme is three-dimensional (3D), dispersion-free and valid for structures with perfect conducting walls. It is especially efficient for the wakefield calculations excited by ultra-short relativistic bunches and is more accurate in long-time simulations than the conventional FDTD approach [36,37].

3.1 The Maxwell Equations

The Maxwell equations are the set of four fundamental equations governing electromagnetism

$$\vec{\nabla} \times \vec{H} = \vec{J} + \frac{\partial \vec{D}}{\partial t} \tag{3.1a}$$

$$\vec{\nabla} \times \vec{E} = -\frac{\partial \vec{B}}{\partial t} \tag{3.1b}$$

$$\vec{\nabla} \cdot \vec{D} = \rho_f \tag{3.1c}$$

$$\vec{\nabla} \cdot \vec{B} = 0 \tag{3.1d}$$

where $\vec{E}$ is the electric field, $\vec{B}$ is the magnetic flux density, $\vec{D}$ is the electric flux density, $\vec{H}$ is the magnetic field, ρ_f is the free charge and $\vec{J}$ is the total current density including both free and bound current. For linear, isotropic and non-dispersive media the electric and magnetic flux densities and the total current density are given by

$$\vec{D} = \varepsilon \vec{E}, \ \vec{B} = \mu \vec{H}, \ \vec{J} = \vec{J}_c + \vec{J}_f \tag{3.2}$$

where ε is the dielectric permittivity, μ is the magnetic permeability, $\vec{J}_f$ is the free current of free moving charge and the bound current $\vec{J}_c$ is given by Ohm's law.

The Maxwell equations in terms of $\vec{E}$ and $\vec{H}$ are the system of eight scalar equations with six variables. Together with initial and boundary conditions the Maxwell equations constitute a well-posed system of hyperbolic partial differential equations.

In free space the Maxwell equations (3.1a) and (3.1b) simplify to

$$\vec{\nabla} \times \vec{H} = \vec{J}_f + \frac{1}{Z_0}\frac{\partial \vec{E}}{\partial \tau}$$

$$\vec{\nabla} \times \vec{E} = -Z_0 \frac{\partial \vec{H}}{\partial \tau}$$

$$(3.3)$$

where $Z_0 = c\mu_0 = (c\varepsilon_0)^{-1} = 376.73\ \Omega$ is impedance of free space, c=$2.9987 \cdot 10^8$m/s is the speed of light in vacuum and the normalized time variable $\tau \equiv c \cdot t$ have been used.

3.1.1 Boundary Conditions

At the interface between two lossless media 1 and 2 the boundary conditions for the electromagnetic fields read as [12, 60]

$$\vec{n} \cdot (\vec{D}_1 - \vec{D}_2) = 0$$

$$\vec{n} \times (\vec{E}_1 - \vec{E}_2) = 0$$

$$\vec{n} \cdot (\vec{B}_1 - \vec{B}_2) = 0$$

$$\vec{n} \times (\vec{H}_1 - \vec{H}_2) = 0$$

$$(3.4)$$

where the subscripts indicate the regions and $\vec{n}$ is the unit vector normal to interface. Using the equation (3.2) we get

$$\vec{n} \cdot (\varepsilon_1 \vec{E}_1 - \varepsilon_2 \vec{E}_2) = 0$$

$$\vec{n} \times (\vec{E}_1 - \vec{E}_2) = 0$$

$$\vec{n} \cdot (\mu_1 \vec{H}_1 - \mu_2 \vec{H}_2) = 0$$

$$\vec{n} \times (\vec{H}_1 - \vec{H}_2) = 0$$

$$(3.5)$$

For the border between the vacuum and Perfect Electric Conductor (PEC) we have [60]

$$\vec{n} \cdot \varepsilon \vec{E} = \rho_s \quad \vec{n} \cdot \mu \vec{H} = 0$$

$$\vec{n} \times \varepsilon \vec{E} = 0 \quad \vec{n} \times \mu \vec{H} = \vec{J}_s$$

$$(3.6)$$

where ρ_s and $\vec{J}_s$ are the surface charge and current densities respectively. The normal $\vec{n}$ is pointing out of the PEC region.

The tangential electric field is zero at the surface of PEC. A nonzero tangential electric field would drive an infinite surface current, which is clearly unphysical. However, this does not imply that the surface current must be zero. In fact, an external field always implies nonzero surface current since the magnetic field has only a tangential component at the PEC surface and the surface current is related to the tangential magnetic field through the fourth condition in (3.6).

3.1.2 The Maxwell Equations in Structures with Cylindrical Symmetry

In cylindrical coordinates $\{r, \varphi, z\}$ the Maxwell equations (3.1) in time domain are given by

$$\frac{1}{r}\frac{\partial H_z}{\partial \varphi} - \frac{\partial H_\varphi}{\partial z} = J_r + \varepsilon\frac{\partial E_r}{\partial t} \qquad \frac{1}{r}\frac{\partial E_z}{\partial \varphi} - \frac{\partial E_\varphi}{\partial z} = -\mu\frac{\partial H_r}{\partial t}$$

$$\frac{\partial H_r}{\partial z} - \frac{\partial H_z}{\partial r} = J_\varphi + \varepsilon\frac{\partial E_\varphi}{\partial t} \qquad \frac{\partial E_r}{\partial z} - \frac{\partial E_z}{\partial r} = -\mu\frac{\partial H_\varphi}{\partial t} \qquad (3.7)$$

$$\frac{1}{r}\frac{\partial (rH_\varphi)}{\partial r} - \frac{1}{r}\frac{\partial H_r}{\partial \varphi} = J_z + \varepsilon\frac{\partial E_z}{\partial t} \qquad \frac{1}{r}\frac{\partial (rE_\varphi)}{\partial r} - \frac{1}{r}\frac{\partial E_r}{\partial \varphi} = -\mu\frac{\partial H_z}{\partial t}$$

The cylindrical symmetry of the electromagnetic problem allows to distinguish the explicit dependence of the EM fields on the azimuthal coordinate φ that can be performed by multipole expansion of the fields [12]

$$\left\{E_r, E_z, H_\varphi\right\}_m (r, \varphi, z, t) = \left\{E_r, E_z, H_\varphi\right\}_m (r, z, t)\cos(m\varphi)$$
$$\left\{H_r, H_z, E_\varphi\right\}_m (r, \varphi, z, t) = \left\{H_r, H_z, E_\varphi\right\}_m (r, z, t)\sin(m\varphi) \qquad (3.8)$$

Where m is an integer and is called the azimuthal mode number.

In accelerators the principal source of external current is the charged particle beam. For a bunch moving at speed of light c with transverse offset a parallel to the axis of a rotationally symmetric structure, the source current $\vec{J}_s$ can be represented via multipole expansion as

$$\vec{J}_s = \frac{\vec{c}\,\rho(z/c - t)\,\delta(r - a)}{\pi a}\sum_{m=0}^{\infty}\frac{\cos(m\varphi)}{1 + \delta_{m,0}} \quad\text{with } \delta_{m,0} = \begin{cases} 1, m = 0 \\ 0, m \neq 0 \end{cases} \qquad (3.9)$$

Where $\rho(z/c - t)$ is the longitudinal charge distribution and $\delta(r - a)$ is the Dirac delta function. For the structures with PEC boundary conditions and external source given by (3.9), the Maxwell equations (3.7) for the m th multipole are read as

$$\frac{m}{r}H_z - \frac{\partial H_\varphi}{\partial z} = \varepsilon\frac{\partial E_r}{\partial t}$$

$$\frac{\partial H_r}{\partial z} - \frac{\partial H_z}{\partial r} = \varepsilon\frac{\partial E_\varphi}{\partial t}$$

$$\frac{1}{r}\frac{\partial (rH_\varphi)}{\partial r} - \frac{m}{r}H_r = J_{z,m} + \varepsilon\frac{\partial E_z}{\partial t}$$

$$-\frac{m}{r}E_z - \frac{\partial E_\varphi}{\partial z} = -\mu\frac{\partial H_r}{\partial t} \qquad (3.10)$$

$$\frac{\partial E_r}{\partial z} - \frac{\partial E_z}{\partial r} = -\mu\frac{\partial H_\varphi}{\partial t}$$

$$\frac{1}{r}\frac{\partial (rE_\varphi)}{\partial r} + \frac{m}{r}E_r = -\mu\frac{\partial H_z}{\partial t}$$

Where we have omitted the azimuthal dependents of the fields, which is given by equations (3.8).

In this chapter we consider the EM problems in structures with perfect electric conducting boundary materials.

3.2 Spatial Discretization and Maxwell Grid Equations

The Maxwell grid equation in finite integration technique (FIT) formalism are based on the integral form of Maxwell equations (3.1) that are given as

$$\oint_{\partial S} \vec{H} \cdot d\vec{l} = \iint_S \left[\vec{J} + \varepsilon \frac{\partial}{\partial t} \vec{E} \right] \cdot d\vec{A}$$

$$\oint_{\partial S} \vec{E} \cdot d\vec{l} = -\frac{\partial}{\partial t} \iint_S \mu \vec{H} \cdot d\vec{A} \qquad (3.11)$$

$$\iint_S \varepsilon \vec{E} \cdot d\vec{A} = \iiint_V \rho \, dV$$

$$\iint_S \mu \vec{H} \cdot d\vec{A} = 0$$

where S is an arbitrary area and ∂S is the path that encloses S.

Then the integral formulation (3.11) is discretized on a rectangular grid by introducing a dual grid $\tilde{G}$ to the primary one G. The EM field electric components are situated on the edges of the primary grid and the magnetic components on the edges of the dual grid. The dual grid is created at the preprocessing stage by defining the nodes of dual cells at the barycenters of primary cells as shown in (Fig. 15).
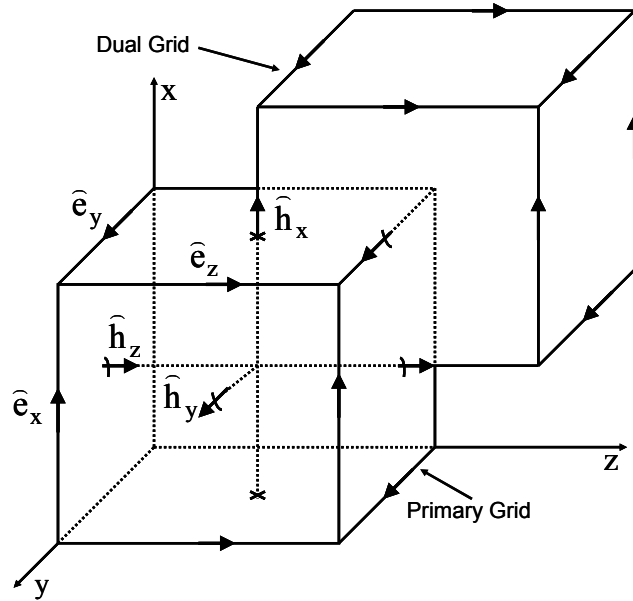
***Figure 15**. Graphical view of electromagnetic field spatial discretization.*

Following the FIT notation [63] for the discrete field components $\{\hat{e}_x, \hat{e}_y, \hat{e}_z\}$, the space steps $\{\Delta x, \Delta y, \Delta z\}$ and $\{i, j, k\}$ indexes for field description in the discrete 3D space, the Maxwell grid equations (MGE) will read as

$$\frac{\widehat{e}_{z,i,j+1,k+\frac{1}{2}} - \widehat{e}_{z,i,j,k+\frac{1}{2}}}{\Delta y} - \frac{\widehat{e}_{y,i,j+\frac{1}{2},k+1} - \widehat{e}_{y,i,j+\frac{1}{2},k}}{\Delta z} = -\mu_x \frac{\partial}{\partial t}\widehat{h}_{x,i,j+\frac{1}{2},k+\frac{1}{2}}$$

$$\frac{\widehat{e}_{x,i+\frac{1}{2},j,k+1} - \widehat{e}_{x,i+\frac{1}{2},j,k}}{\Delta z} - \frac{\widehat{e}_{z,i+1,j,k+\frac{1}{2}} - \widehat{e}_{z,i,j,k+\frac{1}{2}}}{\Delta x} = -\mu_y \frac{\partial}{\partial t}\widehat{h}_{y,i+\frac{1}{2},j,k+\frac{1}{2}}$$

$$\frac{\widehat{e}_{y,i+1,j+\frac{1}{2},k} - \widehat{e}_{y,i,j+\frac{1}{2},k}}{\Delta x} - \frac{\widehat{e}_{x,i+\frac{1}{2},j+1,k} - \widehat{e}_{x,i+\frac{1}{2},j,k}}{\Delta y} = -\mu_z \frac{\partial}{\partial t}\widehat{h}_{z,i+\frac{1}{2},j+\frac{1}{2},k}$$

$$(3.12)$$

$$\frac{\widehat{h}_{z,i+\frac{1}{2},j+\frac{1}{2},k} - \widehat{h}_{z,i+\frac{1}{2},j-\frac{1}{2},k}}{\Delta y} - \frac{\widehat{h}_{y,i+\frac{1}{2},j,k+\frac{1}{2}} - \widehat{h}_{y,i+\frac{1}{2},j,k-\frac{1}{2}}}{\Delta z} = J_{x,i+\frac{1}{2},j,k} + \varepsilon_x \frac{\partial}{\partial t}\widehat{e}_{x,i+\frac{1}{2},j,k}$$

$$\frac{\widehat{h}_{x,i,j+\frac{1}{2},k+\frac{1}{2}} - \widehat{h}_{x,i,j+\frac{1}{2},k-\frac{1}{2}}}{\Delta z} - \frac{\widehat{h}_{z,i+\frac{1}{2},j+\frac{1}{2},k} - \widehat{h}_{z,i-\frac{1}{2},j+\frac{1}{2},k}}{\Delta x} = J_{y,i,j+\frac{1}{2},k} + \varepsilon_y \frac{\partial}{\partial t}\widehat{e}_{y,i,j+\frac{1}{2},k}$$

$$\frac{\widehat{h}_{y,i+\frac{1}{2},j,k+\frac{1}{2}} - \widehat{h}_{y,i-\frac{1}{2},j,k+\frac{1}{2}}}{\Delta x} - \frac{\widehat{h}_{x,i,j+\frac{1}{2},k+\frac{1}{2}} - \widehat{h}_{x,i,j-\frac{1}{2},k+\frac{1}{2}}}{\Delta y} = J_{z,i,j,k+\frac{1}{2}} + \varepsilon_z \frac{\partial}{\partial t}\widehat{e}_{z,i,j,k+\frac{1}{2}}$$

As is seen from this MGE that has been derived by using FIT technique they are equivalent to the discretization of Maxwell equations in differential form using central difference approximation for derivatives.

Now by following matrix notation $\{P_x, P_y, P_z\}$ and $\{\widetilde{P}_x, \widetilde{P}_y, \widetilde{P}_z\}$ for the discrete space derivative operators on primary and dual grids respectively the discrete curl C and divergence S operators on the primary grid can be written as

$$C = \begin{pmatrix} 0 & -P_z & P_y \\ P_z & 0 & -P_x \\ -P_y & P_x & 0 \end{pmatrix} \quad S = \begin{pmatrix} P_x & P_y & P_z \end{pmatrix} \quad (3.13)$$

The dual grid discrete curl operator $\widetilde{C}$ has the same aspect as the primary grid, only the space derivatives for the primary grid P should be replaced by the dual grid operators $\widetilde{P} = P^T$. And the discrete divergence operator $\widetilde{S}$ on the dual grid has the following view

$$\widetilde{S} = \begin{pmatrix} -\widetilde{P}_x & -\widetilde{P}_y & -\widetilde{P}_z \end{pmatrix} \quad (3.14)$$

The vectors of discrete electric and magnetic fields in the space are defined as

$$\widehat{e} = \begin{pmatrix} \widehat{e}_x \\ \widehat{e}_y \\ \widehat{e}_z \end{pmatrix} \quad \widehat{h} = \begin{pmatrix} \widehat{h}_x \\ \widehat{h}_y \\ \widehat{h}_z \end{pmatrix} \quad (3.15)$$

where each element of the vectors is a vector containing component information of the given field in the 3D space. In these notations the Maxwell Grid Equations will read as

$$C\,\widehat{e} = -M_\mu \frac{d}{dt}\,\widehat{h} \qquad S\,\widehat{e} = M_\varepsilon\,\widehat{q}$$

$$\widetilde{C}\,\widehat{h} = M_\varepsilon \frac{d}{dt}\,\widehat{e} + \widehat{\widehat{j}} \qquad \widetilde{S}\,\widehat{h} = 0$$

(3.16)

where we introduced the material matrixes $M_\varepsilon = diag(\varepsilon_x, \varepsilon_y, \varepsilon_z)$ and $M_\mu = diag(\mu_x, \mu_y, \mu_z)$, which are diagonal and with positively defined elements. The material matrixes contain the electric and magnetic properties of the lossless media.

In the presence of a conducting media a conductivity matrix $M_\kappa = diag(\kappa, \kappa, \kappa)$ will appear in the Ohm's law which will contain the conductivity information. Thus the current density with external sources $\widehat{\widehat{j}}_f$ will read

$$\widehat{\widehat{j}} = M_\kappa \widehat{e} + \widehat{\widehat{j}}_f$$

(3.17)

Now via replacing in material matrixes the dielectric permittivity and magnetic permeability by their relative values $\mu \to \dfrac{\mu}{\mu_0}$, $\varepsilon \to \dfrac{\varepsilon}{\varepsilon_0}$ and introducing new variables

$$\tau = c\,t$$

$$e = \frac{1}{Z_0} M_\varepsilon^{1/2}\,\widehat{e} \qquad j = M_\varepsilon^{-1/2}\,\widehat{\widehat{j}}$$

$$h = M_\mu^{1/2}\,\widehat{h} \qquad q = c^{-1} M_\varepsilon^{-1/2}\,\widehat{q}$$

(3.18)

where Z_0 is free space impedance and c - speed of light, the equations system (3.16) will be reduced to the skew-symmetric one

$$\frac{d}{d\tau} e = \widetilde{C}_0\, h + j$$

$$\frac{d}{d\tau} h = -C_0\, e$$

(3.19)

with a new discrete curl operator

$$C_0 = M_\mu^{-1/2}\, C\, M_\varepsilon^{-1/2} = \begin{pmatrix} 0 & -M_{\mu_x}^{-1/2} P_z M_{\varepsilon_y}^{-1/2} & M_{\mu_x}^{-1/2} P_y M_{\varepsilon_z}^{-1/2} \\ M_{\mu_y}^{-1/2} P_z M_{\varepsilon_x}^{-1/2} & 0 & -M_{\mu_y}^{-1/2} P_x M_{\varepsilon_z}^{-1/2} \\ -M_{\mu_z}^{-1/2} P_y M_{\varepsilon_x}^{-1/2} & M_{\mu_z}^{-1/2} P_x M_{\varepsilon_y}^{-1/2} & 0 \end{pmatrix} \equiv$$

$$\equiv \begin{pmatrix} 0 & -P_z^0 & P_y^0 \\ P_z^1 & 0 & -P_x^0 \\ -P_y^1 & P_x^1 & 0 \end{pmatrix}$$

(3.20)

The equation system (3.19) is a time-continuous and space-discrete approximation of the Integral Maxwell equation (3.11).

45

3.2.1 Algebraic Properties of Maxwell Grid Equations

The outstanding feature of Maxwell grid equations when compared with other numerical methods for solving EM field problems is that this set of matrix equations is a consistent discrete representation of the original field equations, i.e. the basic properties of analytical fields are maintained during the transformation of continuous problem to the discrete space [63, 64]. One of the most important properties relating to the primary mesh curl operator C and the dual mesh curl operator $\widetilde{C}$, is the generalized symmetry

$$\widetilde{C} = C^T \tag{3.21}$$

It follows directly from the duality of the pair of staggered meshes and can be easily proven by simple topological considerations.

From the topology of each: the primary and the dual grids, from equations (3.16) the second set of properties is followed

$$S\,C = 0$$
$$\widetilde{S}\,\widetilde{C} = 0 \tag{3.22}$$

It can be interpreted as discrete analogues to the vector-identity $\mathrm{div}\,\mathrm{curl} = 0$ in a continuous case. Applying the equation (3.22) in MGE (3.16) the discrete analogy of charge conservation law is followed:

$$\frac{d}{dt}\widehat{q} + S\,\widehat{\widehat{j}} = 0 \quad\leftrightarrow\quad \frac{d}{dt}\rho + \mathrm{div}\,\vec{J} = 0 \tag{3.23}$$

Finally we define a discrete grad operator $\widehat{G}$ with the properties

$$\widehat{G} = -S^T \quad\text{and}\quad \widetilde{\widehat{G}} = -\widetilde{S}^T \tag{3.24}$$

From equations (3.21) and (3.22) follows $C\widehat{G} = 0$ and $\widetilde{C}\widetilde{\widehat{G}} = 0$ which are the discrete analogues to $\mathrm{curl}\,\mathrm{grad} = 0$ continuous operator property.

3.2.2 Space Stability of Time-Continuous MGE

The time-continuous and space-discrete version of the homogeneous Maxwell grid equation (3.16) for the lossless media case is given be

$$\begin{cases} C\widehat{e} = -M_\mu \dfrac{d}{dt}\widehat{h} \\[2mm] \widetilde{C}\widehat{h} = M_\varepsilon \dfrac{d}{dt}\widehat{e} \end{cases} \quad\Rightarrow\quad M_\varepsilon^{-1}\widetilde{C}M_\mu^{-1}C\widehat{e} = -\dfrac{d^2}{dt^2}\widehat{e} \tag{3.25}$$

Using the property of discrete curl operator (3.23), the square roots $M_\varepsilon^{-1} = M_\varepsilon^{-1/2}\,M_\varepsilon^{-1/2}$ and $M_\mu^{-1} = M_\mu^{-1/2}\,M_\mu^{-1/2}$ of the symmetric positive definite material matrixes, the system matrix of this eigenvalue equation can be transformed into

46

$$M_\varepsilon^{-1} \, C^T \, M_\mu^{-1} \, C = M_\varepsilon^{-1/2} \left(M_\mu^{-1/2} \, C \, M_\varepsilon^{-1/2} \right)^T \left(M_\mu^{-1/2} \, C \, M_\varepsilon^{-1/2} \right) M_\varepsilon^{1/2} \tag{3.26}$$

From this equation follows that this system matrix has only real and non-negative eigenvalues λ_i [55-58, 65]. That means that all eigensolutions of the spatial discretized scheme expressed by this system matrix are related to non-dissipative and non-growing oscillations with a real valued circular frequency $\omega_i = \sqrt{\lambda_i}$ and the time dependency $\hat{e}(t) \sim Re\left(e^{j\omega_i t} \right)$.

3.3 Time Discretization

In this section the explicit and implicit numerical schemes on the Cartesian and cylindrical grids for solving numerically 3D electromagnetic problems in the free space with PEC boundary conditions are described. In time discretization in both (explicit, implicit) cases the central difference method for derivatives is used which is a second-order accurate approximation. For the time a normalized time variable $\tau = ct$ is used. The discrete time step is notated by $\Delta\tau = c\Delta t$.

We consider a problem which reads as follows: in the region Ω which is bounded by a perfect conductor $\partial\Omega$, to find the electromagnetic fields excited by a bunch which is moving with the speed of light c and is characterized by a charge distribution ρ (fig. 16).
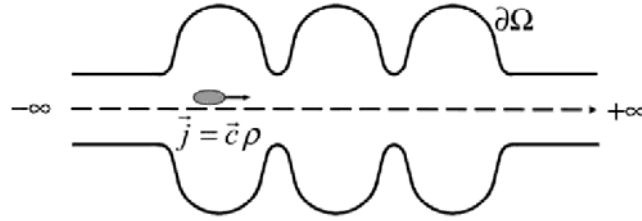
Figure 16*. Charged particle bunch moving through an accelerating structure supplied with infinite pipes.*

The bunch introduces an electric current density $\vec{J} = \vec{e}_z c\rho$ and thus the following system of differential equations is to be solved

$$\begin{cases} \vec{\nabla} \times \vec{H} = \vec{J} + \dfrac{1}{Z_0} \dfrac{\partial \vec{E}}{\partial \tau} \\[2mm] \vec{\nabla} \times \vec{E} = -Z_0 \dfrac{\partial \vec{H}}{\partial \tau} \\[2mm] \vec{\nabla} \cdot \vec{E} = \dfrac{\rho}{\varepsilon_0} \\[2mm] \vec{\nabla} \cdot \vec{H} = 0 \end{cases} \quad , \quad x \in \Omega \tag{3.27}$$

with PEC boundary conditions $\vec{n} \times \vec{E} = 0$, $x \in \partial\Omega$ and given initial conditions

$$\begin{cases} \vec{E}(\tau = 0) = \vec{E}_0 \\[2mm] \vec{H}(\tau = 0) = \vec{H}_0 \end{cases} \quad , \quad x \in \Omega \cup \partial\Omega \tag{3.28}$$

In accelerator applications, the structure is usually supplied by the ingoing and outgoing beam pipe and the analytical solution in a perfectly conducting cylindrical pipe [11] can be used as initial condition.

3.3.1 E/M Splitting Explicit Numerical Scheme

For time discretization an explicit scheme has been suggested by Yee [38] where splitting of electric and magnetic field components have been used (E/M splitting), i.e. on discrete time axis the electric field components are defined at the same time while the magnetic components are shifted by a half-time step relative to the electric one. This numerical scheme yields to the explicit finite difference time domain scheme and in matrix form reads as

$$
\begin{aligned}
e^{n+\frac{1}{2}} &= e^{n-\frac{1}{2}} + \Delta\tau\, M_\varepsilon \left[C_0^T\, h - \Delta\tau\, j \right] \\
h^{n+1} &= h^n - \Delta\tau\, M_\mu\, C_0\, e^{n+\frac{1}{2}}
\end{aligned}
\tag{3.29}
$$

with electric and magnetic field vectors

$$
e = \begin{pmatrix} e_x \\ e_y \\ e_z \end{pmatrix} \qquad h = \begin{pmatrix} h_x \\ h_y \\ h_z \end{pmatrix}
\tag{3.30}
$$

and material matrixes

$$
M_{\varepsilon,\mu} = \begin{pmatrix} M_{\varepsilon_x,\mu_x} & 0 & 0 \\ 0 & M_{\varepsilon_y,\mu_y} & 0 \\ 0 & 0 & M_{\varepsilon_z,\mu_z} \end{pmatrix}
\tag{3.31}
$$

On an equidistant mesh the explicit numerical scheme (3.29) has a second-order local approximation error in the homogeneous region $O\left(\|\Delta\vec{r}\|^2 + \Delta\tau^2 \right)$, $\Delta\vec{r} = (\Delta x, \Delta y, \Delta z)^T$ [38, 54, 55]. Applying Fourier analyses it is easy to get the following stability condition [58, 59] for this numerical scheme that reads as

$$
\Delta\tau \leq \left(\frac{1}{\Delta x^2} + \frac{1}{\Delta y^2} + \frac{1}{\Delta z^2} \right)^{-\frac{1}{2}}
\tag{3.32}
$$

This condition is known in literature as Courant stability condition.

From Fourier analyses follows also the dispersion relation of this explicit numerical scheme in free space [54, 59, 66] that reads as

$$
\frac{\sin^2\left(\frac{\omega}{c} \frac{\Delta\tau}{2} \right)}{\Delta\tau^2} = \frac{\sin^2\left(k_x \frac{\Delta x}{2} \right)}{\Delta x^2} + \frac{\sin^2\left(k_y \frac{\Delta y}{2} \right)}{\Delta y^2} + \frac{\sin^2\left(k_z \frac{\Delta z}{2} \right)}{\Delta z^2}
\tag{3.33}
$$

As can be seen from this relation for an equidistant mesh $\Delta x = \Delta y = \Delta z$, a homogeneous material and the time step $\Delta\tau = \Delta x/\sqrt{3}$, the scheme has no dispersion error along the grid diagonals. This property of the above-described scheme enables us to achieve zero dispersion in a desired direction by the rotation of the mesh. However, this approach has limitations on

discretization, which requires an equidistant mesh to have a non-dispersive numerical scheme in a desired direction.

Consider a problem of electromagnetic field calculation that is excited by a Gaussian charged bunch of rms length σ that moves with the speed of light c in z-direction through a structure of length L. The self-field of the ultra-relativistic bunch has only transverse non-zero field components [11-13] and it is like a plane wave. For the equidistant mesh the dispersion relation (3.33) simplifies to

$$\frac{\sin\left(\dfrac{\omega}{c}\dfrac{\Delta\tau}{2}\right)}{\Delta\tau/2} = \frac{\sin\left(k\dfrac{\Delta z}{2}\right)}{\Delta z/2} \tag{3.34}$$

Assuming that the numerical wave number k differs from the analytical one by some value δk, the Taylor expansion to the lowest order of δk will read as [38, 67]

$$\delta k \approx \frac{1}{24}\left(\frac{\omega}{c}\right)^3 \left[\Delta z^2 - \Delta\tau^2\right] \tag{3.35}$$

The dispersion error could disappear only when the time step is equal to the mesh step $\Delta\tau = \Delta z$. However it contradicts stability condition (3.32). Which means that for any stable time step the Yee's numerical scheme has a dispersion error in the z-direction of the order of

$$\delta k \approx O\left(\left(\frac{\omega}{c}\right)^3 \Delta z^2\right) \tag{3.36}$$

The Gaussian charged bunch excites high frequency fields up to the frequency $\omega \sim c/\sigma$, which means that for the structure of length L the phase error will be of the order of

$$L \cdot \delta k \approx O\left(L \sigma^{-3}\Delta z^2\right) \tag{3.37}$$

This equation means that the Yee's scheme requires very fine mesh for short bunches and long structures. For accurate calculation the mesh step should be chosen in a way that the following relation satisfies

$$\Delta z \ll \sqrt{\frac{\sigma^3}{L}} \tag{3.38}$$

In the next section an implicit scheme will be described that is dispersion free in z-direction for equal time and longitudinal space steps and is in good agreement with the stability condition.

3.3.2 TE/TM splitting implicit numerical scheme

In this section an implicit TE/TM numerical scheme is discussed [33, 49, 50]. The main property of this scheme is the fact that it allows to take a time step $\Delta\tau$ equal to the longitudinal mesh step Δz in which direction the ultra-relativistic charged bunch is propagating. The time discretization of this scheme is as follows: on the discrete time axis the "TE" components of electromagnetic field e_x, e_y, h_z are defined at time level n that corresponds to $\tau = n\Delta\tau$ and the

"TM" components of the field h_x, h_y, e_z at time $\tau = (n + 0.5)\Delta\tau$. Following this consideration and using new vector notations for the EM field and current density components

$$
u = \begin{pmatrix} h_x \\ h_y \\ e_z \end{pmatrix} \quad v = \begin{pmatrix} e_x \\ e_y \\ h_z \end{pmatrix} \quad j_u = \begin{pmatrix} 0 \\ 0 \\ j_z \end{pmatrix} \quad j_v = \begin{pmatrix} j_x \\ j_y \\ 0 \end{pmatrix} \tag{3.39}
$$

the time-continuous scheme (3.19) in equivalent form is read as

$$
\frac{d}{d\tau} u = T_0\, u + L\, v + j_u
$$
$$
\frac{d}{d\tau} v = T_1\, v + L^T\, u + j_v \tag{3.40}
$$

where

$$
T_0 = \begin{pmatrix} 0 & 0 & -P_y^0 \\ 0 & 0 & P_x^0 \\ \widetilde{P}_y^0 & -\widetilde{P}_x^0 & 0 \end{pmatrix}, \quad T_1 = \begin{pmatrix} 0 & 0 & -\widetilde{P}_y^1 \\ 0 & 0 & \widetilde{P}_x^1 \\ P_y^1 & -P_x^1 & 0 \end{pmatrix}, \quad L = \begin{pmatrix} 0 & P_z^0 & 0 \\ -P_z^1 & 0 & 0 \\ 0 & 0 & 0 \end{pmatrix} \tag{3.41}
$$

Applying the suggested time discretization the TE/TM field components are split in time as

$$
\frac{u^{n+\frac{1}{2}} - u^{n-\frac{1}{2}}}{\Delta\tau} = T_0 \frac{u^{n+\frac{1}{2}} + u^{n-\frac{1}{2}}}{2} + L\, v^n + j_u^n
$$
$$
\frac{v^{n+1} - v^n}{\Delta\tau} = T_1 \frac{v^{n+1} + v^n}{2} + L^T u^{n+\frac{1}{2}} + j_v^{n+\frac{1}{2}} \tag{3.42}
$$

where central difference approximation of derivative on time have been used and linear interpolation has been applied.

Similar to Yee's scheme this numerical scheme is also two layer one and can be written in the following form

$$
B\frac{y^{n+1} - y^n}{\Delta\tau} + A\, y^n = f^n \tag{3.43}
$$

where

$$
B = \begin{pmatrix} I - \frac{1}{2}\Delta\tau\, T_0 & 0 \\ \Delta\tau\, L^T & I - \frac{1}{2}\Delta\tau\, T_1 \end{pmatrix}, \quad A = \begin{pmatrix} -T_0 & -L \\ L^T & -T_1 \end{pmatrix}, \quad y^n = \begin{pmatrix} u^{n-\frac{1}{2}} \\ v^n \end{pmatrix}, \quad f^n = \begin{pmatrix} j_u^n \\ j_v^{n-\frac{1}{2}} \end{pmatrix} \tag{3.44}
$$

As is seen, the matrixes in equation (3.43) have the following properties:

$$
A = -A^* \quad \text{with} \quad Q = B - \frac{1}{2}\Delta\tau\, A
$$
$$
Q = Q^* \tag{3.45}
$$

50

In the original variables and in detailed notation the TE/TM scheme for no transverse current density case ($j_v \equiv 0$) read as

TE components

$$\widehat{e}_x^{\#} \equiv \widehat{e}_x^{n-\frac{1}{2}} + \frac{\Delta\tau}{2} M_{\varepsilon_x^{-1}}\left[\widetilde{P}_z \widehat{h}_y^n - \widetilde{P}_y \widehat{h}_z^{n-\frac{1}{2}} \right]$$

$$\widehat{e}_y^{\#} \equiv \widehat{e}_y^{n-\frac{1}{2}} + \frac{\Delta\tau}{2} M_{\varepsilon_y^{-1}}\left[\widetilde{P}_x \widehat{h}_z^{n-\frac{1}{2}} - \widetilde{P}_z \widehat{h}_x^n \right]$$

$$\widehat{h}_z^{n+\frac{1}{2}} = \widehat{h}_z^{n-\frac{1}{2}} + \Delta\tau\left(I + \frac{\Delta\tau^2}{4} M_{\mu_z^{-1}} P_x M_{\varepsilon_y^{-1}} \widetilde{P}_x + \frac{\Delta\tau^2}{4} M_{\mu_z^{-1}} P_y M_{\varepsilon_x^{-1}} \widetilde{P}_y\right)^{-1} M_{\mu_z^{-1}}\left[P_x \widehat{e}_y^{\#} - P_y \widehat{e}_x^{\#} \right]$$

$$\widehat{e}_x^{n+\frac{1}{2}} = \widehat{e}_x^{\#} + \frac{\Delta\tau}{2} M_{\varepsilon_x^{-1}}\left[\widetilde{P}_z \widehat{h}_y^n - \widetilde{P}_y \widehat{h}_z^{n+\frac{1}{2}} \right]$$

$$\widehat{e}_y^{n+\frac{1}{2}} = \widehat{e}_y^{\#} + \frac{\Delta\tau}{2} M_{\varepsilon_y^{-1}}\left[\widetilde{P}_x \widehat{h}_z^{n+\frac{1}{2}} - \widetilde{P}_z \widehat{h}_x^n \right]$$

(3.46)

TM components

$$\widehat{h}_x^{\#} \equiv \widehat{h}_x^n + \frac{\Delta\tau}{2} M_{\mu_x^{-1}}\left[P_z \widehat{e}_y^{n+\frac{1}{2}} - P_y \widehat{e}_z^n \right]$$

$$\widehat{h}_y^{\#} \equiv \widehat{h}_y^n + \frac{\Delta\tau}{2} M_{\mu_y^{-1}}\left[P_x \widehat{e}_z^n - P_z \widehat{e}_x^{n+\frac{1}{2}} \right]$$

$$\widehat{e}_z^{n+1} = \widehat{e}_z^n + \Delta\tau\left(I + \frac{\Delta\tau^2}{4} M_{\varepsilon_z^{-1}} \widetilde{P}_x M_{\mu_y^{-1}} P_x + \frac{\Delta\tau^2}{4} M_{\varepsilon_z^{-1}} \widetilde{P}_y M_{\mu_x^{-1}} P_y\right)^{-1} M_{\varepsilon_z^{-1}}\left[\widetilde{P}_x \widehat{h}_y^{\#} - \widetilde{P}_y \widehat{h}_x^{\#} - \widehat{j}_z^n \right]$$

$$\widehat{h}_x^{n+1} = \widehat{h}_x^{\#} + \frac{\Delta\tau}{2} M_{\mu_x^{-1}}\left[P_z \widehat{e}_y^{n+\frac{1}{2}} - P_y \widehat{e}_z^{n+1} \right]$$

$$\widehat{h}_y^{n+1} = \widehat{h}_y^{\#} + \frac{\Delta\tau}{2} M_{\mu_y^{-1}}\left[P_x \widehat{e}_z^{n+1} - P_z \widehat{e}_x^{n+\frac{1}{2}} \right]$$

with I unit diagonal matrix and $M_{\varepsilon^{-1},\mu^{-1}} \equiv M_{\varepsilon,\mu}^{-1}$.

Realization of the TE/TM Scheme for Rotationally Symmetric Geometries

Below the realization of the implicit TE/TM numerical scheme for the case of rotationally symmetric geometries in cylindrical coordinates $\{r,\varphi,z\}$ is described.
For a bunch moving at the speed of light c with an offset a parallel to the axis of a rotationally symmetric structure, the source current density $\vec{J}_s = \{0,0,J_z\}$ can be represented via multipole expansion eq. (3.9). The numerical scheme (3.46) for an azimuthal mode number m has the form

TE components

$$\hat{e}_\varphi^\# \equiv \hat{e}_\varphi^{n-\frac{1}{2}} + \frac{\Delta\tau}{2} M_{\varepsilon_\varphi^{-1}} \left[\tilde{P}_z \hat{h}_r^n - \tilde{P}_r \hat{h}_z^{n-\frac{1}{2}} \right]$$

$$\hat{e}_r^\# \equiv \hat{e}_r^{n-\frac{1}{2}} + \frac{\Delta\tau}{2} M_{\varepsilon_r^{-1}} \left[m\hat{h}_z^{n-\frac{1}{2}} - \tilde{P}_z \hat{h}_\varphi^n \right]$$

$$\hat{h}_z^{n+\frac{1}{2}} = \hat{h}_z^{n-\frac{1}{2}} + \Delta\tau W_h^{-1} M_{\mu_z^{-1}} \left[P_r \hat{e}_\varphi^\# - m\hat{e}_r^\# \right]$$

$$\hat{e}_\varphi^{n+\frac{1}{2}} = \hat{e}_\varphi^\# + \frac{\Delta\tau}{2} M_{\varepsilon_\varphi^{-1}} \left[\tilde{P}_z \hat{h}_r^n - \tilde{P}_r \hat{h}_z^{n+\frac{1}{2}} \right]$$

$$\hat{e}_r^{n+\frac{1}{2}} = \hat{e}_r^\# + \frac{\Delta\tau}{2} M_{\varepsilon_r^{-1}} \left[m\hat{h}_z^{n+\frac{1}{2}} - \tilde{P}_z \hat{h}_\varphi^n \right]$$

(3.47)

TM components

$$\hat{h}_\varphi^\# \equiv \hat{h}_\varphi^n + \frac{\Delta\tau}{2} M_{\mu_\varphi^{-1}} \left[P_z \hat{e}_r^{n+\frac{1}{2}} - P_r \hat{e}_z^n \right]$$

$$\hat{h}_r^\# \equiv \hat{h}_r^n + \frac{\Delta\tau}{2} M_{\mu_r^{-1}} \left[m\hat{e}_z^n - P_z \hat{e}_\varphi^{n+\frac{1}{2}} \right]$$

$$\hat{e}_z^{n+1} = \hat{e}_z^n + \Delta\tau W_e^{-1} M_{\varepsilon_z^{-1}} \left[\tilde{P}_r \hat{h}_\varphi^\# - m\hat{h}_r^\# - \hat{j}_z^n \right]$$

$$\hat{h}_\varphi^{n+1} = \hat{h}_\varphi^\# + \frac{\Delta\tau}{2} M_{\mu_\varphi^{-1}} \left[P_z \hat{e}_r^{n+\frac{1}{2}} - P_r \hat{e}_z^{n+1} \right]$$

$$\hat{h}_r^{n+1} = \hat{h}_r^\# + \frac{\Delta\tau}{2} M_{\mu_r^{-1}} \left[m\hat{e}_z^{n+1} - P_z \hat{e}_\varphi^{n+\frac{1}{2}} \right]$$

Where due to the azimuthal symmetry of the problem multipole expansion of the electromagnetic fields eq.(3.8) [15] and the following property of a discrete operator of derivative $P_\varphi = mI$ have been used in derivation of the numerical scheme (3.47).

In the staircase approximation of the boundary the material matrixes $M_{\mu^{-1}}$ and $M_{\varepsilon^{-1}}$ are diagonal and following operators of the scheme (3.47)

$$W_e \equiv \left(I + \frac{\Delta\tau^2}{4} M_{\varepsilon_z^{-1}} \tilde{P}_r M_{\mu_\varphi^{-1}} P_r + \frac{\Delta\tau^2}{4} m^2 M_{\varepsilon_z^{-1}} M_{\mu_r^{-1}} \right)$$

$$W_h \equiv \left(I + \frac{\Delta\tau^2}{4} M_{\mu_z^{-1}} P_r M_{\varepsilon_\varphi^{-1}} \tilde{P}_r + \frac{\Delta\tau^2}{4} m^2 M_{\mu_z^{-1}} M_{\varepsilon_r^{-1}} \right)$$

(3.48)

are three-diagonal matrixes. So the equations involving them can be solved easily.

In the next section the stability of the above-introduced scheme will be discussed.

3.3.2.1 Stability Analyses of TE/TM Scheme

The stability of the numerical scheme (3.43) can be studied by the energy inequalities method [55, 56, 58]. Defining the following inner product on complex M-dimensional vectors a and b

$$\langle a, b \rangle = \frac{1}{M} \sum_{i=0}^{M-1} a_i b_i^*$$

(3.49)

The inner product of both sides in equation (3.43) with $y^{n+1} + y^n$ read as

$$\left\langle B\left(y^{n+1} - y^n\right), y^{n+1} + y^n \right\rangle + \Delta\tau \left\langle A y^n, y^{n+1} + y^n \right\rangle = \left\langle \Delta\tau f^n, y^{n+1} + y^n \right\rangle$$

(3.50)

Using the following formula

$$y^n = \frac{\left(y^{n+1} + y^n\right) - \left(y^{n+1} - y^n\right)}{2}$$

(3.51)

the equation (3.50) can be rewritten as

$$\left\langle \left[B - \frac{\Delta\tau}{2} A\right]\left(y^{n+1} - y^n\right), y^{n+1} + y^n \right\rangle + \frac{\Delta\tau}{2} \left\langle A\left(y^{n+1} + y^n\right), y^{n+1} + y^n \right\rangle = \left\langle \Delta\tau f^n, y^{n+1} + y^n \right\rangle$$

(3.52)

Since the operator A is skew-symmetric, the second term in the left-hand side is equal to zero and

$$\left\langle Q y^{n+1}, y^{n+1} \right\rangle - \left\langle Q y^n, y^n \right\rangle = \left\langle \Delta\tau f^n, y^{n+1} + y^n \right\rangle$$

(3.53)

The last relation enables to prove the following theorem [55, 56]:

Theorem: *The condition*

$$Q \equiv B - \frac{1}{2}\Delta\tau A \geq 0$$

(3.54)

is necessary and sufficient for the stability in the Hilbert space of the scheme (3.43) with respect to the initial data y^0 and right-hand side f^n.

The condition (3.54) can be rewritten as

$$\frac{\Delta\tau^2}{4} C_0 C_0^T \leq I \quad \text{or} \quad \Delta\tau \leq \frac{2}{\sqrt{\max(\lambda_i)}}$$

where λ_i are the eigenvalues of the matrix $C_0 C_0^T$.

The last inequalities are direct corollaries of the following Lemma

Lemma: *Let us define a matrix* $\widetilde{A}$ *by relation*

$$\widetilde{A} = \begin{pmatrix} 0 & A \\ A^T & 0 \end{pmatrix}$$

For the square matrix A *the conditions*

(a) $I + \widetilde{A} \geq 0$ *and*
(b) $I - A^T A \geq 0$

are equivalent.

Indeed, the set of eigenvalues $\left\{ \lambda_i^{\widetilde{A}} \right\}$ of the matrix $\widetilde{A}$ can be rewritten in the form

$$\left\{ \lambda_i^{\widetilde{A}} \right\} = \left\{ \sqrt{\lambda_i^{A^T A}} \right\} \cup \left\{ -\sqrt{\lambda_i^{A^T A}} \right\}$$

where $\left\{ \lambda_i^{A^T A} \right\}$ is the set of eigenvalues of the non-negative self-conjugate matrix $A^T A$. Hence, both relations (a) and (b) hold simultaneously.

Now following [57, 65] a discrete energy of electromagnetic field can be defined as

$$W_{TE/TM}^n = \frac{1}{2} \left\langle \left[B - \frac{\Delta\tau}{2} A \right] y^n, y^n \right\rangle \tag{3.55}$$

And the discrete energy conservation law holds

$$\frac{W_{TE/TM}^{n+1} - W_{TE/TM}^n}{\Delta\tau} = -\frac{1}{2} \left\langle \left[\widehat{e}_x^{n+1} + \widehat{e}_x^n, \widehat{e}_y^{n+1} + \widehat{e}_y^n, \widehat{e}_z^{n+\frac{1}{2}} + \widehat{e}_z^{n-\frac{1}{2}} \right], \left[\widehat{j}_x^{n+\frac{1}{2}}, \widehat{j}_y^{n+\frac{1}{2}}, \widehat{j}_z^n \right] \right\rangle \tag{3.56}$$

Note that the discrete energy in numerical schemes defined by relation (3.56) is a second order accurate approximation to the total physical energy of the electromagnetic field. If the right hand side in scheme (3.43) vanishes, the scheme becomes energy conserving $W_{TE/TM}^n = W_{TE/TM}^0$.

Due to the Lemma the stability condition (3.54) can be rewritten in the form

$$\begin{cases} I - \dfrac{\Delta\tau^2}{4} P_z^i \widetilde{P}_z^i \geq 0 \\[2mm] I - \dfrac{\Delta\tau^2}{4} \left(P_x^i \widetilde{P}_x^i + P_y^i \widetilde{P}_y^i \right) \geq 0 \end{cases} \quad \text{with} \quad i = 0, 1 \tag{3.57}$$

The first inequality resembles well-known stability condition of the explicit FDTD scheme for the one-dimensional electromagnetic problem. For the second inequality from the consideration of the maximal eigenvalue of the Laplace operator $\left(P_x^i \widetilde{P}_x^i + P_y^i \widetilde{P}_y^i \right)$ it follows that for the vacuum region with a staircase approximation of the boundary the stability condition read as

$$\begin{cases} \Delta\tau \le \min(\Delta z, \Delta x, \Delta y) \\ \Delta\tau \le \left(\dfrac{1}{\Delta x^2}+\dfrac{1}{\Delta y^2}\right)^{-\frac{1}{2}} \end{cases} \quad (3.58)$$

For the rotationally symmetric case the stability condition reduces to the form

$$\Delta\tau \le \min(\Delta z, \Delta r) \qquad (3.59)$$

Note that the last stability condition does not contain the azimuthal mode number m while Yee's scheme requires reducing the stable time step [54, 68] for higher azimuthal modes

$$\Delta\tau \le \left(\left(1.2+0.4\,m^2\right)\frac{1}{\Delta r^2}+1.2\,\frac{1}{\Delta z^2}\right)^{-\frac{1}{2}} \qquad (3.60)$$

that increases the computational effort considerably.

As will follow from the next section with time step $\Delta\tau$ equal to the longitudinal mesh step Δz the TE/TM numerical scheme (3.43) does not have dispersion in longitudinal direction. The relation (3.58) does not contain information about transverse mesh. Hence, the transverse mesh can be chosen with no stability considerations.

3.3.2.2 Numerical Dispersion

Following the conventional procedure of stability analyses on plane waves [54, 58] the dispersion relations can be obtained for TE/TM numerical scheme in the form

$$\frac{\sin^2\left(\dfrac{\omega}{c}\dfrac{\Delta\tau}{2}\right)}{\Delta\tau^2} = \frac{\sin^2\left(k_z\dfrac{\Delta z}{2}\right)}{\Delta z^2} + \left(\frac{\sin^2\left(k_x\dfrac{\Delta x}{2}\right)}{\Delta x^2}+\frac{\sin^2\left(k_y\dfrac{\Delta y}{2}\right)}{\Delta y^2}\right)\cos^2\left(\dfrac{\omega}{c}\dfrac{\Delta\tau}{2}\right) \quad (3.61)$$

As can be seen from this dispersion equation at the "magic" time step $\Delta\tau = \Delta z$, the scheme is dispersion-free in longitudinal direction. For equal transverse mesh steps $\Delta x = \Delta y \equiv h$ the dispersion relation for the transverse plane waves $k_z = 0$ read as

$$\mathrm{Tan}^2\left(\frac{\omega}{c}\frac{\Delta\tau}{2}\right) = \frac{\Delta\tau^2}{h^2}\left(\sin^2\left(k_x\frac{h}{2}\right)+\sin^2\left(k_y\frac{h}{2}\right)\right) \qquad (3.62)$$

From the dispersion relation (3.61) follows that equation (3.58) is a necessary stability condition for the implicit TE/TM numerical scheme.

The dispersion error cancellation for particular direction is important in electromagnetic field computation due to the fact that the charged particle beams in accelerators have a design orbit and the direction of motion (the longitudinal direction) can be identified. Therefore, the computational domain is very long in the longitudinal direction and relatively short in the transverse plane. Additionally, the electromagnetic field changes very fast in the direction of motion but is relatively smooth in the transverse plane.

Another advantage of dispersion-free scheme is that for an ultra relativistic bunch a mesh moving along with the bunch can be used since the scaled time step is equal to the longitudinal mesh step. The results with the moving mesh for staircase approximation of the geometry are fully equivalent to the stationary global mesh approach. From all this arguments follows that for this scheme the mesh step is independent from the structure length L and related only to the first power of the rms bunch length σ [33, 67] as

$$\Delta z << \sigma \tag{3.63}$$

3.4 Initial Field for Accelerator Application

In accelerator applications the studied structures usually are supplied by ingoing pipe. For the rotationally symmetric structures the analytical solution in a perfect conducting cylindrical beam pipe [11] can be used as initial condition. For ultra relativistic bunch with longitudinal charge distribution $\rho(z)$ moving at an offset a parallel to the symmetry axis of infinitely long perfect conducting beam pipe of radius b the electromagnetic field components of the m th mutipole read as

$$E_r(r, \tau = 0) = \frac{q}{2\pi\varepsilon_0} \frac{2a^m}{1 + \delta_{m,0}} \rho(z) \cos(m\varphi) \begin{cases} \left(\frac{1}{b^{2m}} - \frac{1}{a^{2m}} \right) r^{m-1} & , \quad r \le a \\ \frac{1}{r^{m+1}} + \frac{r^{m-1}}{b^{2m}} & , \quad a < r \le b \end{cases}$$

$$E_\varphi(r, \tau = 0) = \frac{q}{2\pi\varepsilon_0} \frac{2a^m}{1 + \delta_{m,0}} \rho(z) \sin(m\varphi) \begin{cases} -\left(\frac{1}{b^{2m}} - \frac{1}{a^{2m}} \right) r^{m-1} & , \quad r \le a \\ \frac{1}{r^{m+1}} - \frac{r^{m-1}}{b^{2m}} & , \quad a < r \le b \end{cases} \tag{3.64}$$

$$H_r(r, \tau = 0) = -\frac{1}{Z_0} E_\varphi(r, \tau = 0), \quad H_\varphi(r, \tau = 0) = \frac{1}{Z_0} E_r(r, \tau = 0)$$

with

$$\delta_{m,0} = \begin{cases} 1 \, , \, m = 0 \\ 0 \, , \, m \ne 0 \end{cases}$$

As is seen from (3.64) for monopole case $m = 0$, there is no field inside the ring $(r < a)$. The field pattern is uniform inside the beam for $m = 1$ thus resembling the dipole magnet. Similarly for $m = 2$, the field pattern resembles that of a quadrupole magnet and for $m = 3$ a sextupole magnet [13].
If the ingoing pipe is not cylindrical the initial field can be found numerically.

3.5 Longitudinal and Transverse Wake Potentials

In this section, the basic definitions of the longitudinal and transverse wake potential are introduced.

Consider the point charge Q moving along the z axis of the structure with offset $\vec{r}_1$ and velocity v_z close to the speed of light c (Fig.1) and a test charge q moving with the same velocity at a distance s behind the driving charge and the offset $\vec{r}$.
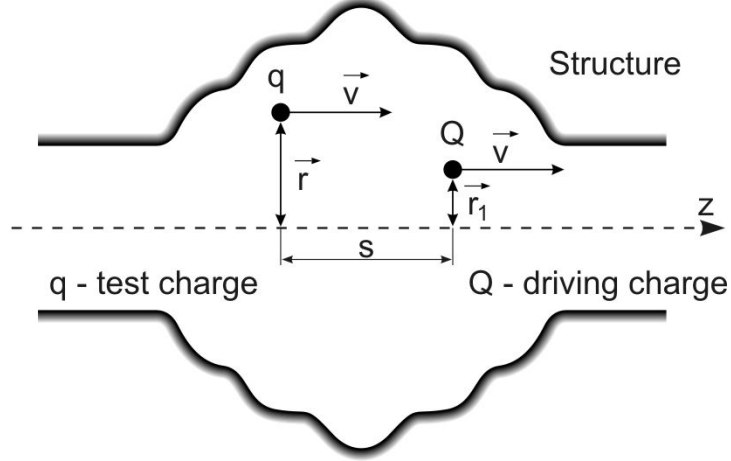
Figure 17. *A driving and test charges traverse the cavity.*

As the driving charge interacts with the structure, it will excite electromagnetic fields (wake fields) with longitudinal and transverse components that act on the test charge. The longitudinal component of the Lorenz force will produce energy gain (or loss) of the test particle, while the transverse component of the Lorenz force will produce a transverse kick of the trailing test particle.

We define the longitudinal point wake potential as the integrated longitudinal Lorenz force experienced by the test particle over the length of the structure in interest

$$w_{//}(\vec{r},\vec{r}_1,s) = \frac{1}{Q}\int_{-\infty}^{+\infty} E_z(\vec{r},\vec{r}_1,z,t=\frac{z+s}{c})\,dz \qquad (3.65)$$

Note, that in our definition, $s < 0$ corresponds to distance in front of the driving charge, $s = 0$ -to the position of the driving charge and $s > 0$ - to the longitudinal position behind the driving charge.

The net energy gain or loss by the test particle following at the distance s behind the driving charge is then given by

$$\Delta U(s) = qQ \cdot w_{//}(s) \qquad (3.66)$$

The transverse components of the electromagnetic fields produce a transverse component of the Lorenz force acting on the test charge. We define the transverse wake potential as an integrated transverse Lorenz force acting on the test charge

$$\vec{w}_{\perp}(\vec{r},\vec{r}_1,s) = \frac{1}{Q}\int_{-\infty}^{+\infty} (\vec{E}+\vec{v}\times\vec{B})_{\perp}(\vec{r},\vec{r}_1,z,t=\frac{z+s}{c})\,dz \qquad (3.67)$$

As it follows from the definition and Lorenz equation of motion the transverse wake potential defines the net transverse kick of the test charge in the wakefields induced by the driving charge

$$\Delta \vec{p}_\perp(s) = qQ\,\vec{w}_\perp(s)/c \tag{3.68}$$

Thus the longitudinal and transverse wake potentials describe the energy gain (loss) and the transverse dynamics of the test particle in the wakefields excited by the driving charge during its passage through the structure (cavity, transitions, discontinuities etc). Note, that from causality principle, for ultrarelativistic driving charge ($v_z \equiv c$) the fields are vanished in front of the driving charge, i.e. $w_{//}(s) = 0$, $\vec{w}_\perp(s) = 0$ for all positions $s < 0$.

An important property of the wake potentials is described by the Panowsky-Wenzel theorem [73] that gives the explicit relation between the longitudinal and transverse wake potentials.

$$\frac{\partial}{\partial s}\vec{w}_\perp(\vec{r},s) = -\vec{\nabla}_\perp w_z(\vec{r},s) \tag{3.69}$$

where $\vec{\nabla}_\perp$ is the transverse gradient operator.

For an extended longitudinal distribution $\rho(s)$ of the driving bunch, the wake potentials are determined by the superposition of the wake functions of individual charges in the bunch that lead to the convolution of the point wake potential and normalized charge distribution

$$W_{//}(s) = \int_{-\infty}^{s}\rho(s')w_{//}(s-s')ds' \qquad \text{with} \quad \int_{-\infty}^{+\infty}\rho(s)ds = 1 \tag{3.70}$$
$$\vec{W}_\perp(s) = \int_{-\infty}^{s}\rho(s')\vec{w}_\perp(s-s')ds'$$

In the next section the convergence of the TE/TM scheme and some numerical tests will be discussed. The following integral parameters will be used: the loss factor $K_{//}$ and the kick factor $K_\perp$ given as

$$K_{//,\perp} = \int_{-\infty}^{+\infty}W_{//,\perp}(s)\rho(s)\,ds \tag{3.71}$$

3.6 Convergence of the Implicit TE/TM Scheme and Numerical Examples for Rotationally Symmetric Geometries.

For illustration, in this section the convergence properties of implicit TE/TM scheme implemented in code ECHO are presented. Some numerical results of the wake field calculations in perfectly conducting rotationally symmetric structures are discussed.

Convergence of the Scheme

On equidistant mesh the implicit TE/TM numerical scheme (3.46) has a second-order local approximation error in homogeneous region $O\left(\|\Delta\vec{r}\|^2 + \Delta\tau^2\right)$, $\Delta\vec{r} = (\Delta x, \Delta y, \Delta z)^T$ [33, 67]. The staircase approximation of the geometry in general makes the scheme first-order accurate. In order to overcome this problem and avoid reduction of the time step, the uniformly stable conformal (USC) approach was developed in [68] which makes the TE/TM scheme second-order

accurate. In the figure 18 the relative error of the loss factor $\delta = \left|K_{//} - \overline{K}_{//}\right|/\overline{K}_{//}$ is shown for a Gaussian bunch with rms length $\sigma = 0.5$ cm passing through a pillbox cavity (fig. 18 left) and a spherical resonator (fig. 18 right).
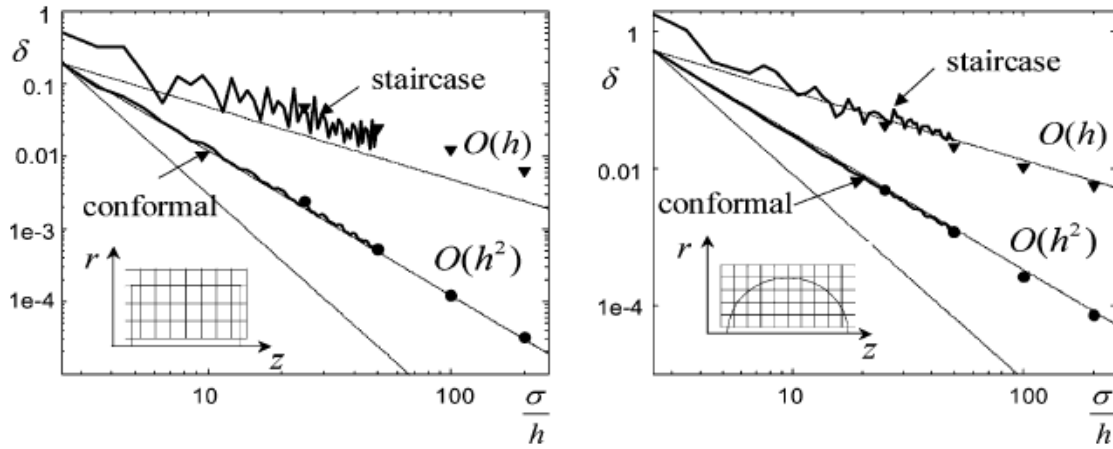
Figure 18. *The relative error of the monopole loss factor for a pillbox (left) and a sphere (right) versus the number of mesh steps per rms bunch length. The solid lines show results for a stationary mesh, the triangles and circles present results for the moving mesh.*

The error is given over the number of mesh steps per bunch length σ/h, where h denotes the equidistant mesh step $h = \Delta z = \Delta r$ in both directions. The pillbox has the length $1.8\,\text{cm}$ and radius $0.9\,\text{cm}$. The sphere diameter is $1.8\,\text{cm}$. The analytical loss factor $\overline{K}_{//}$ for the pillbox is equal to $0.589459\,\text{V/pC}$ and $0.152446\,\text{V/pC}$ for the sphere. Lines demonstrate the error of a computation with a stationary mesh. Triangles and circles show the results for the moving mesh. The mesh covers the Gaussian bunch longitudinally in the range of -5σ to 5σ. As is seen, the staircase scheme shows a first-order rate of convergence and the conformal scheme achieves the second order.

Numerical Examples

The examples of TE/TM numerical scheme applications are given in Ref. [33,50]. First test example is a circular collimator structure shown in Figure 19 (with inner radius b not presented in the figure). Figure 20 shows the wake potential for the collimator with parameters $a = 40\,\text{mm}$, $b = c = 10\,\text{mm}$, $L = 2445\,\text{mm}$ and the bunch with rms length $\sigma = 0.1\,\text{cm}$. The numerical simulations are compared to the analytical solution [74].
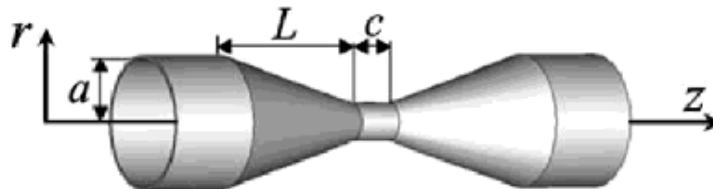
Figure 19. *The geometry of the collimator.*
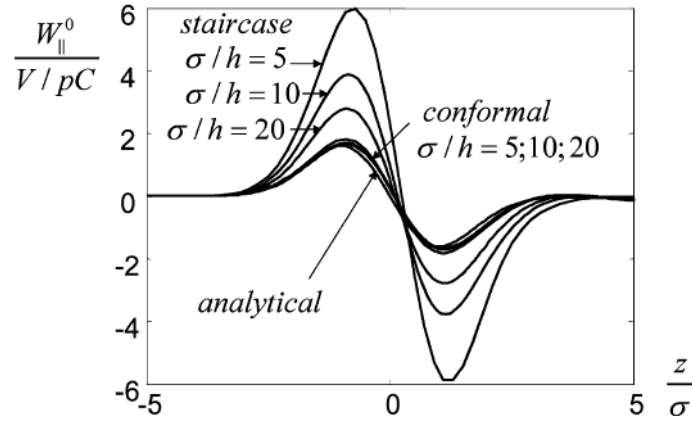
Figure 20. *The monopole wake potential of a collimator. The wakes calculated with different mesh resolutions σ/h are compared to the analytical solution. The results for the staircase scheme show a considerable error. Three curves for the conformal scheme follow the analytical estimation.*

The conformal scheme shows a second-order convergence and gives results of high accuracy with only 5 mesh steps per σ in all tests while for staircase scheme more than 40 mesh points per σ is required to reach the same result. Note that the staircase scheme with 5 steps per σ leads to relative error in excess of 300%.

The next example deals with a structure consisting of the 20 TESLA cavity cells [75] bounded by infinite ingoing and outgoing pipes 35mm in diameter. The side view of the geometry is illustrated in Figure 21.
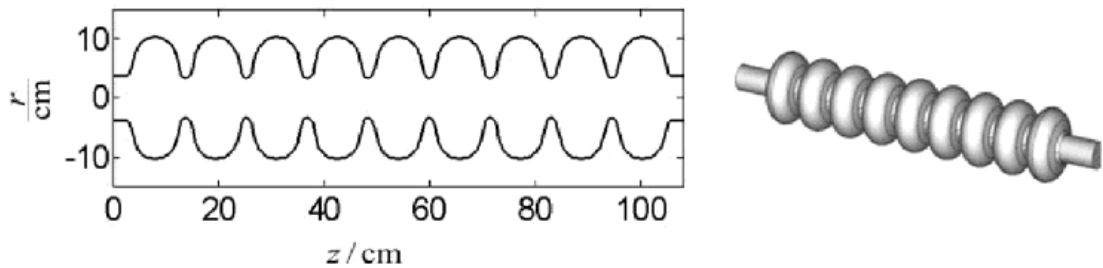
Figure 21. *Side view of the 9-cell TESLA cavity.*

Each cell of this cavity is built using different kinds of geometrical objects: ellipse, line and circle. The contour of the half-cell, called "cups", is shown in figure 22.
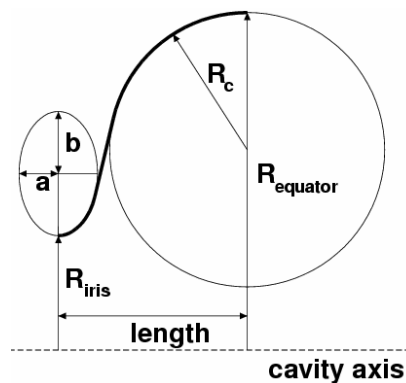
Figure 22. *Contour of a half cell.*

60

It is composed of a circular arc in the equator region and an elliptical section near the iris. The dimensions are listed in Table.2.

Cavity shape parameter	Cups
Equator radius $R_{equ.}$	103.3 mm
Iris radius R_{iris}	35 mm
Radius R_c of circular arc	42.0 mm
Horizontal half axis a	12 mm
Vertical half axis b	19 mm
Length L	57.7 mm

Table 2. TESLA 9-cell cavity middle cup geometry parameters.

The analytical solution (3.64) was used as an initial condition in the ingoing pipe. Figure 23 shows the longitudinal wake potential for a Gaussian bunch with rms length $\sigma = 1\,\mathrm{mm}$.
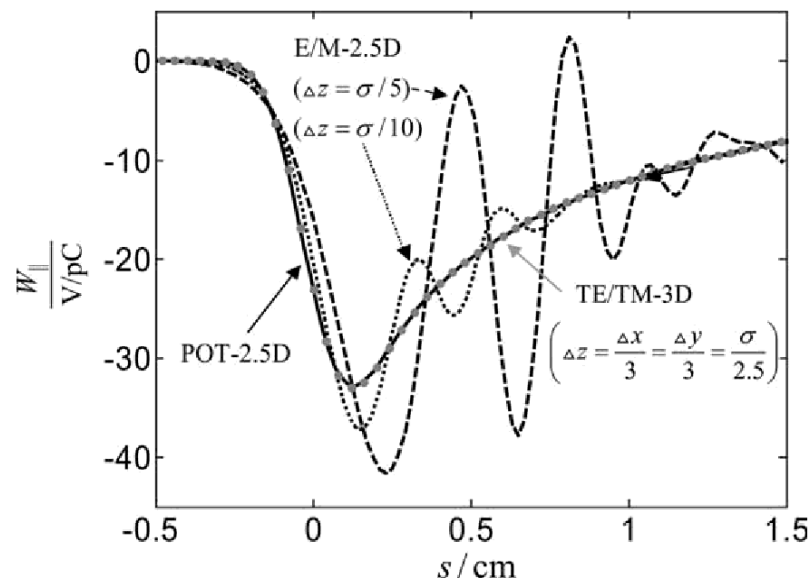
Figure 23. Comparison of the wake potentials obtained by different methods for the structure consisting of 20 TESLA cells excited by a Gaussian bunch with $\sigma = 1\,\mathrm{mm}$. The solid line shows the reference solution obtained with the help of a scheme described in [50]. The dashed and dotted lines describe the solution obtained by the classical Yee's scheme with different number of points per σ. The picture shows coincidence of the reference result (solid line) with the result on the coarse mesh obtained from the 3D TE/TM code (gray points).

The solid line (POT 2.5D) corresponds to the reference solution obtained with the vector potential method [50]. The two other lines show results obtained with different mesh resolutions from the TBCI code [40], which is based on the classical Yee's scheme (E/M – 2.5D). The shown oscillations, are due to the dispersion error of the Yee's scheme. The gray points present the result obtained by the implicit conformal implicit 3D TE/TM numerical scheme. It can be seen that the implicit conformal 3D TE/TM scheme produces very accurate results even for the coarse mesh. Indeed, the conformal method uses 2.5 mesh points per σ in the longitudinal direction while for staircase approximation of the geometry more that 40 mesh points per σ is needed to obtain a similar results.

3.7 Conclusion

In this chapter description of the TE/TM ("transverse electric-transverse magnetic") splitting implicit numerical scheme is given [33, 52]. This scheme models numerically in time domain the continuous EM problem that read as: to calculate three-dimensional (3D) electromagnetic fields excited by ultra-short relativistic bunches in accelerator structures with perfect conducting walls.

The stability and numerical dispersion of the scheme are discussed based on well-known results. The main advantage and outlook of this numerical scheme is the fact that its stability condition allows to cancel numerical dispersion in longitudinal direction. Thus it is important for accelerator structure modeling, the transverse dimensions of the geometry being commonly considerably smaller than the longitudinal.

The realization of this scheme is implemented in the ECHO code, which is for rotationally symmetric geometries. The numerical examples show that the TE/TM splitting numerical scheme is much more accurate in long-time simulations than with the conventional FDTD approach.

Chapter 4.

A New Hybrid Numerical Scheme for Finite Conductivity Modeling in Time Domain

This Chapter is devoted to a new hybrid numerical scheme for calculating the wakefields excited by ultra-short bunches in structures with walls of finite conductivity. Based on the TE/TM splitting numerical scheme described in Chapter 3 a new longitudinally dispersion-free algorithm for resistive structures is developed. The time domain impedance boundary condition in each boundary cell is approximated by one-dimensional EM model described in Chapter 2. The realization of this new hybrid 3D implicit numerical scheme is done for rotationally symmetric geometries and staircase approximation of the boundary surface. A good agreement of the numerical simulations with the well-known analytical results and CST Particle Studio simulations are obtained. The new hybrid scheme was applied to calculate the wake potentials for the various components of FLASH linear accelerator at DESY and the European XFEL project.

4.1 Theory of Wave Propagation in a Conductor

Consider a homogeneous isotropic medium of dielectric constant ε, permeability μ and conductivity κ. Using the material equations $\vec{B} = \mu \cdot \vec{H}$, $\vec{D} = \varepsilon \cdot \vec{E}$ and the Ohm's law $\vec{J} = \kappa \cdot \vec{E}$, the Maxwell's equations in time domain will read as

$$
\begin{aligned}
\mathrm{rot}\,\vec{H} &= \kappa\,\vec{E} + \varepsilon \frac{\partial}{\partial t}\vec{E} \quad & \mathrm{div}\,\vec{H} &= 0 \\
\mathrm{rot}\,\vec{E} &= -\mu \frac{\partial}{\partial t}\vec{H} & \mathrm{div}\,\vec{E} &= 0
\end{aligned}
\tag{4.1}
$$

Since any electromagnetic wave can be described by superposition of plane waves, in further the propagation of the plane wave in a conductor will be considered. For a monochromatic wave with angular frequency ω, i.e. $\vec{E} = \vec{E}_0 e^{-i\omega t}$, the first two Maxwell's equations are rewritten as

$$
\begin{aligned}
\mathrm{rot}\,\vec{H} + i\omega\,(\varepsilon + i\frac{\kappa}{\omega})\vec{E} &= 0 \\
\mathrm{rot}\,\vec{E} - i\omega\,\mu\,\vec{H} &= 0
\end{aligned}
\tag{4.2}
$$

Using the relation $\mathrm{rot}\,\mathrm{rot} = \mathrm{grad}\,\mathrm{div} - \Delta$ for the electric field we get the wave equation

$$
\Delta\vec{E} + \hat{k}^2\vec{E} = 0
\tag{4.3}
$$

where

$$
\hat{k}^2 = \omega^2\mu\,(\varepsilon + i\frac{\kappa}{\omega})
\tag{4.4}
$$

These equations are identical to the non-conducting media case if in the latter the dielectric constant ε is replaced by

$$\hat{\varepsilon} = \varepsilon + i\frac{\kappa}{\omega} \tag{4.5}$$

In addition to the complex wave number $\hat{k}$ and the complex dielectric constant $\hat{\varepsilon}$ we also introduce a complex phase velocity $\hat{v}$ and a complex refractive index $\hat{n}$, which by analogy are defined as

$$\hat{v} = \frac{1}{\sqrt{\mu\hat{\varepsilon}}}, \quad \hat{n} = \frac{c}{\hat{v}} = c\sqrt{\mu\hat{\varepsilon}} = \frac{c}{\omega}\hat{k} \tag{4.6}$$

We set

$$\hat{n} = p\,(1 + i\,\xi) \tag{4.7}$$

where p and ξ are real and expressed in terms of material constants ε, μ and κ. The square of eq.(4.7) is

$$\hat{n}^2 = p^2\,(1 + 2i\,\xi - \xi^2) \tag{4.8}$$

On the other hand

$$\hat{n}^2 = c^2\mu\,\hat{\varepsilon} = c^2\mu\,(\varepsilon + i\frac{\kappa}{\omega}) \tag{4.9}$$

Equating the real and imaginary parts of equations (4.8) and (4.9) we obtain

$$\begin{cases} p^2(1 - \xi^2) = c^2\varepsilon\,\mu \\ p^2\xi = c^2\,\dfrac{\mu\,\kappa}{2\omega} \end{cases} \tag{4.10}$$

or

$$p^2 = \frac{c^2\varepsilon\,\mu}{2}\left\{\sqrt{1 + \frac{\kappa^2}{\varepsilon^2\omega^2}} + 1\right\}$$

$$p^2\xi^2 = \frac{c^2\varepsilon\,\mu}{2}\left\{\sqrt{1 + \frac{\kappa^2}{\varepsilon^2\omega^2}} - 1\right\} \tag{4.11}$$

The positive sign of the square roots is taken in (4.11). Since p and $(p\xi)$ are real the p^2 and $(p^2\xi^2)$ must be positive.

Equation (4.3) is formally identical with the wave equation for non-conducting medium, but the wave number is now complex. The simplest solution is that of a plane, time harmonic wave

$$\vec{E} = \vec{E}_0 e^{i[\hat{k}(\vec{r}\cdot\vec{s}) - \omega t]} \tag{4.12}$$

where $\vec{s}$ is the unit vector in the direction of wave propagation.

If, in accordance with (4.6) and (4.7), we substitute $\hat{k}$ by $\hat{k} = \omega\hat{n}/c = \omega p(1+i\xi)/c$, we get

$$\vec{E} = \vec{E}_0 e^{-\frac{\omega}{c}p\xi(\vec{r}\cdot\vec{s})} e^{i\omega[\frac{p}{c}(\vec{r}\cdot\vec{s})-t]} \tag{4.13}$$

The real part of this expression will read as

$$\mathrm{Re}(\vec{E}) = \vec{E}_0 e^{-\frac{\omega}{c}p\xi(\vec{r}\cdot\vec{s})} \cos\left(\omega\left[\frac{p}{c}(\vec{r}\cdot\vec{s})-t\right]\right) \tag{4.14}$$

which represents the electric vector that is a plane wave with wavelength $\lambda = 2\pi c/\omega p$ and with attenuation given by the exponential term

$$\eta = \frac{\omega}{c}p\xi = \frac{2\pi}{\lambda_0}p\xi = \frac{2\pi}{\lambda}\xi \tag{4.15}$$

Here $\lambda_0 = 2\pi c/\omega$ is the wavelength in vacuum, λ is the wavelength in medium. The constant η is called the absorption coefficient.

The energy density is reduces by e^{-1} factor as the wave penetrates the distance δ, which is called the skin depth and is given by

$$\delta = \frac{1}{\eta} = \frac{c}{\omega}\frac{1}{p\xi} \tag{4.16}$$

This quantity is usually a very small fraction of the wavelength. Returning to equations (4.11) we see that for $\kappa = 0$, the second equation is zero and the first one is $p^2 = c^2\varepsilon\mu$, so the refraction index coincides with the well-known expression $n^2 = c^2\varepsilon\mu$ for dielectrics. For metals $\kappa \neq 0$ the next condition is usually fulfilled

$$\frac{\kappa}{\varepsilon\omega} >> 1 \tag{4.17}$$

Under this condition the equations (4.11) and (4.16) are reduced to

$$p \sim p\xi = c\sqrt{\frac{\mu\kappa}{2\omega}}$$
$$\delta \sim \sqrt{\frac{2}{\mu\kappa\omega}} \tag{4.18}$$

For radiation frequency in infra-red, microwave and long radio wave ranges, the "skin depths" δ for copper with static conductivity $\kappa = 58\cdot10^6\,\Omega/m$, $\varepsilon = \varepsilon_0 = 8.85\cdot10^{-12}$, $\mu = \mu_0 = 4\pi\cdot10^{-7}$ are given in table 3.

Table 3. *Skin depths at the radiation wavlenght range of infra-red, microwave and long radio waves*

Radiation	Infra-red	Microwaves	Long radio waves
λ_0	10^{-5} m	0.1 m	10^3 m
δ	$1.2\cdot10^{-8}$ m	$1.2\cdot10^{-6}$ m	$1.2\cdot10^{-4}$ m

A perfect conductor is characterized by infinitely large conductivity $\kappa \to \infty$ and in this limiting case $\xi \to 1$ and $p \to \infty$. For such a conductor, an incident wave is completely reflected from the surface.

We have seen that the basic equations related to the propagation of a plane harmonic wave in a conducting medium differ from those related to propagation in dielectric media by replacement of the real constants ε and k by complex ones $\hat{\varepsilon}$ and $\hat{k}$. Now consider the wave propagation from dielectric into a conductor. Both media are assumed to be of infinite extent fig.24.
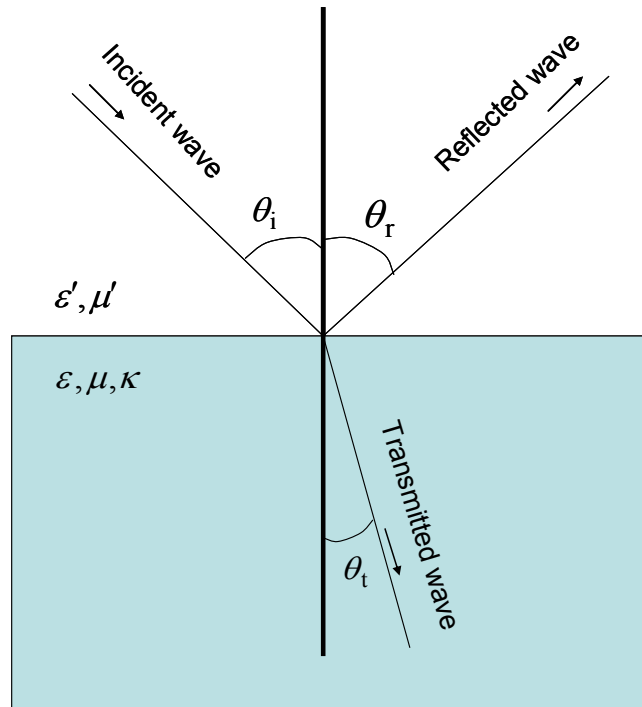
Figure 24 . *Transmission and reflection of EM wave on dielectric-conductor boundary surface*

By analogy with refraction law for dielectrics for a conductive media case we can write [76]

$$\sin\theta_t = \frac{1}{n(\theta_i, \kappa, \omega)} \sin\theta_i \tag{4.19}$$

For dielectrics the refraction index is constant and real while for conductors it is complex and depends on incident angle, conductivity and frequency of incident wave

$$n^2(\theta_i, \kappa, \omega) = \frac{1}{2}\left[\sin^2\theta_i + g(\theta_i, \kappa, \omega)\, p^2\,(1+\xi^2) + 1 - \xi^2\right] \tag{4.20}$$

where

$$g^2(\theta_i, \kappa, \omega) = 1 - 2\frac{1-\xi^2}{p^2(1+\xi^2)^2}\sin^2\theta_i + \frac{1}{p^4(1+\xi^2)^2}\sin^4\theta_i \tag{4.21}$$

Here we should keep in mind that p and ξ are functions of frequency and conductivity. When condition (4.17) is satisfied, the parameters p, ξ in equation (4.11) are approximated as

$$p^2 \rightarrow \frac{c\sqrt{\varepsilon\mu}}{2}\frac{\kappa}{\varepsilon\omega} = \frac{1}{2}\frac{\kappa}{\varepsilon\omega}$$ (4.22)

$$\xi \rightarrow 1$$

where the relation $c = 1\big/\sqrt{\varepsilon_0\mu_0}$ is used.

Using these expressions it is easy to see that the refraction index is much larger than unity $n(\theta_i, \kappa, \omega) \gg 1$, thus the inverse value is very small. This means, that when the condition (4.17) is fulfilled, the incident waves are propagating not parallel to the boundary surface and are transmitted perpendicular to the boundary surface ($\theta_t \sim 0$), i.e. only the tangential components of electric and magnetic fields survive in the conducting media.

In accelerators the spectrum of excited EM field due to bunch interaction with the surrounding structure extends to frequencies up to several $\omega_b \sim c/\sigma$ with σ the rms bunch length. In advanced accelerators the vacuum chambers are usually made of high conducting materials like stainless steel, aluminum or copper and the condition (4.17) is actually satisfied. As an example, for stainless steel vacuum chamber $\kappa = 1.4 \cdot 10^6 \, \Omega^{-1}\text{m}^{-1}$ and for a bunch with rms length of 1μm we get $\kappa/(\varepsilon_0 \omega) \approx 527$.

Thus for high conducting media only the tangential component of the wave in the resistive region (transmitted wave) can be taken into account and the task is reduced to one-dimensional electromagnetic problem in metal. The so-called 1D conducting line model can be applied instead of full space electromagnetic field description.

4.2 A New Hybrid TE/TM Splitting Implicit Numerical Scheme for Finite Conductivity Modeling in Accelerating Structures

In this section a hybrid TE/TM splitting implicit numerical scheme for finite conductivity modeling in accelerating structures is discussed [33, 49, 50]. The problem is read as: To calculate electromagnetic fields excited by ultra-relativistic charged particle Gaussian bunch moving with the speed of light in vacuum bounded with walls of finite but high conductivity assuming that the following condition is fulfilled

$$\kappa/(\varepsilon_0\omega) \gg 1$$ (4.23)

It is well known that in such a system the bunch of Gaussian charge distribution with rms bunch length σ excites the electromagnetic fields up to the frequencies of $\omega \sim c/\sigma$. This allow to write the condition (4.23) in terms of bunch rms length as

$$\kappa Z_0 \, \sigma \gg 1$$ (4.24)

with impedance of free space $Z_0 = 1/c\varepsilon_0$.

As shown in the previous section, the condition (4.24) allows the modeling of the conductivity part as one-dimensional (1D) electromagnetic problem. In this section we will introduce a new hybrid 3D numerical scheme for finite high conductivity modeling as a modification of the 3D dispersion-free numerical scheme for the perfect electric boundary condition problem introduced in chapter 3.

In the new hybrid scheme for the vacuum part the 3D TE/TM splitting numerical scheme is used where the boundary cells of the grid are supplied by 1D electromagnetic problem for EM field calculation in the conductive region. In this model the tangential components of electric field on the boundary are applied for EM field update in the boundary cells of vacuum region.

The excitation source for the 1D problem will be the tangential components of the magnetic field in the boundary cell. Such a scheme is implemented for the simple 1D case introduced in chapter 2. To describe the tangential components of electromagnetic fields in the boundary cells we introduce a local coordinate system $\{p, \varphi, s\}$ connected to the boundary for cylindrical grid as shown in fig.25.
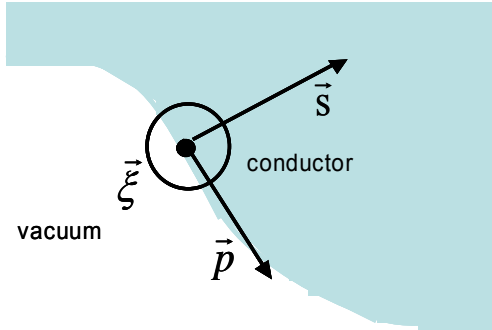
Figure 25. *Boundary local coordinate system.*

As can be seen from the figure 25 the s - axis of the local coordinate system is always directed along the normal vector to the surface. Thus according to the previous section the electromagnetic fields components which are tangential to the surface will be propagated into the conductive region in the direction of s -axis at each local point of the surface.

In this chapter we consider the boundary interface by staircase approximation [77, 78]. It is zero order approximation of the boundary while the 3D numerical scheme in free space introduced in chapter 3 has second-order accuracy [33]. Thus due to boundary zero order approximation the accuracy of the 3D numerical scheme (with boundary) is reduced to the first order. The first-order approximation of the boundary can be reached by conformal methods which have been already implemented for perfect electric boundary condition (PEC) problems [68]. With conformal method the order of the 3D numerical scheme in the vacuum is unchanged (second order). The first numerical experiments with direct application of conformal method to hybrid scheme result in serious instabilities and rigorous study is necessary to improve the stability. Thus we will introduce the hybrid scheme only for staircase approximation of the boundary.

The TE/TM splitting hybrid numerical scheme is realized for the electromagnetic problems with rotational symmetric geometries. A cylindrical coordinate $\{r, \varphi, z\}$ system is used, where z is the longitudinal coordinate. We will consider a Gaussian charged bunch moving at the speed of light c in longitudinal direction with an offset a parallel to z -axis (fig. 26). Using the multipole expansion of the source (3.9) and electromagnetic fields (3.8) the dependence of the fields on azimuthal coordinate φ in the numerical scheme can be taken analytically. The task is to flow then into two-dimensional (2D) mesh for the geometry description in the discrete space. Thus the space discretization is required for two directions $\{r, z\}$.
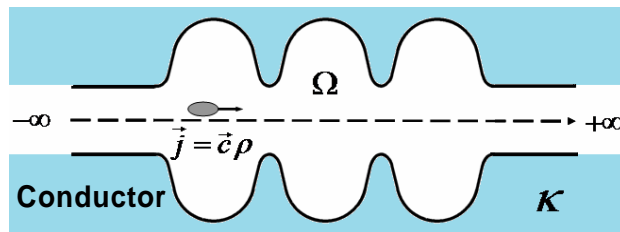
Figure 26. *Ultra-relativistic charged particle moving through an accelerating structure with finite conductive walls supplied with infinite perfect conducting pipes.*

Usually the accelerating structures are supplied with ingoing and outgoing beampipes. Thus in our problem we will supply the structures with perfect conducting pipes which will enable us to use analytics in PEC pipe to define the initial electromagnetic fields and to implement indirect method for wake potential calculation introduced in Chapter 3.

The special parts of our problem are the boundary cells of the grid, which are in touch with conductive region and need a careful consideration. The goal is to model the impedance boundary condition (IBC) in time domain. The thickness of the modeling conductor is taken much smaller than the skin depth of the given problem. Such a 1D problem has been discussed in chapter 2. As an excitation source of the 1D electromagnetic problem the magnetic field components in boundary cell of the vacuum region will be used. This field is tangential to the boundary surface and perpendicular to the tangential electric fields. Thus the IBC modeling in time domain is converted into a 1D electromagnetic problem in the metal.

According to the section 2.3 of chapter 2 the implicit 1D numerical scheme will be applied for our 1D problem to model the conductor. This numerical scheme according to equations 2.104 can be rewritten as

$$
\hat{h}_c^{\#} = \hat{h}_c^n + \frac{\Delta\tau}{2}\frac{1}{Z_0}P\,\hat{e}_c^n
$$

$$
W\left(\hat{e}_c^{n+1} - \hat{e}_c^n\right) = \hat{e}_c^n (A-1) + Z_0\,B\,P^*\,\hat{h}_c^{\#} \tag{4.25}
$$

$$
\hat{h}_c^{n+1} = \hat{h}_c^{\#} + \frac{\Delta\tau}{2}\frac{1}{Z_0}P\,\hat{e}_c^{n+1}
$$

with three-diagonal matrix

$$
W \equiv I - \frac{\Delta\tau}{4}B\,P^*P \tag{4.26}
$$

and I the unit diagonal matrix. The $\Delta\tau$ in equation (4.25) is the discrete time step. The index c is used to note that we are considering the EM fields in conductive region. The two-banded matrices P and P^* in the 1D numerical scheme plays the role of discrete differential operators and depends on the discrete space step Δx. The matrices A and B are diagonal with entries

$$
\begin{aligned}
&a_{0,0} = e^{-\tilde{\kappa}\Delta\tau\frac{\Delta x}{\Delta x+\Delta x_0}} \quad a_{i,i} = e^{-\tilde{\kappa}\Delta\tau} \\
&b_{0,0} = \frac{2}{\tilde{\kappa}}\left(1-a_{0,0}\right) \quad a_{i,i} = \frac{1}{\tilde{\kappa}}\left(1-a_{i,i}\right)
\end{aligned} \quad \text{for } i \geq 1 \tag{4.27}
$$
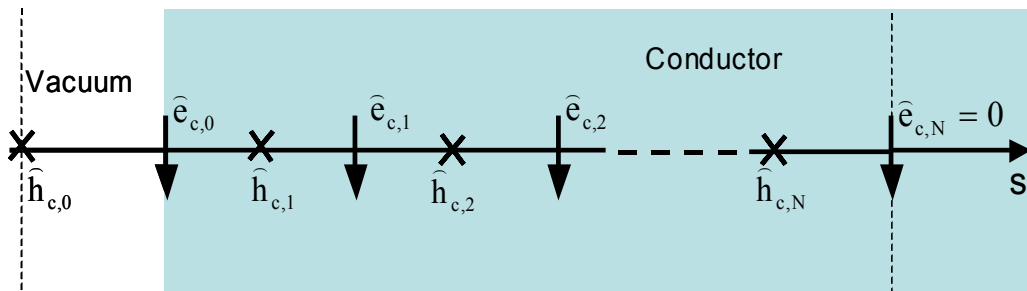
Figure 27. *The geometric view of the 1D numerical scheme in conductive region.*

According to the figure 27 the boundary conditions at the interfaces for 1D electromagnetic problem read as $\widehat{e}^n_{c,N} = 0$ and $\widehat{h}^n_{c,0} = \widehat{h}^n_{\xi,\text{vacuum}}$. This approach is applicable when the thickness of the modeling conductor is taken much larger than the skin-depth of the considered problem.

From multipole expansion of the fields eq.(3.8) follows that for the monopole case ($m = 0$) the non zero field components are E_r, E_z, H_φ. Thus the monopole case will be considered separately from higher order multipole cases.

Monopole case (m=0)

Graphically the discretization of the problem is illustrated in figure 28 where the 1D conductive lines for finite conductivity modeling are shown.

Figure 28. *Vacuum grid with 1D conductive lines at the boundaries for monopole case.*

As can be seen from the figure in the cells like cell **A** the magnetic field component $\widehat{h}_{\varphi_{i,j}}$ is the excitation source for 1D electromagnetic problems in transverse and longitudinal directions, i.e. both 1D problems are equivalent. Thus the electric field components tangential to the boundary will be equal at any time step $\widehat{e}^n_c \equiv \widehat{e}^n_{cr} = \widehat{e}^n_{cz}$. This means that for each mesh cell the number of 1D problems is reduced to one instead of two. Finally the TE/TM numerical scheme for monopole case can be written in the following steps

TE component

1. $\qquad \widehat{e}_r^{\,n+\frac{1}{2}} = \widehat{e}_r^{\,n-\frac{1}{2}} - \Delta\tau\, M_{\varepsilon_r^{-1}}\, \widetilde{P}_z\, \widehat{h}_\varphi^{\,n}$

TM components

$$\widehat{h}_{\varphi}^{\#} \equiv \widehat{h}_{\varphi}^{n} + \frac{\Delta\tau}{2} M_{\mu_{\varphi}^{-1}} \left[P_z \, \widehat{e}_r^{n+\frac{1}{2}} - P_r \, \widehat{e}_z^{n} + l_c \, \widehat{e}_c^{n} \right]$$

2.

$$\widehat{e}_z^{n+1} = \widehat{e}_z^{n} + \Delta\tau \left(I + \frac{\Delta\tau^2}{4} M_{\varepsilon_z^{-1}} \widetilde{P}_r M_{\mu_{\varphi}^{-1}} P_r \right)^{-1} M_{\varepsilon_z^{-1}} \left[\widetilde{P}_r \, \widehat{h}_{\varphi}^{\#} - \widehat{j}_z^{n} \right]$$

3. By updating EM fields of 1D problems using the scheme (4.25) the tangential electric field at next time level $\widehat{e}_c^{n+1}$ is defined. As an excitation source for the 1D problem, the tangential component of magnetic field $\widehat{h}_{\varphi}^{n}$ in vacuum boundary cell is taken.

4. $$\widehat{h}_{\varphi}^{n+1} = \widehat{h}_{\varphi}^{\#} + \frac{\Delta\tau}{2} M_{\mu_{\varphi}^{-1}} \left[P_z \, \widehat{e}_r^{n+\frac{1}{2}} - P_r \, \widehat{e}_z^{n+1} + l_c \, \widehat{e}_c^{n+1} \right]$$

where $\widehat{e}_c^{n}$, $\widehat{e}_c^{n+1}$ are the voltages at the conductive surface and l_c is conductive edge length. The conductive edge length for the cells like **A** (fig.28) is $l_c = 2$, and for cells like **B** is $l_c = 1$.

Higher-Order Multipole Case (m>0)

For a higher-order multipole case all six components of the field should be taken into account. The $\widehat{e}_r^{n}$, $\widehat{e}_z^{n}$, $\widehat{h}_{\varphi}^{n}$ components of EM field are graphically shown on 2D mesh in fig.28.
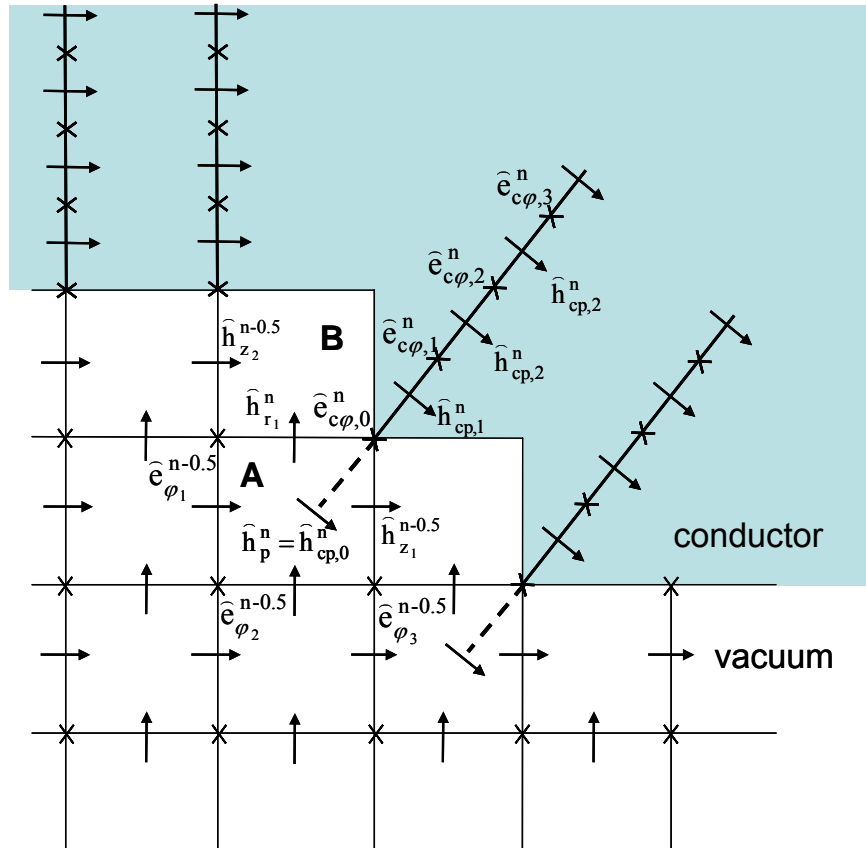
***Figure 29**. 2D view of cylindrical mesh of vacuum region.*

The other three components $\hat{h}_r^n$, $\hat{h}_z^n$, $\hat{e}_\varphi^n$ of the field are illustrated in fig.29. Note that for 3D case, to find the tangential components of electric field in each direction, 1D EM problems should be solved, i.e. for finite conductivity, modeling of each boundary cell in vacuum should be supplied by three separate 1D problems. For rotational symmetry geometries the 1D problems for each cell are reduced to two. In multipole case a second electric field $\hat{e}_{c\varphi}^n$ tangential to the boundary interface should be obtained. To calculate the $\hat{e}_{c\varphi}^n$ field, the second 1D problem in conductor should be solved. As an excitation source for this 1D problem, the $\hat{h}_p^n$ (fig.29) magnetic field from boundary cell in vacuum is taken. For the cells like **A** (fig.29) this magnetic field vector is defined as a sum of magnetic field vectors $\hat{h}_r^n$ and $\hat{h}_z^n$ projected on the cell diagonal Fig.(30).
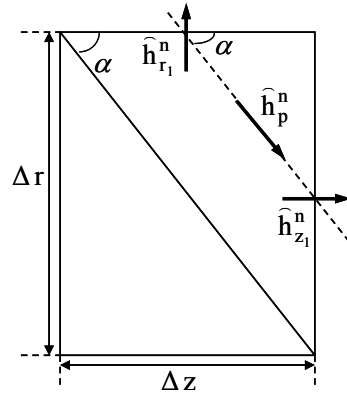
Figure 30. *Overview of the discrete magnetic field components in the grid cell.*

Following the notations illustrated in figure 30, the $\hat{h}_p^n$ field will read as

$$\hat{h}_p^n = \hat{h}_{z_1}^n \cos\alpha + \hat{h}_{r_1}^n \sin\alpha$$

$$\mathrm{tg}\,\alpha = \frac{\Delta r}{\Delta z}$$

(4.28)

For the cells like **B** (fig.26) the $\hat{h}_p^n$ field is equal to the $\hat{h}_z^n$, i.e. $\hat{h}_p^n = \hat{h}_{z_2}^n$.

Note that in the TE/TM numerical scheme the longitudinal component of magnetic field $\hat{h}_z$ on the discrete time axis is defined at time level $(n+0.5)$. Thus, this field at time level n could be found by following the interpolation procedure

$$\hat{h}_z^n = \frac{\hat{h}_z^{n-\frac{1}{2}} + \hat{h}_z^{n+\frac{1}{2}}}{2}$$

Finally for IBC modeling in time domain we should connect two 1D EM problems to each vacuum boundary cell. The electromagnetic fields in each 1D problems should be taken $\{\hat{h}_{c\varphi}^n, \hat{e}_{cp}^n\}$ and $\{\hat{h}_{cp}^n, \hat{e}_{c\varphi}^n\}$ pairs respectively.

Finally the TE/TM hybrid numerical scheme for an azimuthal mode number m read as

TE components

1.

$$\hat{e}_\varphi^\# \equiv \hat{e}_\varphi^{n-\frac{1}{2}} + \frac{\Delta\tau}{2} M_{\varepsilon_\varphi^{-1}} \left[\tilde{P}_z \hat{h}_r^n - \tilde{P}_r \hat{h}_z^{n-\frac{1}{2}} \right]$$

$$\hat{e}_r^\# \equiv \hat{e}_r^{n-\frac{1}{2}} + \frac{\Delta\tau}{2} M_{\varepsilon_r^{-1}} \left[m \hat{h}_z^{n-\frac{1}{2}} - \tilde{P}_z \hat{h}_\varphi^n \right]$$

$$\hat{h}_z^{n+\frac{1}{2}} = \hat{h}_z^{n-\frac{1}{2}} + \Delta\tau \left(I + \frac{\Delta\tau^2}{4} M_{\mu_z^{-1}} P_r M_{\varepsilon_\varphi^{-1}} \tilde{P}_r + \frac{\Delta\tau^2}{4} m^2 M_{\mu_z^{-1}} M_{\varepsilon_r^{-1}} \right)^{-1} M_{\mu_z^{-1}} \cdot$$
$$\cdot \left[P_r \hat{e}_\varphi^\# - m \hat{e}_r^\# + \hat{e}_{c\varphi}^n \right]$$

$$\hat{e}_\varphi^{n+\frac{1}{2}} = \hat{e}_\varphi^\# + \frac{\Delta\tau}{2} M_{\varepsilon_\varphi^{-1}} \left[\tilde{P}_z \hat{h}_r^n - \tilde{P}_r \hat{h}_z^{n+\frac{1}{2}} \right]$$

$$\hat{e}_r^{n+\frac{1}{2}} = \hat{e}_r^\# + \frac{\Delta\tau}{2} M_{\varepsilon_r^{-1}} \left[m \hat{h}_z^{n+\frac{1}{2}} - \tilde{P}_z \hat{h}_\varphi^n \right]$$

TM components

2.

$$\hat{h}_\varphi^\# \equiv \hat{h}_\varphi^n + \frac{\Delta\tau}{2} M_{\mu_\varphi^{-1}} \left[P_z \hat{e}_r^{n+\frac{1}{2}} - P_r \hat{e}_z^n + 1_c \hat{e}_{cp}^n \right]$$

$$\hat{h}_r^\# \equiv \hat{h}_r^n + \frac{\Delta\tau}{2} M_{\mu_r^{-1}} \left[m \hat{e}_z^n - P_z \hat{e}_\varphi^{n+\frac{1}{2}} + \hat{e}_{c\varphi}^n \right]$$

$$\hat{e}_z^{n+1} = \hat{e}_z^n + \Delta\tau \left(I + \frac{\Delta\tau^2}{4} M_{\varepsilon_z^{-1}} \tilde{P}_r M_{\mu_\varphi^{-1}} P_r + \frac{\Delta\tau^2}{4} m^2 M_{\varepsilon_z^{-1}} M_{\mu_r^{-1}} \right)^{-1} M_{\varepsilon_z^{-1}} \cdot$$
$$\cdot \left[\tilde{P}_r \hat{h}_\varphi^\# - m \hat{h}_r^\# - \hat{j}_z^n \right]$$

3. The updates of EM fields of 1D problems using the scheme (4.25) give the tangential electric fields $\hat{e}_{cp}^{n+1}$ and $\hat{e}_{c\varphi}^{n+1}$ at time level (n+1). For the field updates of 1D problems the $\hat{h}_p^n$ and $\hat{h}_\varphi^n$ magnetic fields from vacuum boundary cells are used as input parameters.

4.

$$\hat{h}_\varphi^{n+1} = \hat{h}_\varphi^\# + \frac{\Delta\tau}{2} M_{\mu_\varphi^{-1}} \left[P_z \hat{e}_r^{n+\frac{1}{2}} - P_r \hat{e}_z^{n+1} + 1_c \hat{e}_{cp}^{n+1} \right]$$

$$\hat{h}_r^{n+1} = \hat{h}_r^\# + \frac{\Delta\tau}{2} M_{\mu_r^{-1}} \left[m \hat{e}_z^{n+1} - P_z \hat{e}_\varphi^{n+\frac{1}{2}} + \hat{e}_{c\varphi}^{n+1} \right]$$

where the discrete derivative operators P_r, P_z for normal and $\widetilde{P}_r$, $\widetilde{P}_z$ for dual mesh have been applied, I is unit diagonal matrix.

The material matrices M_ε and M_μ have been used which contain the information about lengths of mesh edges normalized on discrete space steps and the normalized mesh areas respectively. Thus, for staircase approximation of the boundaries the elements of material matrices are equal to one for vacuum region and zero for the conductive part.

The simulation experiments show that the numerical dispersion properties of the hybrid TE/TM numerical scheme are preserved, i.e. as for the original TE/TM scheme (Chapter 3) the hybrid scheme also has no dispersion in longitudinal direction at the magic time step which is equal to the longitudinal space step $\Delta\tau = \Delta z$.

In the next section the stability and convergence of the hybrid scheme for rotational symmetric geometries will be discussed.

4.3 The Stability of the Hybrid Scheme.

The 3D Hybrid implicit numerical scheme is designed in a way that the stability properties of 3D scheme in the vacuum region (3.58), (3.59) and 1D scheme in conductor (2.137) are preserved. Thus the stability conditions for hybrid scheme on cylindrical mesh will read

$$\begin{cases} ---\text{vacuum}--- \\ \Delta z < \sigma_b \\ \Delta\tau \le \min(\Delta z, \Delta r) \\ ---\text{conductor}--- \\ \Delta x_c^2 \ge \dfrac{2\Delta\tau}{\kappa \cdot Z_0} \\ \Delta x_c \le \min(\Delta z, \Delta r) \end{cases} \qquad (4.29)$$

where σ_b is rms bunch length, κ is the conductivity, Z_0-impedance of free space, $\Delta\tau$ is the time step normalized to the speed of light, $\{\Delta r, \Delta z\}$ are the space steps in vacuum region and Δx_c is the space step of 1D scheme for conductive region.

The stability conditions (4.29) of the hybrid TE/TM implicit numerical scheme have been tested and approved by a number of numerical experiments. The numerical dispersion property (3.61) of the scheme also holds. Thus at the "magic" time step $\Delta\tau = \Delta z$ the developed hybrid scheme is dispersion free in longitudinal direction.

The hybrid numerical scheme can model the IBC in time domain for electromagnetic problems, where the following relation is satisfied [see section 4.1]

$$\kappa Z_0 \sigma_b \gg 1 \qquad (4.30)$$

In advanced accelerators the vacuum chambers usually are made of high conducting materials ($\kappa \ge 10^5$) like aluminum or copper and the condition (4.30) is usually satisfied. As an example, for stainless steel vacuum chamber $\kappa = 1.4\cdot10^6\,\Omega^{-1}\text{m}^{-1}$ and bunch rms length of $1\mu\text{m}$, $\kappa Z_0 \sigma_b \approx 527$. Thus the above numerical scheme is applicable to high energy accelerators like FLASH and European XFEL project where the beam rms length varies from $25-50\,\mu\text{m}$.

4.4 Convergence of the Hybrid Scheme.

The convergence study of the 3D hybrid numerical scheme is performed based on the comparison of the numerical results with the steady state solutions of Gaussian bunch wake potentials in a round pipe with finite conductive walls. For the points charge moving in infinite round pipe of radius b with the offset a parallel to the symmetry axis the analytical steady state solution of the longitudinal wake potential of m-th multipole is well known [79] and read as

$$w_{//,m}(s) = q_m \, r^m \cos(m\varphi) F_m(s) \tag{4.31}$$

with q_m the m-th multipole charge moment and the function $F_m(s)$ are given as

$$q_m = \frac{\int\limits_0^{2\pi}\int\limits_0^{b} \rho(r,\varphi) r^{m+1}\cos(m\varphi)\,dr\,d\varphi}{\int\limits_0^{2\pi}\int\limits_0^{b} r^{2m+1}\cos^2(m\varphi)\,dr\,d\varphi} = \frac{(m+1)}{\pi}\frac{a^m}{b^{2(m+1)}}$$

$$F_m(s) = -\frac{4}{\varepsilon_0}\left[\frac{1}{3}e^{-\eta^{2/3}\frac{s}{s_0}}\cos\left(\sqrt{3}\,\eta^{2/3}\frac{s}{s_0}\right) - \frac{\sqrt{2}}{\pi}\eta\int\limits_0^{\infty}\frac{x^2}{x^6+8\eta^2}e^{-x^2\frac{s}{s_0}}dx\right]$$

$$\tag{4.32}$$

where $\eta = (m+1+\delta_{m,0})/2$ with $\delta_{m,0}$ Kronecker delta function and s_0 is so called characteristical distance given as

$$s_0 = \left(\frac{2cb^2\varepsilon_0}{\kappa}\right)^{1/3} \tag{4.33}$$

In the case of Gaussian bunch distribution $\rho(s)$ with rms length σ the longitudinal wake potential read

$$W_{//,m}^G(s) = \int\limits_{-5\sigma}^{s} w_{//,m}(s-s')\rho(s')\,ds'$$

$$\rho(s) = \frac{1}{\sqrt{2\pi}\sigma}e^{-\frac{s^2}{2\sigma^2}}$$

$$\tag{4.34}$$

Applying the Panowsky-Wenzel theorem (3.70) and the eq.(3.71) the transverse wake potential $W_{\perp,m}^G$ and loss (kick) factor for Gaussian charge distribution can be derived. Note that the wake potentials are given per unit length of the round pipe.

The convergence of the hybrid scheme is analyzed for the Gaussian bunch of rms length $\sigma = 1\,\text{mm}$ moving in round pipe of radius $a = 1\,\text{cm}$ and wall conductivity $\kappa = 10^5\,\text{S/m}$. To check the convergence the linear dependence on time step of the discrete space step in conductive region is required that will fulfill the stability condition (1.137) within the range of research. In this special case due to high conductivity the relation $\Delta x_c = 100\Delta\tau\cdot\sqrt{2/\kappa}$ is applicable.

a)
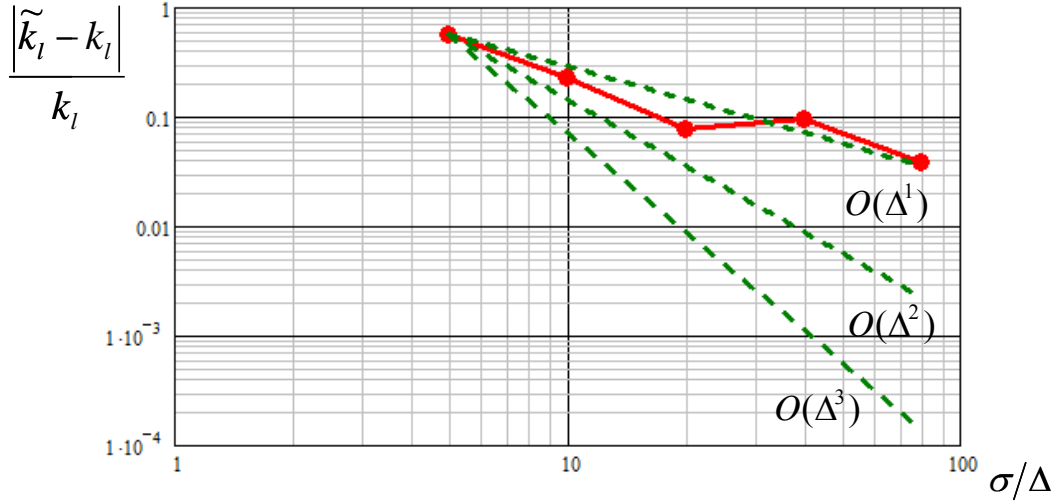
b)
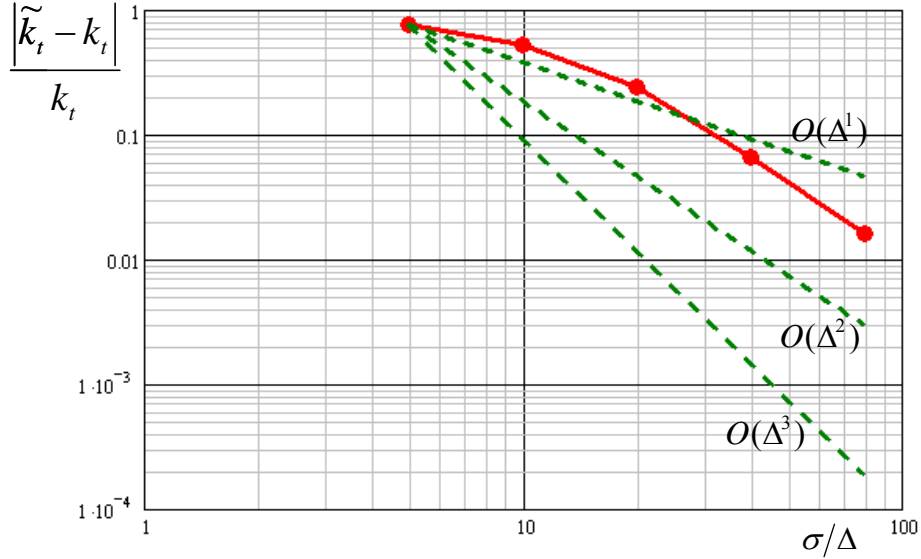
Figure 31. *Convergence (logarithmic scale) of the monopole loss and dipole kick factors (red) and the prediction until 3rd order (green dashed).*

The results of the study is presented in figure 31, the convergence of the numerically calculated loss (a) and dipole kick (b) factors is compared to the analytical values $k_l = 1.31 \, \text{V/pC}$ and $k_t = 75.5 \, \text{V/pC/m}$ respectively. In those plots the horizontal axis corresponds to the number of discretized point on 1σ bunch rms length and Δ is the space step. All calculations in this and further sections are done with equidistance mesh and "magic" time step, i.e. normalized time step is equal to the longitudinal space step $\Delta \equiv \Delta\tau = \Delta z = \Delta r$. As is seen the numerical scheme is first order accurate as was predicted due to the staircase approximation of the boundary interface. Note that for convergence study the geometrical mesh should be shifted from boundary interface, otherwise we will observe a second-order convergence. The next section shows the results of numerically calculated steady state solutions of longitudinal monopole and transverse dipole wake potentials when the geometric mesh coincides with the boundary interface.

Similar tests on convergence of the hybrid scheme have been performed for higher-order harmonics and it was observed that the convergence behaves similar to dipole case.

4.5 Numerical Tests on Rotational Symmetric Geometries

In this section several examples of the wake potentials calculations in various resistive structures are presented. The results are compared with known analytical solutions and the results obtained by other advanced numerical codes. As an example the following typical structures are taken: infinitely long resistive tube, resistive insert and resistive tapered collimator.

Steady State Resistive Wake Potentials.

As the first test we calculate the steady state longitudinal and transverse short-range wake potentials of the Gaussian bunch with rms length $\sigma = 1 \text{mm}$ moving in a round pipe of radius $a = 1 \text{cm}$ and walls conductivity $\kappa = 10^5 \, \text{S/m}$. For this simple geometry the adjustment of the geometric mesh with boundary interface is possible.

a)

b)
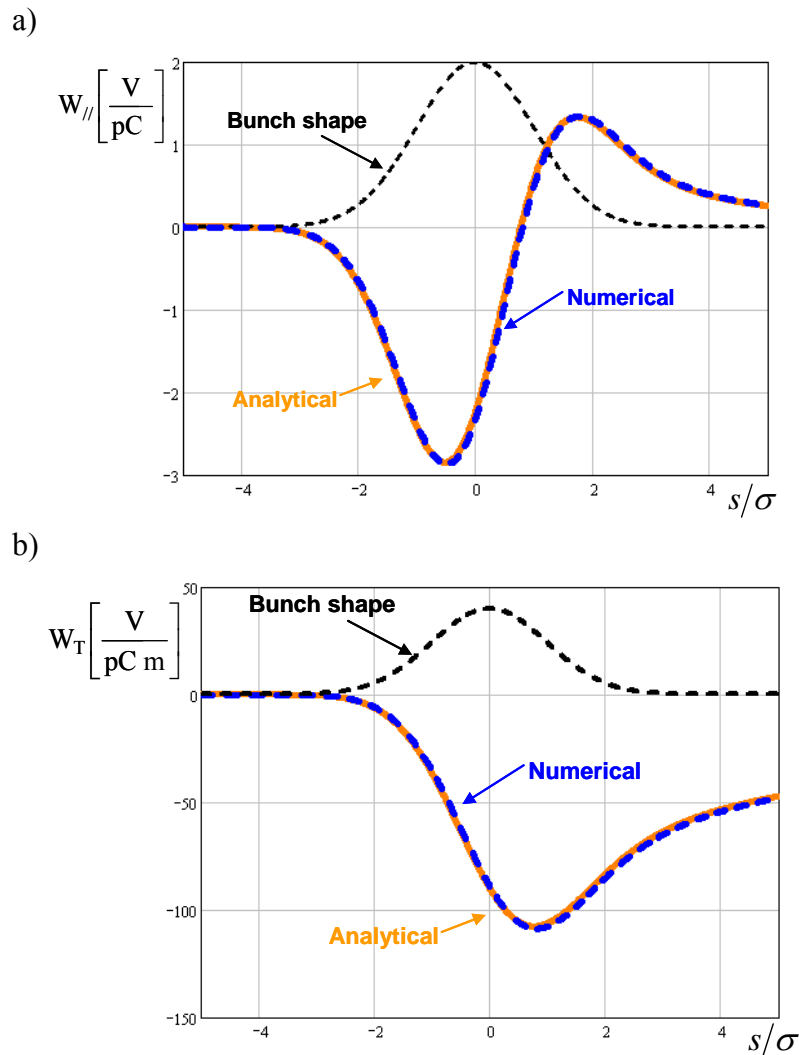
Figure 32*. Comparison of the numerical longitudinal monopole and transverse dipole wake potentials (blue dashed) with analytical solutions (orange solid).*

Figure 32 shows the comparison of the numerically calculated longitudinal monopole (a) and transverse dipole (b) wake potentials with analytical wakes. The numerical results are given for the mesh resolution of 10 points in 1σ. In this case (mesh coincides with boundary interface) the error in loss and kick factors is about 3% while to obtain same accuracy of the calculation in staircase approximation (mesh is shifted from boundary interface) we will need more than 40 points on 1σ.

The Wake Potentials for Resistive Insert.

As the second test we calculate the longitudinal and transverse wake potentials of the Gaussian bunch passing through the finite length resistive cylinder supplied with infinitely long perfectly conducting beam pipes (Fig. 33). The resistive part of cylinder has radius $a = 1\,\text{cm}$, length $g = 10\,\text{cm}$ and conductivity $\kappa = 10^4\,\text{S/m}$.
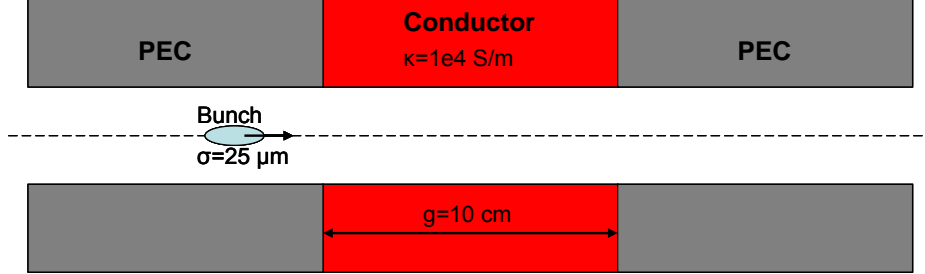
Figure 33. *Cross section of the finite-length resistive cylinder supplied with infinitely long perfectly conducting pipes.*

The analytical solutions for monopole loss k_l and dipole kick k_t factors of the Gaussian bunch in such structure are given in Ref. [80]

$$
k_l = \frac{c\,Z_0\,g}{2\,\pi^2\,a\,\sqrt{2\,\kappa\,Z_0\,s_g^{3/2}}}\,K_l\!\left(\frac{\sigma}{s_g}\right)
$$
$$
k_t = \frac{c\,Z_0\,\sqrt{g\,s_g}}{\pi^2\,a^3}\,K_t\!\left(\frac{\sigma}{s_g}\right)
\qquad \text{with}\quad s_g = \sqrt{\frac{g}{2\,Z_0\,\kappa}}
\qquad (4.35)
$$

where the functions K_l and K_t are given by

$$
K_l(u) = \int_0^\infty dx\; x^{-3/2}\, e^{-x^2 u^2}\left[1 - e^{-x^2} + \frac{2\,x}{\sqrt{\pi}} - e^{-x^2}\,\mathrm{erfi}(x)\right]
$$
$$
K_t(u) = \int_0^\infty dx\; x^{-5/2}\, e^{-x^2 u^2}\,\mathrm{erfi}(u\,x)\left[1 - e^{-x^2} + \frac{2\,x}{\sqrt{\pi}} - e^{-x^2}\,\mathrm{erfi}(x)\right]
\qquad (4.36)
$$

Figure 34 presents the numerically obtained longitudinal monopole (a) and transverse dipole (b) wake potentials (blue) and the analytical steady state wakes (orange) [11, 12] for the Gaussian bunch of rms length $\sigma = 25\,\mu\text{m}$

a)
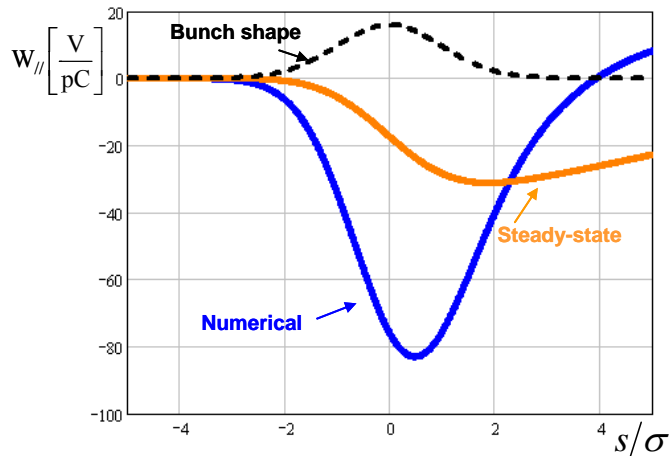
b)
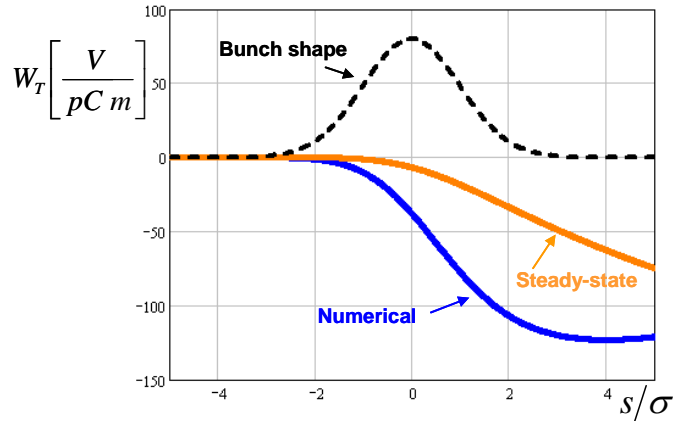
Figure 34. Comparison of transient (blue solid) and steady state (orange solid) wake potentials.

The numerically obtained loss and kick factors are equal to 58 V/pC and 42.6 V/pC/m respectively. The numerical results are coincidental with the analytical prediction (4.35) for loss factor (57 V/pC) and kick factor (41.5 V/pC/m) with accuracy of 1.7% and 2.3% respectively.

The steady state loss factor for such an insert is equal to 16 V/pC, the loss factor being underestimated. The same situation is with steady state kick factor that is equal to 9.6 V/pC/m. In the demonstrated example of the 10cm-long resistive insert it is clearly seen that the steady state loss and kick factors compromise the exact results by 75%.

Wake Potentials in Rotational Symmetric Tapered Collimator.

For the third example we take a rotational symmetric tapered collimator (fig. 35) with parameters d=10mm, b=6mm, L_1=200 mm, L_2 =100mm and conductivity $\kappa = 10^4$ S/m .
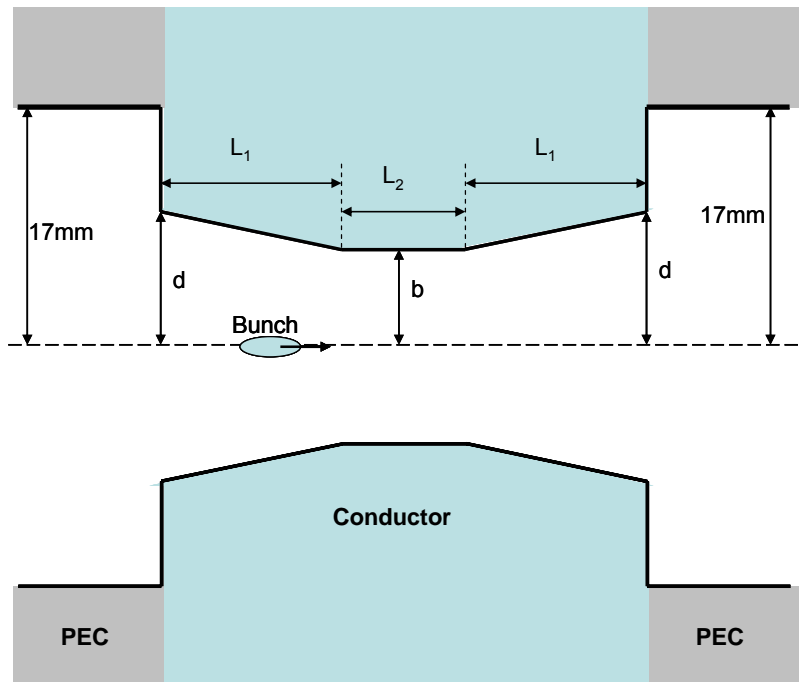
Figure 35. Cross section of the tapered collimator.

The numerical calculation of longitudinal monopole shot range wake potential (Fig. 36) of the Gaussian bunch with rms length $\sigma = 50\mu m$ results in the 270 V/pC loss factor for

conductive walls that is twice larger than for perfectly conducting walls (133 V/pC). Thus the real wake can not be obtained as a direct sum of the geometric and the steady-state solutions. A similar situation is observed for transverse wake potential.
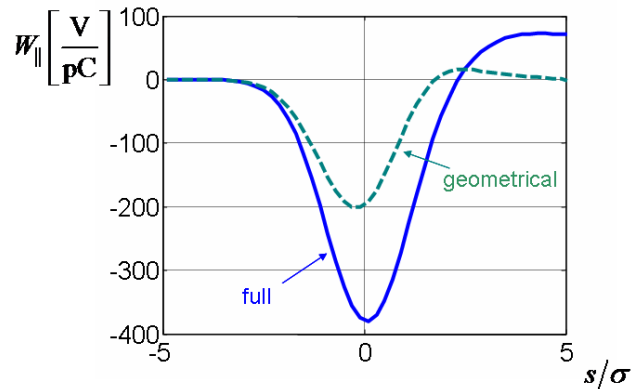
Figure 36. Comparison of the longitudinal wake potentials for tapered collimator with finite (blue solid) and perfect (green dashed) conducting walls.

In the last example we compare the wake potentials computed by the hybrid numerical scheme and by CST Microwave Studio. To be able to obtain an accurate result with CST Microwave Studio the Gaussian bunch is taken longer $\sigma = 20\,mm$ and the tapered collimator (fig. 35) is taken shorter with new parameters d=10mm, b=6mm, L_1=L_2 =30 mm and conductivity κ=100 S/m. Note that the conductivity was reduced to obtain larger wake potential than for the PEC case.

Fig. 37 presents the comparison of the longitudinal wake potentials obtained by CST Particle Studio (CST-PS) and by the new hybrid numerical code. The wake potentials calculated by the new code is done by 40 discrete points on 1σ bunch rms length and is in good agreement with the accurate result obtained by CST-PS. An equidistant mesh and staircase approximation of boundary interface was used for calculation with the new code.
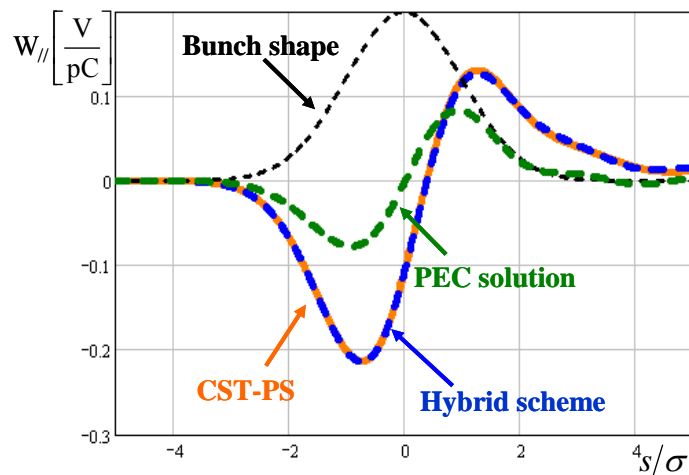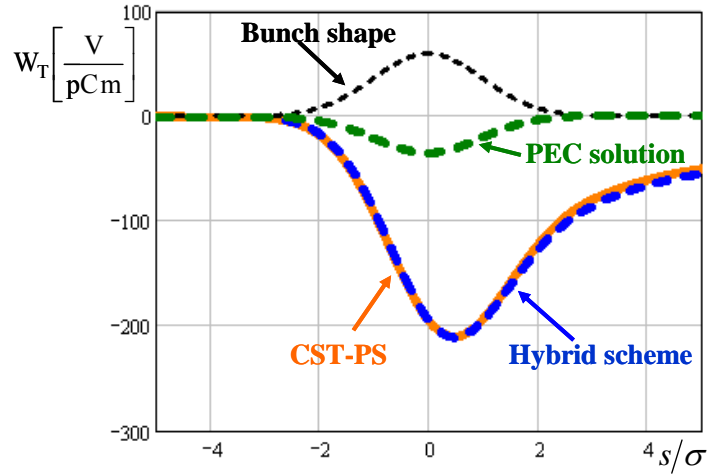
Figure 37. *Comparison of longitudinal wake potential calculated by CST Particle Studio (orange solid) and by hybrid scheme (blue dashed).*

Note that for this particular example to obtain an accurate solution with CST-PS a few hours is needed while for the new code (with implementation of moving mesh approach) the computational time is less than a minute.

4.6 Practical Applications to European XFEL and FLASH Facilities

In this section we present the application of the new numerical hybrid code for calculation of the longitudinal and transverse wake potentials for various resistive components of the FLASH and the European XFEL facilities.

FLASH Tapered Collimators

On the FLASH facility four collimators of the same type are installed. The collimators have a length of 500mm (L_1=200mm, L_2=100mm) (fig.35) and are made of copper material ($\kappa = 5.8 \cdot 10^7$ S/m). Each of the collimators has different geometrical options, presented in table 4 in accordance with fig.35.

Table 4. *FLASH collimator geometry parameters*

	Set 1	Set 2	Set 3
b	2 mm	3 mm	6 mm
d	4.5 mm	5.5 mm	8 mm

For those three geometry options of the collimator the longitudinal and transverse wake potential have been calculated using the new hybrid scheme for a Gaussian bunch of rms length σ =50 μm. To compare the contribution of the walls finite resistivity into the total wake potentials the geometric wakes were calculated using the numerical code ECHO.

Figure 38 presents the longitudinal monopole and dipole transverse wake potentials calculated by the new hybrid scheme and ECHO for Set 1 collimator geometry (table 4).
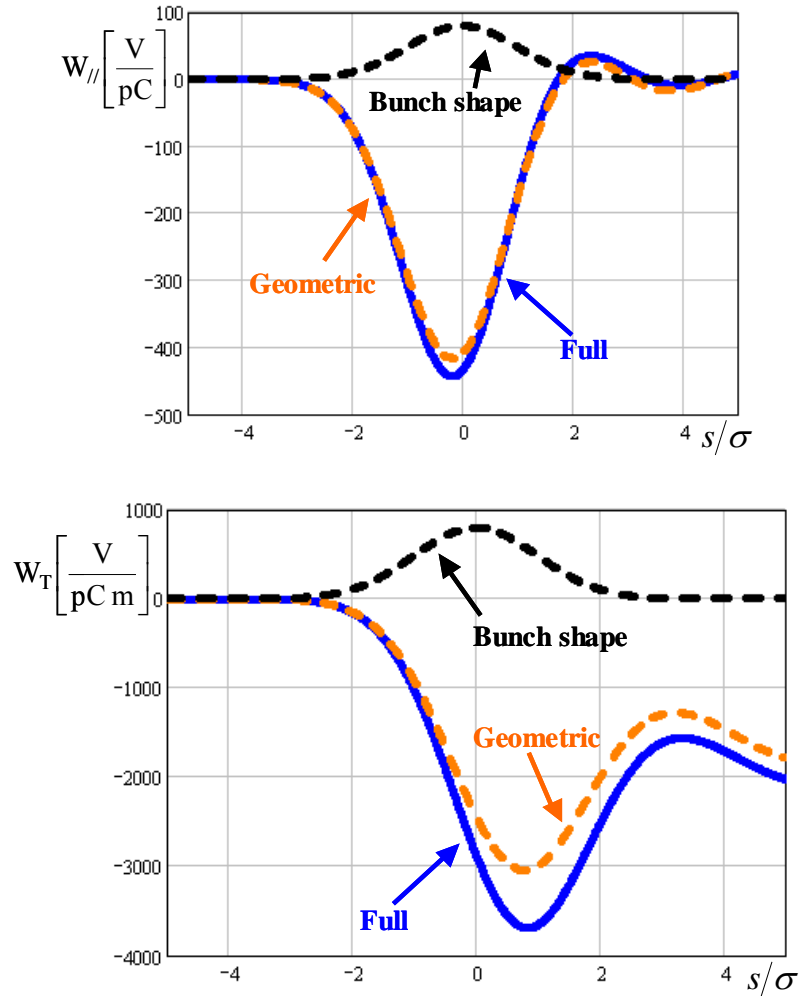
Figure 38 . *Geometric (orange dashed) and full (blue solid) wake potentials for the FLASH collimator geometry Set 1.*

In table 5 the loss (kick) and rms loss (kick) factors for collimator different geometry sets (table 4) obtained by the new hybrid scheme and ECHO code are presented. As is seen, the finite resistivity of the walls increases the monopole loss and rms loss factors by about 4% and 9% respectively. The dipole kick and the rms kick factors are increased by about 20%, 10.5%, and 5.5% for each geometry sets of the collimators.

Table 5. *The geometric and full loss (kick) factors of the FLASH collimator.*

	Geometric				Full			
	Loss factor V/pC	Rms Loss factor V/pC	Kick factor V/pC/m	Rms Kick factor V/pC/m	Loss factor V/pC	Rms Loss factor V/pC	Kick factor V/pC/m	Rms Kick factor V/pC/m
Set 1	279.4	129.5	2037	900	292.4	141.2	2424	1114
Set 2	244.1	103.4	1123	594	253.3	113.4	1240	670
Set 3	157.5	63.6	266	157.9	163.4	69.5	280.7	167.3

Rotationally Symmetric Step Collimator for European XFEL project

As the next application of the hybrid numerical scheme the longitudinal and transverse wake potentials of rotationally symmetric step collimator (fig. 39) designed for European XFEL

project [3] are presented. This collimator is made from titanium ($\kappa = 6 \cdot 10^5$ S/m) and has the length of L=500 mm. The calculations are done for the σ =25 μm rms length Gaussian bunch.
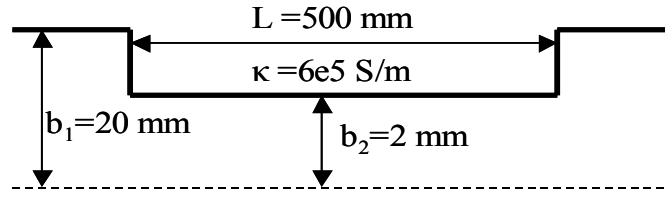
Figure 39. *Geometry of the step collimator for European XFEL project.*

The longitudinal and transverse wake potentials can be estimated by summation of geometric and steady-state resistive wakes.(4.31). The geometric longitudinal monopole and transverse dipole wake potentials can be calculated using the results derived in Ref. [81]

$$W_{//}(s) = \frac{Z_0\,c}{\pi} \ln\left(\frac{b_1}{b_2}\right) \rho(s)$$

$$W_T(s) = \frac{Z_0\,c}{\pi} \left(\frac{1}{b_2^2} - \frac{1}{b_1^2}\right) \theta(s)$$

(4.37)

where $\rho(s)$ is the Gaussian bunch distribution function and the function $\theta(s)$ is related to the error function $erf(x)$ as

$$\theta(s) = \int_{-\infty}^{s} \rho(s')\,ds' = \frac{1 + erf\left(\dfrac{s}{\sqrt{2}\,\sigma}\right)}{2}$$

(4.38)

Figure 40 presents the longitudinal monopole and transverse wake potentials calculated by the hybrid scheme (numerically) and analytical estimation (geometric + steady-state resistive). Note that the numerical calculation takes into account also the transient resistive wake fields while in analytics it is omitted.

83
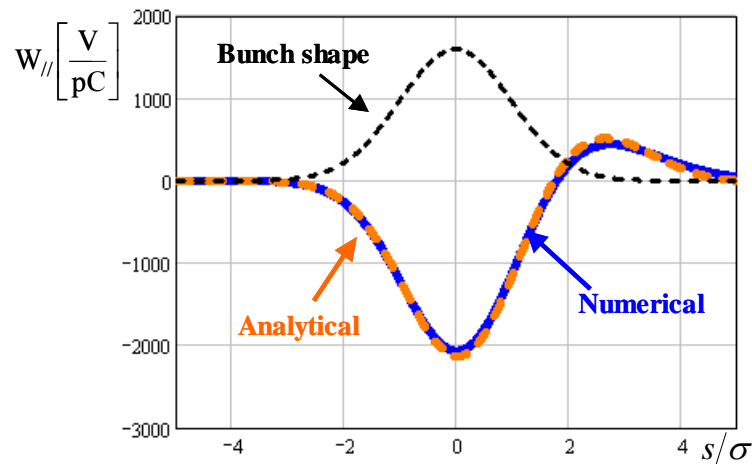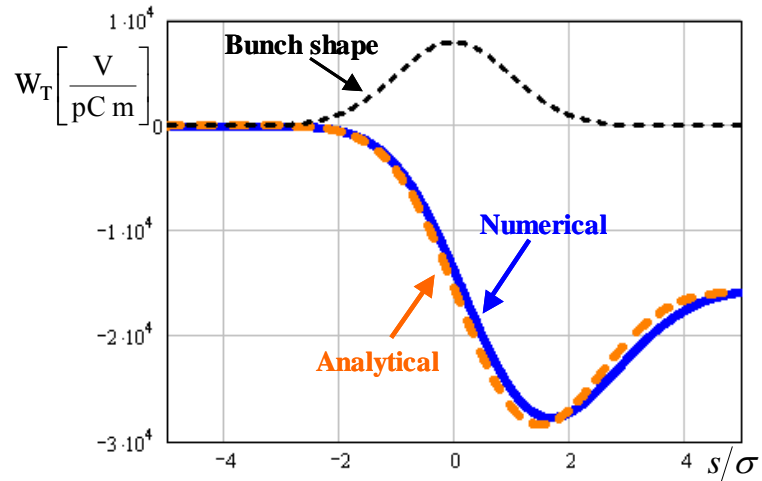
Figure 40. *Longitudinal monopole and transverse dipole wake potentials of step collimator calculated numerically (blue solid) and analytical (orange dashed) expression (geometric + steady state).*

Table 6 presents the numerical results for monopole loss and dipole kick factors with their rms deviations.

Table 6. *The loss and kick factors of the European XFEL step collimator.*

Loss factor kV/pC	Rms Loss factor kV/pC	Kick factor kV/pC/m	Rms Kick factor kV/pC/m
1.4	0.65	14	8.7

In this example the contribution of transient resistive part into the loss and kick factors is of the order of 3% .

Wake Potentials in Undulator Intersections of European XFEL

Finally we calculate the wake potentials for the undulator intersection designed for European XFEL project (fig. 41). The undulator cell consist of the 5161-mm long undulator section with the 890-mm length intersection.
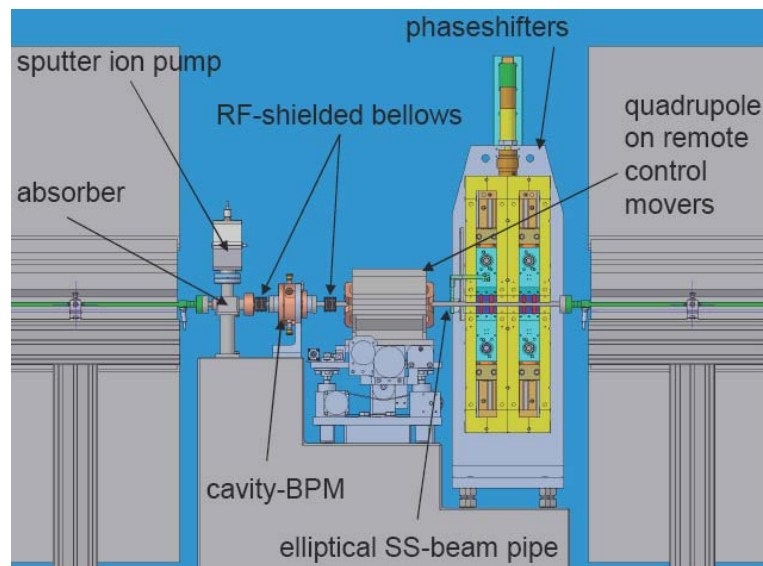
Figure 41. *Undulator intersection of European XFEL project.*

The intersection consists of pump, absorber, bellows, BPM (Beam Position Monitor) and round pipe of radius 5mm. In the table 7 are presented the lengths and the conductivities of the undulator section elements [82].

Table 7. *The list of undulator intersection elements.*

N	Element	Length	Material	Conductivity
1	Elliptical pipe	5161 mm	Aluminum	3.66E+07
2	Pump	105 mm	Aluminum	3.66E+07
3	Absorber	22 mm	Copper	5.80E+7
4	Bellow	30 mm	BeCu 174	2.78E+7
5	BPM	51 mm	Stainless Steel 304	1.4E+6
6	Bellow	30 mm	BeCu 174	2.78E+7
7	Round pipe	652 mm	Copper	5.80E+7

The geometries of the undulator intersection elements are presented in Figure 42.

a. Bellow

b. Beam Position Monitor (BPM)

c. Absorber

Figure 42. Geometries of undulator intersection elements: bellow (a), BPM (b), absorber (c).

In figure 43 are presented longitudinal monopole and transverse dipole wake potentials calculated by the hybrid scheme and analytical estimation (geometric+resistive) for the Gaussian bunch of σ =25 μm rms length passing the undulator intersection.
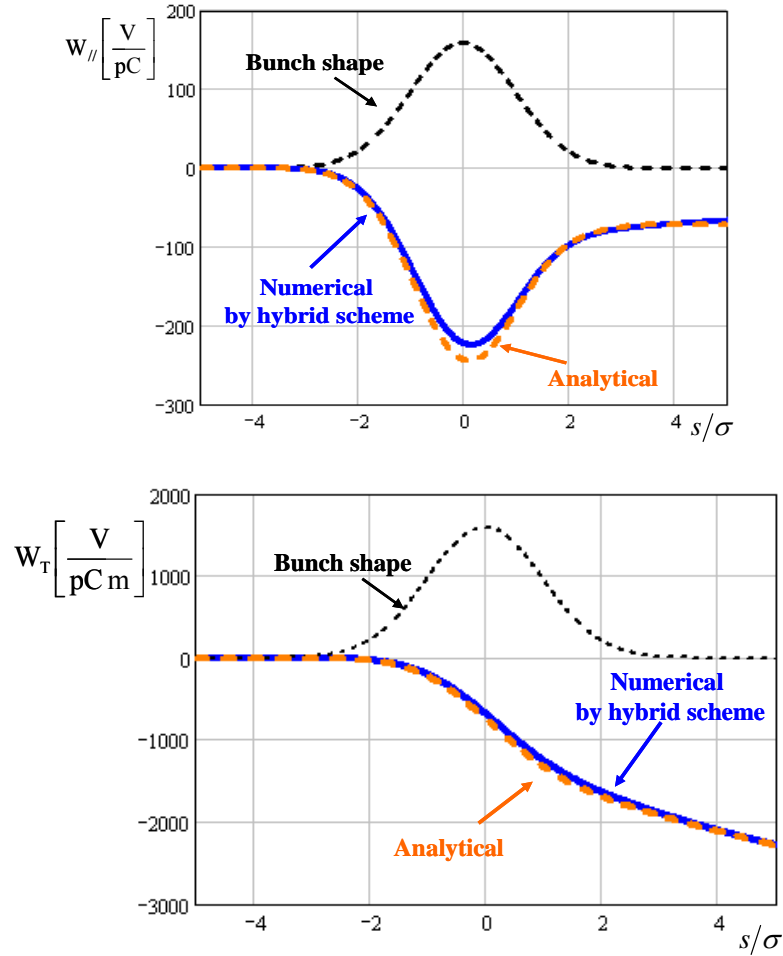
Figure 43. Longitudinal monopole and transverse dipole wake potentials for undulator intersection of European XFEL project calculated by new hybrid numerical scheme (blue solid) and analytically (geom.+resistive) (orange dashed).

Obtained loss and kick factors are presented in table 8.

Table 8. Loss and kick factors of the European XFEL undulator intersection.

	Loss factor V/pC	Rms Loss factor V/pC	Kick factor V/pC/m	Rms Kick factor V/pC/m
Hybrid scheme	167.4	56.04	713.6	460.8
Geom.+Resistive	180.9	61.7	766.0	482.1

86

The effects of "in" and "out" undulator intersection transitions are taken into account in calculations by adding 3cm long round aluminum pipes of radius 4.4 mm at both sides of the intersection. In the calculation the resistive wake potentials are estimated for the following elements: pump, absorber (4 mm radius), BPM (straight section) and round pipe. As is seen (fig. 43 and table 8) the monopole loss and dipole kick factors obtained analytically lead to 8% overestimation of the losses calculated with hybrid scheme (transient resistive effects included).

4.7 Conclusion

In this chapter a new hybrid numerical scheme for rotational symmetric structures was introduced. This hybrid scheme was developed for wake field calculations excited by ultra short bunches moving through the structures with finite conductive walls. The new hybrid scheme is fully time domain and is dispersion-free in longitudinal direction that allows to calculate the wakefields for very long (L>1m) structures without loss of calculation accuracy. The realization of the scheme was done for staircase approximation of the boundary that reduces the calculation accuracy to the first order. Several tests have been performed to improve the hybrid scheme. The results are in good agreement both with analytics and numerical results obtained by CST-PS. The new hybrid scheme was applied to calculate the wake potentials for the various accelerator elements of FLASH linear accelerator at DESY and the European XFEL project.

Summary

The acceleration of electron bunches with very small longitudinal and transverse phase space volume is one of the most actual challenges for the future International Linear Collider and high brightness X-Ray Free Electron Lasers. The exact knowledge on the wake fields generated by the ultra-short electron bunches during its interaction with surrounding structures is a very important issue to prevent the beam quality degradation and to optimize the facility performance. The high accuracy time domain numerical calculations play the decisive role in correct evaluation of the wake fields in advanced accelerators. Although various analytical and numerical methods have been developed to evaluate these fields, the calculation of the wake fields generated by ultra-short bunches in 3D structures with finite conductivity walls still remains a challenging problem.

The one problem associated with accumulation of numerical dispersion errors during the wake field calculation in accelerators is successfully solved by implementation of the dispersion-free numerical scheme for structures with perfectly conducting walls.

To model the conductive boundaries, the numerical scheme for one-dimensional electromagnetic problems with Impedance Boundary Condition has been derived. This scheme is an approximation of electromagnetic properties of the 3D metallic boundaries, since for high conductivity materials the incident waves are transmitted perpendicular to the boundary surface.

To calculate the wake fields produced by ultra short bunches in structures with resistive walls, a new 3D time-domain dispersion-free hybrid numerical scheme is developed. The stability of the new hybrid numerical scheme in vacuum, conductor and bound cell is studied. The stability conditions have been tested and approved by a number of numerical experiments. The convergence of the new scheme is analyzed by comparison with well-known analytical solutions.

The realization of this new hybrid 3D implicit numerical scheme is done for rotationally symmetric geometries and staircase approximation of the boundary surface. A good agreement of the numerical simulations with the well-known analytical results and CST Particle Studio simulations are obtained. The new hybrid scheme was applied to calculate the wake potentials for the various components of FLASH linear accelerator at DESY and the European XFEL project.

Reference

1. K. Kubo, A. Seryi, N. Walker, A. Wolski, Beam dynamics challenges for the ILC, ICFA Beam Dyn. Newslett., v. 44, pp. 3-35, 2007.

2. LCLS Design Study Report, SLAC-R-521, December, 1998.

3. M. Altarelli et al, XFEL. The European X-Ray Free-Electron Laser, Technical Design Report, DESY 2006-097, Hamburg, July 2006.

4. A. Oppet et al, Toward a Low Emittance X-ray FEL at PSI, Proceedings of FEL 07, Novosibirsk, Russia, 26-31 Aug 2007 .

5. K. Bochetta et al, Fermi @ Elettra: A Free Electron Laser for EUV and soft X-ray radiation, Synchrotron Radiat.News 18, N 6: 30-35,2005.

6. G. Datolli, A. Renieri, Review of Existing Soft and Hard X-Ray FEL Projects, FEL-2005, 21-26 August 2005, Stanford, CA, USA, 442-446, 2005.

7. J. Murphy and C. Pellegrini, Free Electron Lasers for the XUV Spectral Region, Nucl. Instr. and Meth., pp.159-167, 1985.

8. Ya. S. Derbenev, A.M. Kondratenko and Y.L. Saldin, Nucl. Instr. and Meth., A193, pp. 415-421, 1982.

9. Z. Huang, K. Kim, A Review of X-ray Free-Electron Laser Theory, Phys. Rev. STAB, 0348201, 2007.

10. M. Dohlus, J. Rossbach, and P. Schmuesser, Ultraviolet and Soft X-ray Free-Electron Lasers, , Springer, New York, 2008.

11. A.W. Chao , Physics of Collective Beam Instabilities in High Energy Accelerators, New York, John Willey & Sons, Inc., 371 pp., 1993.

12. B.W.Zotter and S.A. Kheifetz, Impedances and Wakes in High-Energy Particle Accelerators, Singapore, World Scientific, 405 pp., 1997.

13. H. Wiedemann, Particle Accelerator Physics, Springer, Nederland, vol.2, 473 pp., 1999.

14. T.O. Raubenheimer, Electron Beam Acceleration and Compression for Short Wavelength FELs, Nucl. Instr. Meth. A, 40, pp. 358-369, 1995.

15. A.Hofmann, Beam Instabilities, CAS Proceedings, Rhodes, Greece, CERN – 95-06, pp. 307-326, 1995.

16. J.-L. Laclare, Coasting Beam Longitudinal Coherent Instabilities, CAS Proc., Finland, CERN – 94-01, pp. 345-405, 1994.

17. T. Weiland and R. Wanzenberg, Wake Field and Impedances, Joint US-CERN Accelerator Courses, Hilton Head, pp. 39-79,1990.

18. K. L. Bane, P. B. Wilson, T. Weiland, Wake Fields and Wake Field Acceleration, SLAC-PUB-3528,56 pp., December 1984.

19. P. Wilson, AIP Conf. Proc., vol.87, New York, pp. 450-583, 1982.

20. D. Briggs, Low frequency transverse resistive instability in the collider, SSCL-512-REV1, 15 pp., Jun 1992.

21. F. Ruggiero, Single beam collective effects in the LHC, Part. Accel. 50, pp. 83-104, 1995.

22. R. Nagaoka, Study of Resistive-wall Effects on SOLEIL, EPAC 2004, Lucerne, Switzerland, pp. 2038-2040, 2004.

23. I.Hoffmann, G.Franchetti, A.Fedotov, AIP Conf.Proc.642: 248-252,2003.

24. A. Piwinski, IEEE Trans. Nucl. Sci. 24, No.3, pp. 1364-1366, 1977.

25. R.Gluckstern and B.Zotter, Analysis of shielding charged particle beams by thin conductors, Phys. Rev. ST Accel. Beams, 4, 024402, 2001.

26. X. E. Lin, RF loss in and leakage through thin metal film, SLAC-PUB-7924, 7 pp., August 1998.

27. T. Weiland and B. Zotter, Particle Accelerator 11, 143-151 (1981)

28. H. Henke and O. Napoly, in Proceedings of the Second European Particle Accelerator Conference, Nice, France, *1990* (Editions Frontiers, Gif-sur-Yvette, 1991), pp. 1046–1048, 1990.

29. A. W. Chao, Coherent Instabilities Of A Relativistic Bunched Beam, Technical Report No. 2946, SLAC-PUB, 173 pp., 1982, also AIP Conf.Proc. 105, pp. 353-523,1983.

30. S. Ratschow and T. Weiland, Analytical calculation of the wake potential of a spherical resonator, Phys. Rev. ST Accel. Beams, v.5, 052001, 2002.

31. A. Tsakanian, Analytical calculation of wake fields in conical cavity, Nucl. Instr. Meth. A548, pp. 298-305, 2005.

32. Th. Weiland, A discretization Method for the Solution of Maxwell Equations for Six-Component Fields, Int. J. Elect. Comm., v. 31, pp 116-128, 1977.

33. I. Zagorodnov, T. Weiland, TE/TM scheme for computation of electro-magnetic fields in accelerators, J. Comput. Phys., v. 207, pp. 69-91, 2005.

34. K. Fujita, H. Kawaguchi, I. Zagorodnov, T. Weiland, Time domain wake field computation with boundary element method, IEEE Trans. Nucl. Sci., v. 53, pp.431-439, 2006.

35. R. W. Hockney and J. W. Eastwood, Computer Simulation Using Particles, IOP Publishing Ltd., Bristol, 1988.

36. K.S. Yee, IEEE Trans. Antennas Propag. 14, 302 (1966).

37. T. Weiland, in Proceedings of the 11th International Conference on High-Energy Accelerators, Geneva, Switzerland, 1980 (Brikhauser-Verlag, Basel), pp. 570-575.

38. K. S. Yee, Numerical Solution of Initial Boundary Value Problems Involving Maxwell's Equations in Isotropic Media, IEEE Trans. Antennas Propag. 14, 302 (1966).

39. MAFIA Collaboration, MAFIA manual, CST GmbH, Darmstadt, 1997.

40. T. Weiland, TBCI and URMEL – New computer codes for wake field and cavity mode calculations, IEEE Trans. Nucl. Science 30, 2489 (1983).

41. A. D. Greenwood, K. L. Cartwright, J. W. Luginsland, and E. A. Baca, Journal of Comput. Phys. 201, 665 (2004).

42. S. Wang, F. L. Teixeira, Dispersion-relation-preserving FDTD algorithms for large-scale three- dimensional problems, IEEE Trans. Antennas Propag. 51, 1818 (2003).

43. N. V. Kantartzis, T. T. Zygiridis, T. D. Tsiboukis, An unconditionally higher order ADI-FDTD technique for the dispersionless analyses of generalized 3D EMC structures, IEEE Trans. Magn. 40, 1436 (2004).

44. J. B. Cole, High-accuracy Yee algorithm based on non-standard finite differences: new developments and verifications, IEEE Trans. Antennas Propag. 50, 1185 (2002).

45. T. Kashiwa, et al.., Phase velocity errors of the non-standard FDTD method and comparison with other high accuracy FDTD methods, IEEE Trans. Magn. 39, 2125 (2003).

46. R. Hampel, I. Zagorodnov, T. Weiland, New discretization scheme for wake field computation in cylindrically symmetric structures, in Proceedings of the EPAC 2004, Lucerne, p. 2556.

47. A. Mosnier, A. Novokhatskii, Wakefield dynamics in quasi-periodic structures, in Proceeding of the PAC 1997, Vancouver, Canada.

48. A. Novokhatskii, M. Timm, T. Weiland, Transition dynamics of the wake fields of ultra short bunches, TESLA Report 2000-03, DESY, 2000.

49. I. Zagorodnov, T. Weiland, Calculation of Transverse Wake Potential for Short Bunches, Proceeding of the ICAP 2002, East Lansing.

50. I. Zagorodnov, R. Schumann, T. Weiland, Long-Time Computation of Electromagnetic Fields in the Vicinity of a Relativistic Source, J. Comput. Phys. 191 (2003) 525.

51. CST Microwave Studio is a trademark of CST GmbH.

52. I. Zagorodnov, T. Weiland, TE/TM field solver for particle beam simulations without numerical Cherenkov radiation, Phys. Rev. ST-AB 8, 042001, 2005.

53. E. Gjonaj, T. Lau, T. Weiland (TUD, TEMF, Darmstadt) , R. Wanzenberg (DESY, Hamburg), Computation of Short Range Wake Fields with PBCI, Published in ICFA Beam Dyn. Newslett. 45: 38-52, 2008.

54. A. Taflove, S. C. Hagness, Ed., Computational Electrodynamics: The Finite-Difference Time-Domain Method, Artech House, London, 2000.

55. A. A. Samarskii, The Theory of Difference Scheme, Marcel Dekker, New York, 2001.

56. A. A. Samarskii, P. P. Matus, P. N. Vabischevich, Difference Schemes with Operator Factors, Kluwer Academic Publishers, London, 2002.

57. F. Edelvik, R. Schuhmann, T. Weiland, A General Stability Analysis of FIT/FDTD Applied to Lossy Dielectrics and Lumped Elements, Int. J. Numer. Model. 17 (2004) 407.

58. K. S Kunz., R. J. Luebbers, The Finite-Difference Time-Domain Method for Electromagnetism, CRC Press, New York, 1993.

59. M. Levy, Parabolic Equation Methods for Electromagnetic Wave Propagation, Cornwall, England, 2000.

60. J.D.Jackson, Classical Electrodynamics, 2 nd edition , New York, 1975.

61. M. Dohlus, Dissertation "Ein Beitrag zur numerischen Berechnung elektromagnetischer Felder im Zeitbereich", TEMF, Darmstadt, Germany.

62. Rob F. Remis, On the Stability of the Finite-Difference Time-Domain Method, Journal of Comput. Phys. 163, 249-261 (2000).

63. T. Weiland, Time Domain Electromagnetic Field Computation with Finite Difference Methods, Int. J. Numer. Model. 9 (1996) 295.

64. T. Weiland, On the Unique Numerical Solution of Maxwellian Eigenvalue Problems in Three Dimensions, Particle Accelerators 17 (1985) 227.

65. R. Schuhmann, T. Weiland, Conservation of Discrete Energy and Related Laws in the Finite Integration Technique, PIER Manograph Series 32, 2001, p. 301.

66. S. Wang, F. L. Teixeira, Dispersion Relation Preserving FDTD Algorithms for Large Scale Three-Dimensional Problems, IEEE Trans. Antennas Propag. 51 (2003) 1818.

67. M. Dohlus, I. Zagorodnov, Explicit TE/TM Scheme for Particle Beam Simulations, Journal of Comput. Phys. 228 (2009) 2822-2833.

68. I. Zagorodnov, R. Schuhmann, T. Weiland, A Uniformly Stable Conformal FDTD Method on Cartesian Grids, Int. J. Numer. Model. 16 (2003) 127.

69. T. Weiland, Transverse Beam Cavity Interaction, Part I: short range forces, Nucl. Instrum. Methods 212 (1983) 329.

70. T. Weiland, Comment on Wake Field Computation in Time Domain, Nucl. Instr. Meth. 216 (1983) 13.

71. O. Napoly, Y. Chin, B. Zotter, A Generalized Method for Calculating Wake Potential, Nucl. Instr. Meth. 344 (1993) 255.

72. I. Zagorodnov, Indirect Methods for Wake Potential Integration, Phys. Rev. ST-AB 9, 102002 (2006).

73. W. K. H. Panowsky, W. A. Wenzel, Some Considerations Concerning the Transverse Deflection of Charged Particles in Radio-Frequency Fields, Rev. Sci. Instr. 27 (1956) 947.

74. K. Yokoya, Impedance of slowly tapered structures, Tech. Rep. SL/90-88 (AP), CERN, 1990.

75. TESLA Technical Design Report, DESY 2001-011, Hamburg, Germany, 2001, Part II.

76. M. Born, E. Wolf, Principles of Optics, 1986.

77. A. C. Cangellaris and D. B. Wright, Analysis of the numerical error caused by the stair-stepped approximation of a conducting boundary in FDTD simulations of electromagnetic phenomena, IEEE Trans. Antennas Propagat., vol. 39, pp. 1518–1525, Oct. 1991.

78. J. B. Schneider and K. L. Shlager, "FDTD simulations of TEM horns and the implications for staircased representations," IEEE Trans. Antennas Propagat., vol. 45, pp. 1830–1838, Dec. 1997.

79. K. L. F. Bane and M. Sands, in: *Micro Bunches Workshop*, edited by E. B. Blum, M. Dienes, J. B. Murphy, AIP Conf. Proceedings No. 367 (AIP, New York, 1996), p. 131; see also K. L. F. Bane, SLAC Report No. SLAC-AP-87, 1991.

80. S. Krinsky, B. Podobedov, R. L. Gluckstern, Impedance of finite length resistive cylinder, Phys. Rev. ST-AB 7, 114401, 2004.

81. G. Stupakov, K.L.F. Bane, I. Zagorodnov, Optical approximation in the theory of the geometrical impedance, Phys. Rev. ST-AB 10, 054401, 2007.

82. O. Zagorodnova, European XFEL Database, DESY, 2009.